Accepted Manuscript

Research opportunities with compact accelerator-driven neutron sources

I.S. Anderson, C. Andreani, J.M. Carpenter, G. Festa, G. Gorini, C.-K. Loong, R. Senesi

PII: S0370-1573(16)30195-8
DOI: http://dx.doi.org/10.1016/j.physrep.2016.07.007
Reference: PLREP 1921

To appear in: *Physics Reports*

Accepted date: 19 July 2016

Please cite this article as: I.S. Anderson, C. Andreani, J.M. Carpenter, G. Festa, G. Gorini, C.-K. Loong, R. Senesi, Research opportunities with compact accelerator-driven neutron sources, *Physics Reports* (2016), http://dx.doi.org/10.1016/j.physrep.2016.07.007

Research Opportunities with Compact Accelerator-driven Neutron Sources

I. S. Anderson
Oak Ridge National Laboratory, Oak Ridge, TN USA

C. Andreani*
Università degli Studi di Roma "Tor Vergata", Physics Department and NAST Centre, Via della Ricerca Scientifica 1, 00133 Roma, Italy
CNR-IPCF Sezione di Messina, Messina, Italy
Museo Storico della Fisica e Centro Studi e Ricerche Enrico Fermi, Roma, Italy

J. M. Carpenter
Argonne National Laboratory, Argonne, IL USA

G. Festa*
Università degli Studi di Roma "Tor Vergata", Physics Department and NAST Centre, Via della Ricerca Scientifica 1, 00133 Roma, Italy
Museo Storico della Fisica e Centro Studi e Ricerche Enrico Fermi, Roma, Italy

G. Gorini
Università degli Studi di Milano—Bicocca, Milano, Italy

C.-K. Loong
Università degli Studi di Roma "Tor Vergata", Centro NAST, Via della Ricerca Scientifica 1, 00133 Roma, Italy

R. Senesi
Università degli Studi di Roma "Tor Vergata", Physics Department and NAST Centre, Via della Ricerca Scientifica 1, 00133 Roma, Italy
CNR-IPCF Sezione di Messina, Messina, Italy
Museo Storico della Fisica e Centro Studi e Ricerche Enrico Fermi, Rome, Italy

ABSTRACT

Since the discovery of the neutron in 1934 neutron beams have been used in a very broad range of applications, As an aging fleet of nuclear reactor sources is retired the use of compact accelerator–driven neutron sources (CANS) are becoming more prevalent. CANS are playing a significant and expanding role in research and development in science and engineering, as well as in education and training. In the realm of multidisciplinary applications, CANS offer opportunities over a wide range of technical utilization, from interrogation of civil structures to medical therapy to cultural heritage study. This paper aims to provide the first comprehensive overview of the history, current status of operation, and ongoing development of CANS worldwide. The basic physics and engineering regarding neutron production by accelerators, target-moderator systems, and beam line instrumentation are introduced, followed by an extensive discussion of various evolving applications currently exploited at CANS.

KEYWORDS:

Compact neutron sources, neutronics, accelerator, nuclear reactions, neutron scattering neutron interrogation, cultural heritage, detectors

*Corresponding Authors. e-mail: carla.andreani@uniroma2.it, giulia.festa@uniroma2.it

TABLE OF CONTENTS:

1. Introduction: purpose and scope 4
2. The Neutron 4
2.1 Basic properties 4
3. Neutron Sources 6
3.1 A Little History 6
3.1.1 Reactors 7
3.1.2 Accelerator-driven Neutron Sources 8
3.2 Production Reactions 9
3.2.1 Fission 9
3.2.2 Spallation 9
3.2.3 Fusion 12
3.2.4 Neutron production by nuclear reactions driven by low-energy charged particles 13
3.2.5 Photonuclear reactions 15
4. Compact Accelerator-driven Neutron Sources 17
4.1 CANS in Operation: Status and Future Trends 19
4.1.1 Bariloche Electron-linac-driven Neutron Source 19
4.1.2 The Compact Pulsed Hadron Source of Tsinghua University 20
4.1.3 The quasi-monoenergetic neutron beam facility at CYRIC 21
4.1.4 The Frascati Neutron Generator 22
4.1.5 Gaerttner Linear Accelerator at Rensselaer Polytechnic Institute 23
4.1.6 GELINA—The Geel Electron Linear Accelerator Facility 24
4.1.7 HUNS—The Hokkaido University Neutron Source 26
4.1.8 iThemba in South Africa 27
4.1.9 KOMAC-NST, KIRAMS-MC-50, and PAL-PNF facilities in Korea 28
4.1.10 KUANS—The Kyoto University Accelerator-driven Neutron Source 29
4.1.11 KURRI-LINAC—The Kyoto University Research Reactor Institute–Electron Linear Accelerator 30
4.1.12 LENS—The Low-Energy Neutron Source 31
4.1.13 PKUNIFTY—Peking University Neutron Imaging Facility 32
4.1.14 RANS—RIKEN Accelerator-driven Neutron Source 33
4.1.15 The Svedberg Laboratory neutron facility 34
4.2 CANS under Development 35
4.2.1 The ESS-Bilbao Project, Spain 35
4.2.2 The Frankfurt Neutron Source at the Stern-Gerlach-Zentrum (FRANZ), Germany 36
4.2.3 LENOS—The Legnaro Neutron Source, Italy 37
4.2.4 n@BTF, The Frascati electron-driven source 37
4.2.5 The nELBE Time-of-flight Facility at the Helmholtz-Zentrum Dresden-Rossendorf 38
4.2.6 NEPIR facility at the SPES source of the Laboratori Nazionali di Legnaro 39
4.2.7 The Nagoya University Accelerator-driven Neutron Source (NUANS) 41
4.2.8 UTCANS—U-Tokyo 41

4.2.9 Van de Graaff facility at the Institute for Reference Materials and Measurements of the Joint Research Centre of the European Commission in Geel, Belgium. 43
4.3 Preferred Characteristics of CANS Applications 44
5. Neutron Interaction 46
5.1.1 Condensed matter scattering of slow neutrons 47
5.1.2 Non-scattering interactions 51
5.1.3 Neutron capture–induced radiation 53
5.1.4 Neutron-induced radiation effects 55
5.1.5 Neutron slowing-down and thermalization 56
5.1.6 Magnetic interactions 57
5.2 Neutron Detectors 58
6. Applications 61
6.1 Experimental Neutronics and Device Development 60
6.2 Materials Characterization 61
6.3 Interrogation 61
6.3.1 Civil structures 62
6.3.2 Cultural heritage 63
6.3.3 Detection of explosives 64
6.3.4 Detection of antipersonnel landmines 65
6.3.5 Well-logging and mineralogy 65
6.4 Irradiation Effects of Electronics 66
6.5 Nuclear Data 69
6.6 Experimental Nuclear Astrophysics 69
6.7 Neutron Capture Therapy 70
6.8 Isotope Production 72
7. Perspectives 74
8. Conclusions 74

1. Introduction: purpose and scope

Neutron beams are used in a wide range of applications, mainly aimed at determining and understanding the properties of condensed matter. For those applications that require at least moderate fluxes of neutrons, measurements are typically carried out at large-scale neutron beam facilities, including nuclear fission reactors and accelerator-driven sources which operate as user facilities. Historically, reactor sources have predominated; but as reactor technology, and the resulting available fluxes, plateaued in the 1960s, accelerator-driven sources became more prevalent. Furthermore, nonproliferation policies, and the difficulties associated with manufacturing suitable fuel elements, have prevented the replacement of reactor facilities. The smaller reactor facilities were often used as testing and training grounds, while the larger facilities provided the capability for more advanced or flux-limited measurements. High-power accelerator-driven spallation neutron sources have already established themselves as the flagship facilities, eventually targeted to replace the high-flux reactors; however, the demise of the small-scale reactors presents a shortfall in the number of available beams, as the community of users grows and demands more effective instruments. [1, 2] On the other hand, accelerator-driven neutron sources based on low-energy neutron-producing reactions, which are inexpensive to build and operate and are suitable for university and small laboratory installations, have become an attractive alternative. These compact accelerator-driven neutron sources, or CANS, can effectively serve many of the needs that were hitherto served by small reactors and are the focus of this report.

As the reader will quickly ascertain, there are a wide range of accelerator-driven neutron sources in operation or being built across the world. This article aims at providing a comprehensive overview of CANS, defined for our purposes as accelerator-driven facilities with particle energies less than 100 MeV and a power level below 100 kW for neutron production. This working definition, which is based on engineering and physical considerations, delineates the distinctive role of CANS with respect to high-power spallation sources and nuclear reactors. We have attempted to provide a comprehensive overview that includes the basic physics and engineering behind neutron sources and the interaction of neutron beams with condensed matter, as well as descriptions of known CANS—those currently in operation and under construction or study—and their applications. The prospect of CANS against a backdrop of the changing landscape of neutron research will be discussed at the end.

2. The Neutron

2.1 Basic properties

The neutron, together with the proton, is one of the building blocks of materials at the nuclear scale. Neutrons are generally categorized according to their means of production, their energies, and their use in conventional and special applications. We extend the term “slow neutrons” to include all those having energies that are currently used in the neutron characterization of materials, $E < 1000$ eV. We term as “fast neutrons” all those of higher energies, $E > 1000$ eV. A detailed summary of neutron properties is given in Table 2.1. As a nucleon, the neutron distinguishes itself with characteristics unlike those of the photon and the electron, which undergo only electromagnetic interactions with atomic electrons. Photons and electrons do not perturb the nuclear structure unless at very high energies or powers, e.g., high-energy x/γ rays and relativistic electrons. Thermal and cold neutrons, owing to their very low energies compared with the electronic energies of atomic orbitals, interact with atomic nuclei and the magnetic electrons via nuclear and magnetic scattering, respectively, without altering the chemistry of materials. Slow and fast neutrons also interact with matter via non-scattering reactions. Because accelerator-driven neutron sources may produce quasi-monoenergetic neutrons or, by means of moderators or beam shaping assemblies, deliver a broad range of slow to fast neutrons, they lend themselves to basic materials research and a variety of applications.

Figure 2.1 shows the expected neutron spectrum emitted from a 100 K liquid methane moderator of the Intense Pulsed Neutron Source (IPNS) neutron source, one of the first spallation slow neutron sources based on a proton synchrotron which operated between 1982 and 2008 at Argonne National Laboratory (ANL).

Table 2.1 Neutron attributes, categorization, and relationships

Fundamental properties						
Mass	$m_n = 1.674927351 \times 10^{-27} kg = 1.0086474\ amu$					
Magnetic moment μ_N = nuclear magneton	$\mu_{n=} - 1.9130427\mu_N = -0.96623647 \times 10^{-26} J/T = -6.0307740 \times 10^{-9}\ meV/gauss$					
Larmor frequency	$\omega_L = \gamma_n \lvert\vec{B}\rvert = 1.83247179X10^4 \lvert\vec{B}\rvert$					
Gyromagnetic ratio	$\gamma_n = 2\mu_n \hbar = 1.83247179 \times 10^4$ radians/s/gauss					
Numerical conversions of neutron attributes [units]						
$E[\text{meV}]$	$k^2[\text{Å}^{-2}]$	$1/\lambda^2[\text{Å}^{-2}]$	$v^2[\text{m}^2/\text{s}^2]$	$f[\text{Thz}]$	$T[\text{K}]$	$B[\text{gauss}]$
E	$\hbar^2k^2/2m_n$ $= 2.072\ 125\ k^2$	$h^2/(2m_n\lambda^2)$ $= 81.804\ 21/\lambda^2$	$m_n v^2/2$ $= 5.227\ 0374 \times 10^{-6} v^2$	hf $= 4.135\ 667\ 42\ f$	$k_B T$ $= 0.086\ 173\ 32\ T$	$\lvert\vec{\mu_n}\rvert\lvert\vec{B}\rvert$ $= 6.0307740 \times 10^{-9} B$
$\lambda[\text{Å}] = h/m_n v = 3956.0340/v$, v = neutron speed [m/s].						
Neutron categories according to energy distribution						
Slow neutrons: $E < 1000$ eV			Fast neutrons: $E > 1000$ eV			
Thermal neutrons: $0.005\text{ eV} < E < 0.5$ eV			Epithermal neutrons: $0.05\text{ eV} < E < 1000$ eV			
Cold neutrons: $E < 0.005$ eV		Very cold neutrons: $\sim 8\ \mu\text{eV} < E < 800\ \mu\text{eV}$		Ultracold neutrons: $E < 8\ \mu$eV		

Nucleons are confined within atomic nuclei by the strong forces, unless the nuclei are outside of the valley of nuclear stability in the Z-N plane, wherein spontaneous decay occurs in various ways.

A free neutron decays by e^- emission to a proton, accompanied by an electron anti-neutrino, and has a mean lifetime t_e = 881.5 seconds = 14.7 minutes and a half-life $t_{1/2}$ = 611.0 seconds:

$$\text{n} \xrightarrow{T_{1/2}=611s} \text{e}^- + \text{p} + \bar{\nu}_e + 782\text{ keV}\ . \qquad (0.1)$$

Although the decay process is interesting from a fundamental physics point of view, we do not need to account for it in materials science applications, since the lifetimes of free neutrons far exceed the duration of our measurements.

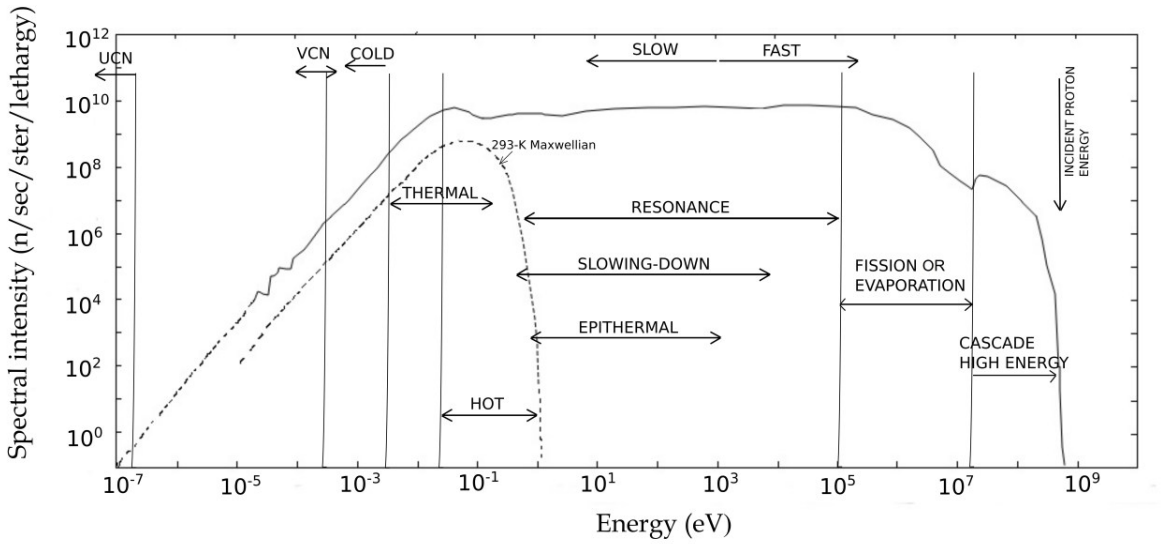

Figure 2.1 The Monte Carlo–simulated spectrum of neutrons, labeled according to the nomenclature for different neutron energies and ranges, from the cadmium-decoupled, poisoned 100 K liquid methane moderator at the IPNS, see [Chapter 2 for a more detailed description]. Although in this example the target is Uranium similar spectra would be observed for different targets.

3. Neutron Sources

3.1 A Little History

The very earliest slow-neutron scattering experiments were in-principle demonstrations using neutrons from radioisotope neutron sources, as by James Chadwick in his 1932 discovery of the existence of the neutron. The research of Enrico Fermi, of Eugene Wigner, and of Meitner, Hahn and Strassmann characterizing fundamental aspects of neutron-matter interactions, was based on isotope-driven $^{4}\mathrm{He}$-n neutron sources. Later, low-energy cyclotron-driven sources provided higher-energy charged particles that enabled a wide range of nuclear physics discoveries and higher neutron production. Atmospheric neutrons were discovered, which arise from high-energy cosmic-ray proton spallation reactions. Available slow-neutron beam intensities grew immensely with the development of fission reactors after Fermi's demonstration in 1942. Pulsed electron linear accelerators providing bremsstrahlung photoneutrons entered the scene but were soon overshadowed by reactors and proton-accelerator–driven pulsed sources that provided greater neutron fluxes. Figure 3.1 shows the history of the development of neutron sources, which includes—not exclusively—low-energy charged-particle sources, fission reactors, and spallation sources.

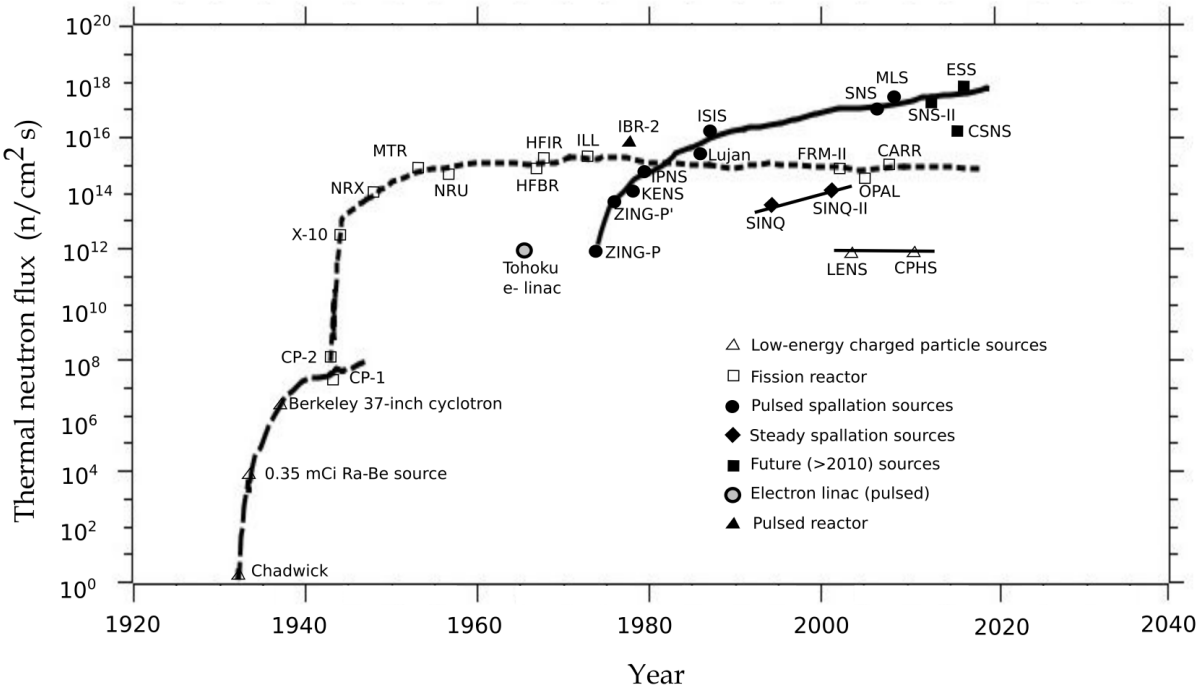

Figure 3.1 History of development of neutron sources, updated from [3]. The effective thermal neutron flux is shown to highlight the utilization of these sources for materials research.

3.1.1 Reactors

The pioneering work dates back to Enrico Fermi and to his discovery, in October 1934, of the "slowing down of neutrons". In this experiment, performed using the water of the goldfish fountain located at the Institute of Physics in Rome, Enrico Fermi established for the first time, in the afternoon of 22 October 1934, the crucial role of hydrogenous substances on neutron induced radioactivity, thus paving the way for the use of slow neutrons in nuclear fission chain reactions [4]. Fermi's Nobel Prize in 1938 acknowledged his seminal work. Eight years later, on 2 December 1942, scientists under the leadership of Fermi successfully demonstrated the artificial self-sustaining nuclear chain reaction, as witnessed by the criticality of the world's first nuclear reactor, the Chicago Pile One (CP-1) [5] . In the early years, the principal sources of neutron beams were the first nuclear reactors pursued in the course of developments for the atomic bomb. Researchers were mostly physicists investigating, on the side, what kinds of measurements would be possible [6]. Soon, scientists began to apply neutron scattering methods to probe the properties of materials rather than just characterizing the nuclear interactions. Subsequent work by Enrico Fermi, Walter Zinn, Ernest Wollan, Clifford Shull, and Bertram Brockhouse took place at reactors built in the 1940s and 1950s. The early reactors also contributed to the important development of instrumentation, in parallel with technical discoveries. Ever more powerful research reactors evolved until the late 1960s when reactor technology reached engineering heat transfer limits. The available thermal neutron flux stabilized at around 10^{15} n/cm^2•s, as it became difficult and costly to achieve even modest increases in neutron flux. The 1994 Nobel Prize in Physics was awarded to Clifford Shull and Bertram Brockhouse in recognition of their early work. Meanwhile, a great deal of effort was placed on making more efficient use of the existing neutron fluxes. Instruments and techniques were invented that enabled a greater variety and precision of measurements and a broader range of scientific investigations.

Those developments continue to this day, carried out at small reactors as well as the largest, flagship facilities. A milestone in this regard was the establishment of the Institut Laue-Langevin (ILL) in Grenoble, France in conjunction with the advent of the High Flux Reactor (HFR) in 1972. The ILL remains to this day a premier resource for neutron beam research. Cryogenic (for example liquid hydrogen) moderators that shift the neutron spectrum to greater-than-thermal-neutron wavelengths were developed in the 1960s at the research reactors at Harwell, UK. The ILL reactor, equipped with two cryogenic moderators (20 K liquid D_2) and neutron guides, permits effective delivery of cold neutrons outside the reactor confinement building so as to accommodate a large number of instruments at the guide halls. Nowadays, widespread use of neutron guides has increased significantly the capacity of cold-neutron utilization and the variety of instruments available to the scientific community. Similarly, a hot source of 2000°C graphite extended the spectrum of useful neutrons to shorter-than-thermal wavelengths. Over the years older, less powerful reactors have retired to make room for new, highly optimized reactors to fulfill demands for better-performance facilities. The small sources, by virtue of their moderate fluxes and flexible beamline configuration, have been the powerhouses for development of neutronic and scattering hardware and the classrooms for inculcation of users and technical personnel to feed large facilities. On the other side of the coin, closing down small facilities will significantly curtail the opportunities for research of instrumentation and methodology, for validation of moderator designs, for evaluation of instrument components such as neutron polarizers and detectors, for conducting experiments that are not neutron-flux limited, and for training of young scientists and engineers.

Figure 3.1 shows that the neutron yield from fission reactors has reached a maximum in the 1960s owing to the onerous requirement of heat removal – about 180 MeV of energy per neutron produced from the reactor core. This technical challenge in conjunction with the concern of proliferation of nuclear substances implies that all future sources will be accelerator-driven.

3.1.2 Accelerator-driven Neutron Sources

Early work at accelerator-driven sources was based on cyclotrons and pulsed electron-linac–driven bremsstrahlung photoneutron sources. In these sources the gamma rays produced in the bremsstrahlung process go on the produce neutrons by photoneutron reactions. The e-linac-driven sources soon reached a power limit of about 50 kW, imposed by heat transfer engineering constraints on target design which is subjected to about 2000-MeV heating per neutron production. The bremsstrahlung photoneutron sources also produced high-energy gamma ray backgrounds that can be problematic for many neutron scattering applications. Starting in the early 1970s as proton beam power exceeded the 100-MeV energy level, accelerator-driven spallation neutron sources have since come to the fore. Spallation is the process induced by high-energy particles delivered by accelerators (around GeV protons) striking nuclei in a massive target, which promptly emits neutrons (and other radiation) to cool off. A spallation reaction produces several orders of magnitude less heat (about 30 MeV per neutron) to be dissipated than the bremsstrahlung photonuclear reaction and about one-tenth as much heat as fission. Pulsed operation, the natural mode of most accelerator types – "on" and producing neutrons and heat during only a small fraction of the time and "off" the remainder of the time – alleviates the heat load averaged over time yet the instantaneous power and neutron flux are very high. All accelerator-driven sources require appropriate moderators to surround the target for neutron slowing down to energies of the thermal- and cold neutron regime. Typically, for neutron scattering applications, moderators contain high-hydrogen density substances, such as liquid hydrogen, water, or sold hydrocarbons, cryogenically cooled if necessary, since the light molecular masses and the ample energy levels corresponding to the degrees of freedom of molecular motion in these media allow effective energy transfer during the neutron slowing-down processes. The centroid of the neutron energy spectrum depends to a certain extent on the temperature of the moderator owing to the Maxwell distribution of kinetic energies although there is always a residual component of epithermal neutrons that are under moderated. Furthermore, the neutron pulse width can be

modified to suit experimental requirements by tailored moderator-reflector configurations or by application of poisoning neutron absorbers such as cadmium. The pulses from accelerator-driven short-pulse spallation sources (SPSSs) are short enough to differentiate the neutron flight times of events corresponding to most resolution requirements. Pulses from long-pulse spallation sources (LPSSs) are typically too long for most TOF instruments without the use of additional pulse shaping, but the duty-cycle heat transfer advantage remains.

The established achievements of pulsed-source instruments across the board attest to the versatility and potentiality of accelerator-driven neutron sources combined with employment of state-of-the-art beam transport, optics, sample environment, and detector systems. [6]

Today's high-power SPSSs include the MW-level sources, *i.e.*, the Spallation Neutron Source (SNS) in the US and the Japan Spallation Neutron Source (JSNS of J-PARC), and the sub-MW-level sources, *i.e.*, the ISIS at UK. Additionally, a MW-level steady-state spallation source, SINQ, has been in operation for twenty years in Switzerland. A new LPSS, the European Spallation Source (ESS), is currently under construction in Sweden.

However, as mentioned earlier, these flagship facilities cannot carry out the role of training and experimental testing that small fission reactors had assumed until now yet are uncertain about future operation. Hence, we see a plethora of new small or compact accelerator-driven sources being developed across the world. Given the flexibility in design, these sources are quite diverse: differing in accelerator systems, neutron-production reactions, targets-moderator designs, and emphases in application.

3.2 Production Reactions

3.2.1 Fission

Fission reactor sources rely on a neutron-propagated chain reaction in the fuel (usually ^{235}U or ^{239}Pu). In addition to a net yield of about one neutron, each fission—an exothermic process—splits the nucleus into two highly excited fragments of roughly equal mass, these fission products deposit ~180 MeV of energy in terms of heat along with β and γ radiation and neutrinos. Most of the neutrons emerge promptly from the excited fission fragment nuclei. A small fraction (~1%) of neutrons emerges seconds or minutes after the fission event. These so-called delayed neutrons arise from delayed decay (usually beta-decay) of certain groups of fission products.Fission fragments remain radioactive for a long time.

3.2.2 Spallation

Spallation is an endothermic process caused, for example, by protons in heavy nuclei, requiring a threshold energy of ~100 MeV. Figure 3.2 shows the neutron yield for protons of different energies and different target materials, from Fraser et al.[3]

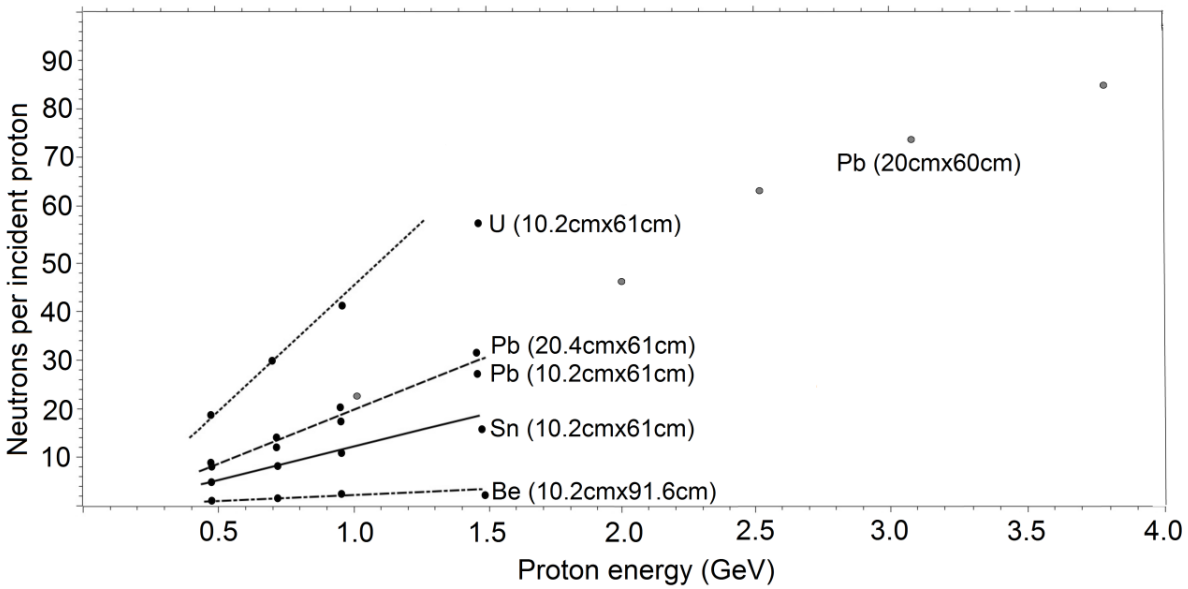

Figure 3.2. Thick-target yields of neutrons as a function of incident proton energy and target material. [7, 8]

A function that reasonably well correlates the Fraser data is

$$Y(E,A)=\begin{cases} 0.1(E_{GeV}-0.120)(A+20) \text{ except for fissionable materials} \\ 50(E_{GeV}-0.120) \text{ for } {}^{238}U \end{cases} \tag{3.1}$$

The yield is approximately a linear function of the mass number, A, of the target material; and up to 1 GeV, the neutron yield is a linear function of the incident particle energy. For higher energies, the yield falls off from the linear relationship because of the production and subsequent nonproductive decay of π_0 particles into pairs of 70-MeV photons. Hence, above 1 GeV, the yield can be represented as approximately $E^{0.8}$. [9] A yield proportional to proton energy implies a constant neutron production rate per unit of time-averaged proton beam power, independent of the proton energy. For example, a 1-GeV proton on tungsten (A=184) produces 18 neutrons and deposits ~30 MeV of heat per neutron, which is, significantly, less than the counterpart for neutrons from fission. This heat is a significant engineering concern. Residual nuclei, either from the spallation products or from neutron-activated target material, decay slowly, releasing heat long after the end of irradiation, which must be embodied in the safeguard of operation, e.g., the loss-of-coolant scenario.

Spallation involves first the intranuclear cascade of high-energy p, n, and pions, which in turn causes an external cascade of n, p, d, t, α, β, γ, pions, muons, and neutrinos via a variety of nuclear reactions. As a result, the residual debris includes a large component of nuclei somewhat lighter than the original nuclei of the target and a smaller component of fission products and light nuclei. Beta-delayed decay of certain light spallation products, for example ^{8}He, ^{9}He, and ^{11}Li, leads to delayed emission of neutrons. Delayed neutrons are, at least approximately, monoenergetic (100s of keV) because they come from neutron decay of specific excited nuclear states.

High-energy gamma rays from beta-delayed spallation products and target-nucleus activation produce delayed neutrons in (γ, n) interactions with ^{2}H and Be in the surroundings. Delayed neutrons, although relatively small in number and emerging at nearly a constant rate between accelerator pulses, can constitute an important background in TOF applications. Figure 3.3 illustrates the spallation process.

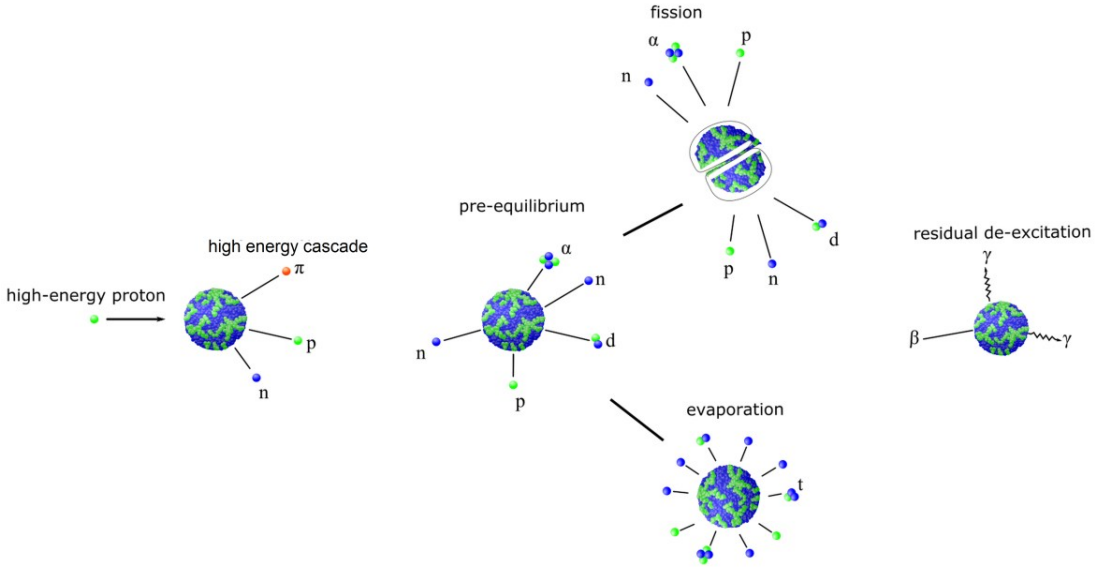

Figure 3.3 Schematic illustration of the spallation process. The initial impact gives rise to high energy cascades within the nucleus and the emission of particles with energies close to the incident energy. Later production processes including pre-equilibrium, fission, evaporation lead to lower energy particles and daughter nuclei. Refer to Fig 2.1 for the typical energy spectra of these processes.

Neutrons from fission and from spallation have similar spectra, since both arise from evaporation of neutrons from excited nuclei. Figure 3.4 shows the evaporation spectrum of neutrons born from the source nuclei. The function is

$$f(E) \propto \sqrt{E}\exp(-0.775E), \tag{3.2}$$

for which the mean energy is approximately 2.0 MeV. More generally,

$$f(E) = a\exp\left(-E/b\right)\sinh\left(\sqrt{cE}\right), \tag{3.3}$$

in which b and c depend on the evaporating nucleus, but the mean energy is always around 2 MeV.

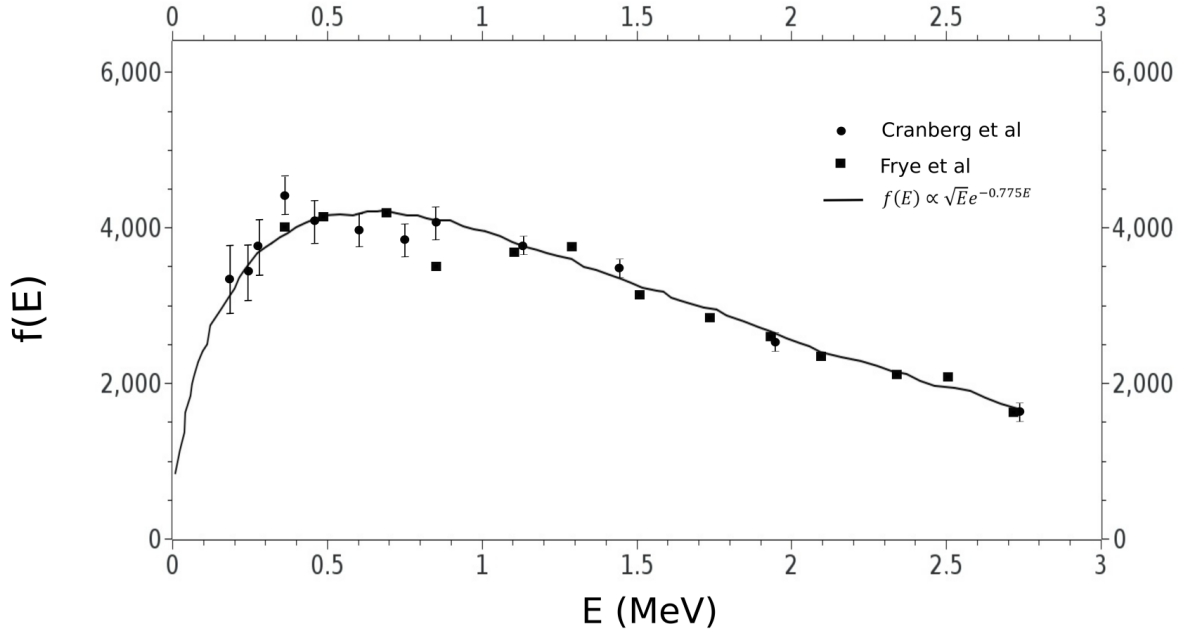

Figure 3.4 The spectrum of neutrons evaporating promptly from fission fragments. (Cranberg et al., and Frye et al [10])

Most of the spallation neutrons appear in the evaporation spectrum. But a few (~2%) are cascade neutrons, distributed with energies up to the incident proton energy and traveling in forward directions. These few neutrons, above ~100 MeV, demand much more massive shielding than is required for reactor sources.

3.2.3 Fusion

Two commonly used fusion reactions are $d + d \rightarrow n + {}^{3}He + 3.26$ MeV and $d + t \rightarrow n + {}^{4}He + 17.6$ MeV. The threshold for the (d, t) reaction is lower than that for the (d, d). In low-energy accelerator sources, the target nuclei, d, or t, are usually incorporated in a solid matrix as TiD_x or TiT_x. In particular, the (d, t) reaction which has been under testing at the JET [11] and Tokamak Fusion Test Reactor (TFTR) [12] is the most likely candidate reaction for future fusion power plants.

The fusion reactions mentioned are well understood and are now commonly used in small compact neutron generators that are commercially available. The neutron yield in general is low, but these devices are small, inexpensive, and easily deployed for a number of applications.

Table 3.1 shows the major characteristics of products of several reactions.

Table 3.1 Neutron production from high power nuclear reactions

Reactions (examples)	**Neutron yield (net) and energy distribution**	**Heat release (MeV)**	**Residual products and radiation**
Thermal fission (^{235}U or ^{239}Pu)	~1 n/fission Maximum ~0.8, mean ~2 MeV, extending to ~10 MeV	~200 exothermic	Fission products; β, γ, neutrinos

Spallation (~1GeV p on mercury target)	25-30 n/p Peak at ~2 MeV extending to near the incident proton energy	30 MeV/n (W target) Endothermic, heat deposited on target vessel by incident protons	Spallation and fission products; p, d, t, α, β, γ, pions, muons, neutrinos
Fusion	14. MeV neutrons 2.4 MeV neutrons	2.7 MeV heat 0.8 MeV heat	α and ^{3}He of very short range

Neutron production from spallation and fission involves energetic protons or neutrons traversing the target or the fuel elements over a mean free path as large as many centimeters, hence limiting the brightness of the source. Inertial fusion employs a small (millimeter size) *d-t* pellet that can be ignited in principle by a high-power laser beam. Recently, Taylor *et al*. [13] suggested a super-high-flux neutron source based on laser-ignited inertial fusion. A single target is a pellet of d-t mixture, which, upon ignition, sustains the fusion reaction $\mathrm{d}+\mathrm{t}\rightarrow\alpha(3.5\mathrm{MeV})+\mathrm{n}(14.1\mathrm{MeV})$. However, the fluxes of very high power-density α particles will impose severe problems in heat removal and radiation damage to reactor components that are unsolved by present-day technology. A tritium resupply cycle needs also to be worked out. Laser-ignited inertial fusion is included in Table 3.1 as an option among high-power neutron sources for the future.

3.2.4 Neutron production by nuclear reactions driven by low-energy charged particles

At energies below ~50 MeV, the de Broglie wavelength of the proton or deuteron is comparable to the size of a nucleus (~10^{-13} cm), so the particle-nucleus reaction can be considered as occurring through only one or two reaction channels. Although our knowledge of nuclear structures is not sufficiently complete to predict accurately the state wave functions of the compound nucleus and the transition probability of the reaction channels, experiments have been carried out to measure the cross sections of many low-energy nuclear reactions. Figures 3.5 and 3.6 show the estimated global neutron yields from measured cross sections of various target materials over two different energy ranges of incident particles. The neutron yield and cross sections of a number of (p, n), (d, n), (t, n), and (α, n) reactions, listed in Table 3.2, were evaluated by Drosg [14]. In general the targets are light elements, and the neutron yields from low-energy charged particles are smaller than those from spallation and fission by several orders of magnitude. Yet the density of heat deposited in the target is large because of the very short range of low-energy charged particles in a solid target. Thus care must be taken for the (often windowless) entrance of the incident beam and for the protection of the target against damage by heat deposition, radiation shock, and accumulation of gaseous hydrogen at the end of the range of charged particles in the target material. For example, the damage caused by the end-of-range stopping, evidenced by the well-known “Bragg peak” (not the diffraction peak), of incident protons in beryllium metal is well documented [15] . A few at. % of hydrogen accumulation causes the metal to disintegrate.

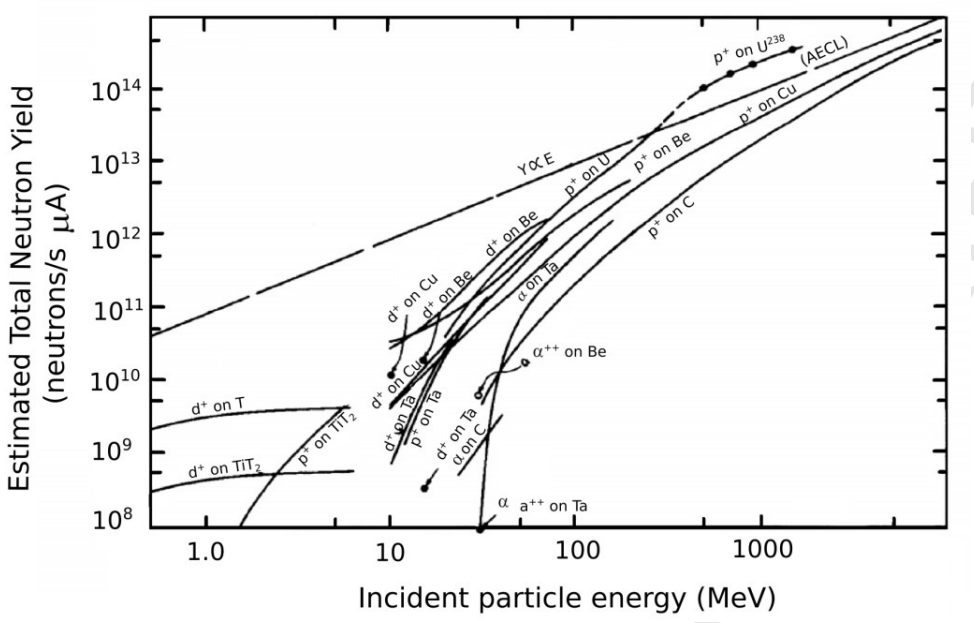

Figure 3.5 Estimated global neutron yields from nuclear reactions of particles incident on thick targets of various materials. [16, 17]

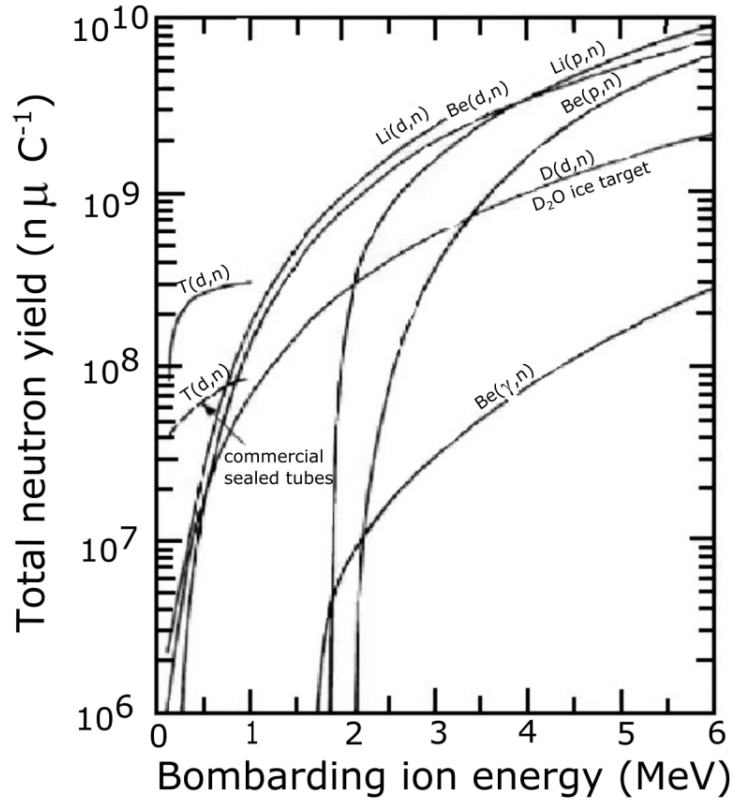

Figure 3.6 Estimated global neutron yield from low-energy nuclear reactions. [18]

Table 3.2 The neutron-producing reactions considered by [14] as candidates for monoenergetic neutron sources

Reaction types	Examples
(p,n)	^{3}H(p,n)^{3}He, ^{6}Li(p,n)^{6}Be, ^{7}Li(p,n)^{7}Be, ^{9}Be(p,n)^{9}B, ^{10}Be(p,n)^{10}B, ^{10}B(p,n)^{10}C, ^{11}B(p,n)^{11}C, ^{12}C(p,n)^{12}N, ^{13}C(p,n)^{13}N, ^{14}C(p,n)^{14}N, ^{15}N(p,n)^{15}O, ^{18}O(p,n)^{18}F, ^{36}Cl(p,n)^{36}Ar, ^{39}Ar(p,n)^{39}K, ^{59}Co(p,n)^{59}Ni
(d,n)	^{2}H(d,n)^{3}He, ^{3}H(d,n)^{4}He, ^{7}Li(d,n)^{8}Be, ^{9}Be(d,n)^{10}B, ^{11}B(d,n)^{12}C, ^{13}C(d,n)^{14}N, ^{1}4N(d,n)^{15}O, ^{15}N(d,n)^{16}O, ^{18}O(d,n)^{19}F, ^{20}Ne(d,n)^{21}Na, ^{24}Mg(d,n)^{25}Al, ^{28}Si(d,n)^{29}P, ^{32}S(d,n)^{33}Cl
(t,n)	^{1}H(t,n)^{3}He
(α,n)	^{3}H(α,n)^{6}Li, ^{7}Li(α,n)^{10}B, ^{11}B(α,n)^{14}N, ^{13}C(α,n)^{16}O, ^{22}Ne(α,n)^{25}Mg

3.2.5 Photonuclear reactions

Neutron production based on the photonuclear reaction from electron bremsstrahlung has played an important role in the development of accelerator-driven sources (see Figure 3.7). Energetic electrons striking high-mass targets slow down to emit bremsstrahlung (e,γ) photons. Photons proceed to interact with target nuclei to produce (γ,n) photoneutrons. Figure 3.7 shows the global neutron yields, the number of neutrons of all energies in all directions per unit of electron beam energy, as functions of electron energy for a range of materials.[19] Heavy elements are clearly best as bremsstrahlung photoneutron sources and yield plateaus at high electron energies.

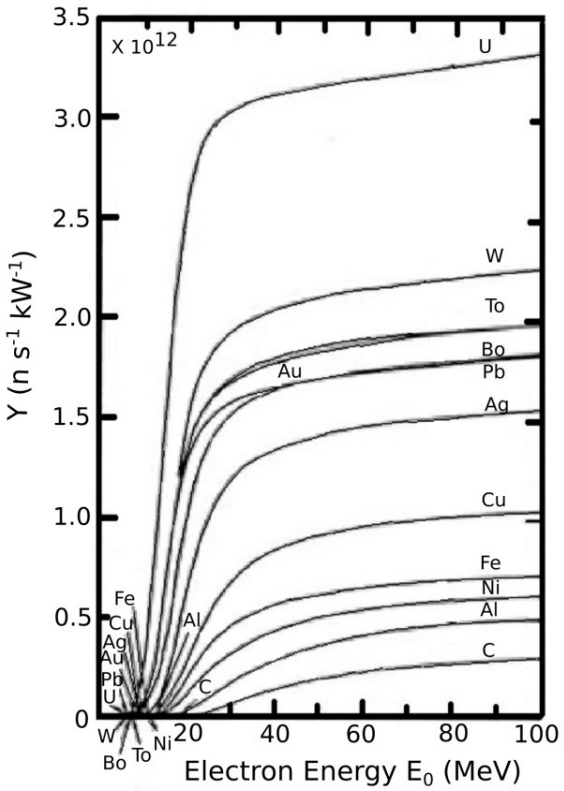

Figure 3.7 Global yield of bremsstrahlung photoneutrons as a function of electron energy for different targets. [19]

Most of the neutrons are emitted in an evaporation spectrum according to

$$N(E) \propto \sqrt{E}\exp(-E/T) \tag{3.4}$$

with $T \approx$1-2 MeV. Most of the electron energy dissipates as heat, which must be removed from the target; consequently the process is rather inefficient. The yield saturates for electron energies above ~100 MeV,

$$Y(E \geq 100 \text{ MeV}) = 2.35\times10^{12} \text{ n/sec/kW} = 2.35 \times10^{9} \text{ n/joule} \tag{3.5}$$

for tungsten (W). This amounts to 2,800 MeV of heat per useful neutron.

In practice, target heat transfer limitations constrain power on targets a few cm in diameter to about 50 kW. More power would melt even refractory metals like tungsten, as in electron-beam welding.

Recently being recognized as a prospective neutron source is photonuclear neutron production based on gamma rays arising from inverse Compton scattering (ICS). ICS is the process in which a relativistic electron collides more or less head-on with a laser photon, whereby the photon gains a significant fraction of the electron kinetic energy. The process can produce photons in the gamma-ray range for electrons of ~GeV energy. For example, a 0.06-J, 1-μm-wavelength laser pulse colliding with a 2×10^9 bunch of 875 MeV electrons could produce 3×10^7 photons of 14-MeV energy. [20] Such energetic γ rays, exciting heavy nuclei through the giant dipole reaction, lead to substantial production of evaporation (~1-MeV) neutrons. The process is about ten times more efficient than bremsstrahlung photoneutron production because it avoids the intermediate, inefficient step of bremsstrahlung radiation and consequent target heating. A 1-kW beam of 15-MeV photons incident on a small tantalum target would produce about 10^{13} neutrons [21].

Table 3.3 Neutron production from low-energy nuclear reactions. Typical values are tabulated though exact values will depend on the incident particle energies and targets.

Reaction types	**Examples**	**Neutron yield per event**	**Heat deposit (MeV)**	**Residual products and radiation**
(p/d, xn)	^{7}Li(p,n)^{7}Be ^{9}Be(p,n)^{9}B ^{9}Be(d,n)^{10}B	~10^{-3} – 10^{-2} n/p or n/d	~3,000	Mostly γ, possibly *t* and accumulation of hydrogen
Fusion	^{2}H(d,n)^{3}He ^{3}H(d,n)^{4}He	~10^{-5} n/d	>3,000	Mainly γ
Photonuclear	35 MeV e$^-$ on a W target	~10^{-2} n/e	~2,000	Mainly γ
Tabletop laser–driven	All of above	Above combined	?	Much debris

Table 3.3 lists the key characteristics of nuclear reactions driven by low-energy charged particles. Here, we include neutron production driven by very high-power (>10^{18} W cm^{-2}) tabletop lasers. This research began in the 1990s with studies of the motions of electrons subjected to a very high electric field of the order of GV/m sustained by relativistic plasma waves driven by lasers. The conditions in terms of the

laser power and pulse length, target setup, and so on were subsequently formulated to achieve acceleration of intense, quasi-monoenergetic "hot" electrons that are capable of triggering photonuclear reactions in a solid target for neutron production. These conditions were further extended to apply for the generation and acceleration of other charged particles, such as *p* and *d*, hence the prospect for inducing low-energy neutron-producing nuclear reactions. A number of experiments have been reported to successfully demonstrate these capabilities. The obvious merits of these tabletop laser–driven neutron sources are the achievable compact size, the very short neutron pulses, and the concentrated neutron intensity in the forward direction. However, the practice of harvesting the useful neutrons within the complex emission background and the conditioning of the target for sustained operation has yet to be worked out. [22, 23]

4. Compact Accelerator-driven Neutron Sources

In the 1970s, the ZING-P prototype pulsed spallation source at ANL (sub-microampere 200 MeV protons) verified the principles and performance estimates of pulsed spallation neutron sources, including synchrotron injection by negative hydrogen ion stripping; the effectiveness of decoupled beryllium reflectors; and the effectiveness of time-focused pulsed-source diffractometers and crystal analyzer spectrometers. The results of most of these tests and demonstrations are now standard components of all of the large accelerator-driven neutron sources. IPNS (ANL, 7 kW) and KENS (KEK, 5 kW) have been shut down and the Lujan Center (LANS, 80 kW), is still working at significantly reduced operation, giving way to larger, higher-power facilities including ISIS (UK, 160 kW), JSNS, and SNS. Each of the smaller facilities operated for about 25 years as national-scale capabilities serving many research applications and serving also as prototypes for larger installations and as centers where new techniques, instruments, and source components evolved, enabling the development of the megawatt sources. They were big enough to support significant scientific research, yet not so large as to preclude experimentation on sources, techniques, and components. They are currently being replaced by a very diverse suite of CANS, each with a wide range of applications. The CANS are all designed to run at power levels of less than 100 kW with user programs tailored to specialized or multipurpose applications. The following subsections describe the missions, major components, and current status—operational or under development—of the CANS facilities. We obtained this information by contacting the facilities' managing staffs or through perusal of the literature. The design parameters of each facility are given in a table, and the layout of its source and beam lines are illustrated in schematic drawings or photographs. Table 4.1 lists the CANS that are covered in this paper.

Table 4.1: Accelerator-driven neutron sources, mostly CANS: in operation and under development

Name	Country	Accelerator type/reaction type	Status
Bariloche Linac	Argentina	Electron linac	Operational since 1969
CPHS—Compact Pulsed Hadron Source of Tsinghua University	P. R. China	Proton linac	Operational since 2013
CYRIC: Quasi-monoenergetic neutron beam facility at CYRIC	Japan	Azimuthal varying field cyclotron	Operational since 2004
FNG: the Frascati Neutron Generator	Italy	Deuteron electrostatic accelerator	Operational
Gaerttner linear accelerator at Rensselaer Polytechnic Institute	USA	Electron linac	Operational
GELINA: Geel Electron Linear Accelerator Facility	Belgium	Electron linac	Operational
HUNS: the Hokkaido University Neutron Source	Japan	Electron linac	Operational since 1974
iThemba	South Africa	Proton cyclotron	Operational
KOMAC-NST, KIRAMS-MC-50, and PAL-PNF	Korea	Tandem accelerator, cyclotron, electron linac	Operational since 2000
KUANS: Kyoto University Accelerator-driven Neutron Source	Japan	Proton radio frequency quadrupole (RFQ)	Operational
KURRI-LINAC: Kyoto University Research Reactor Institute, Electron Linear Accelerator	Japan	Electron linac	Operational
LENS: the Low-Energy Neutron Source	USA	Proton RFQ + 2 linacs	Operational since 2005
PKUNIFTY	P. R. China	RFQ linac	Operational
RANS: RIKEN Accelerator-driven Neutron Source	Japan	Proton RFQ+ linac	Operational since 2013
TSL neutron facility	Sweden	Proton and H_2^+ cyclotron	Operational
ESS Bilbao Project	Spain	Proton linac	Under study or ongoing development
FRANZ: Frankfurt Neutron Source at the Stern-Gerlach-Zentrum	Germany	Proton linac	Under study or ongoing development

LENOS: Legnaro Neutron Source	Italy	Proton RFQ	Under study or ongoing development
n@BTF-The Frascati electron-driven source	Italy	Electron linac	Under upgrade
nELBE: Time-of-flight facility at the Helmholtz-Zentrum Dresden-Rossendorf (HZDR)	Germany	Superconducting electron accelerator	Under study or ongoing development
NEPIR facility at the SPES source of Laboratori Nazionali di Legnaro	Italy	Proton cyclotron	Under construction
NUANS: Nagoya University Accelerator-driven Neutron Source	Japan	DC accelerator (dynamitron)	Under construction
UTCANS—University of Tokyo	Japan	Electron linac	Under study or ongoing development
Van de Graaff facility at the Institute for Reference Materials and Measurements (IRMM)	Belgium	Tandem	Under study or ongoing development

4.1 CANS in Operation: Status and Future Trends

4.1.1 Bariloche Electron-linac-driven Neutron Source

The Neutron Physics group at Centro Atómico Bariloche (CNEA, Argentina) operates a small 25 MeV linear electron accelerator, the Bariloche Linac, dedicated to the use and development of neutron methods to tackle problems of basic science and technological applications. Historically the facility has been used to determine the total cross sections of materials as a function of neutron energy by means of transmission experiments for thermal and sub-thermal neutrons. This technique is at present exploited for its sensitivity to the structure and dynamics of condensed matter over distances ranging from the "first-neighbor scale" up to the microstructural level or "grain scale." It also allowed testing of theoretical models for the generation of scattering kernels and cross sections. Through the years, research activities moved from classic pulsed neutron diffraction, which included the development of high-precision methods for determining very low hydrogen content in metals, toward deep inelastic neutron scattering (DINS), a powerful tool for determining atomic momentum distribution in condensed matter and for nondestructive mass spectroscopy. [24] More recently, nonintrusive techniques aimed at the scanning of large cargo containers have started to be developed with the Bariloche Linac CANS, testing the capacity and limitations with regard to detecting special nuclear material and dangerous substances in thick cargo arrangements. Also, the ever-present bremsstrahlung radiation has been recognized and tested as a useful complement to instrumental neutron activation, as it permits detection of other nuclear species through high-energy photon activation.

The facility is also used for graduate and undergraduate students' experimental work within the frame of Instituto Balseiro Physics and Nuclear Engineering courses of study and MSc and PhD thesis program. At present, the accelerator is out of operation and a replacement of the injector power supply to provide higher beam power on the target is under way.

Table 4.1.1 Parameters of the Bariloche electron-linac–driven neutron source

Electron linac	Target station	Major activities
25 MeV, 25–30 μA Short pulse, width 1.4 μs up to 100 Hz	Lead target, water cooled ~6×10^{11} n/s	Total cross section measurements Diffraction, deep inelastic neutron scattering Device/moderator research and development Education

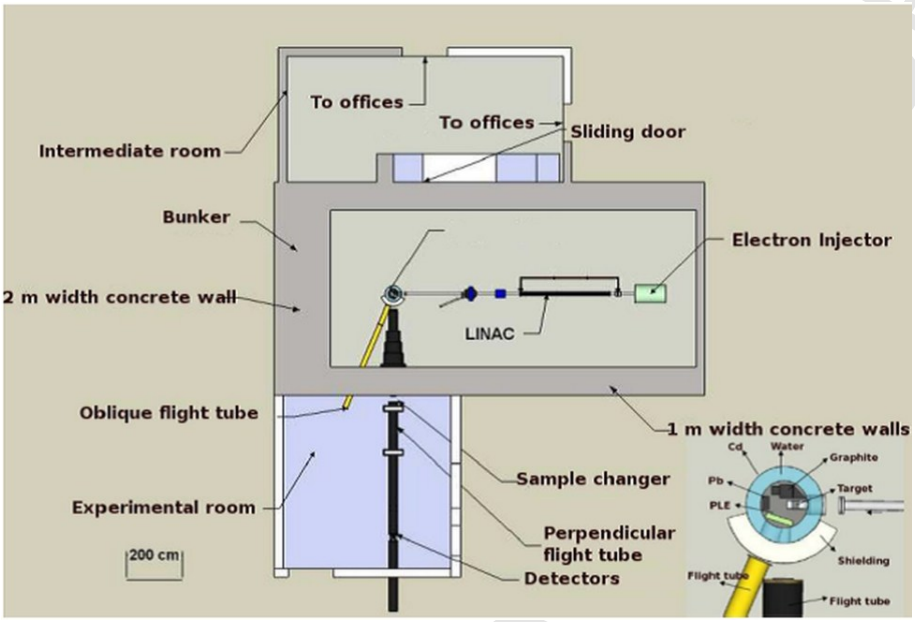

Figure 4.1.1 Layout of the e-LINAC, its bunker, and the neutron extraction tubes.

4.1.2 The Compact Pulsed Hadron Source of Tsinghua University

The Compact Pulsed Hadron Source (CPHS), located at Tsinghua University (Beijing), is the first multipurpose pulsed neutron source in China. It aims to attain a neutron yield of ~10^{13} n/s in the energy range from cold to epithermal for education, instrumentation development, and industrial applications. [25] Since July 2013, a 3-MeV proton beam has been delivered to the beryllium target, and two beam lines are in operation with a room-temperature moderator for neutron detector R&D and neutron imaging. Construction of a drift tube linac for an upgrade of the proton energy to 13 MeV is under way.

Table 4.1.2 Parameters of the Compact Pulsed Hadron Source of Tsinghua University

Proton linac	Target station	Major activities
3 MeV (initial) 13 MeV (final), 16 kW 50 mA (peak), 1.25 mA (average) Long pulse, width 0.5 ms, 50 Hz	Be (p, n) PE (initial), solid methane (final) ~5×10^{13} n/s	Imaging, small-angle neutron scattering Detector/device R&D Education

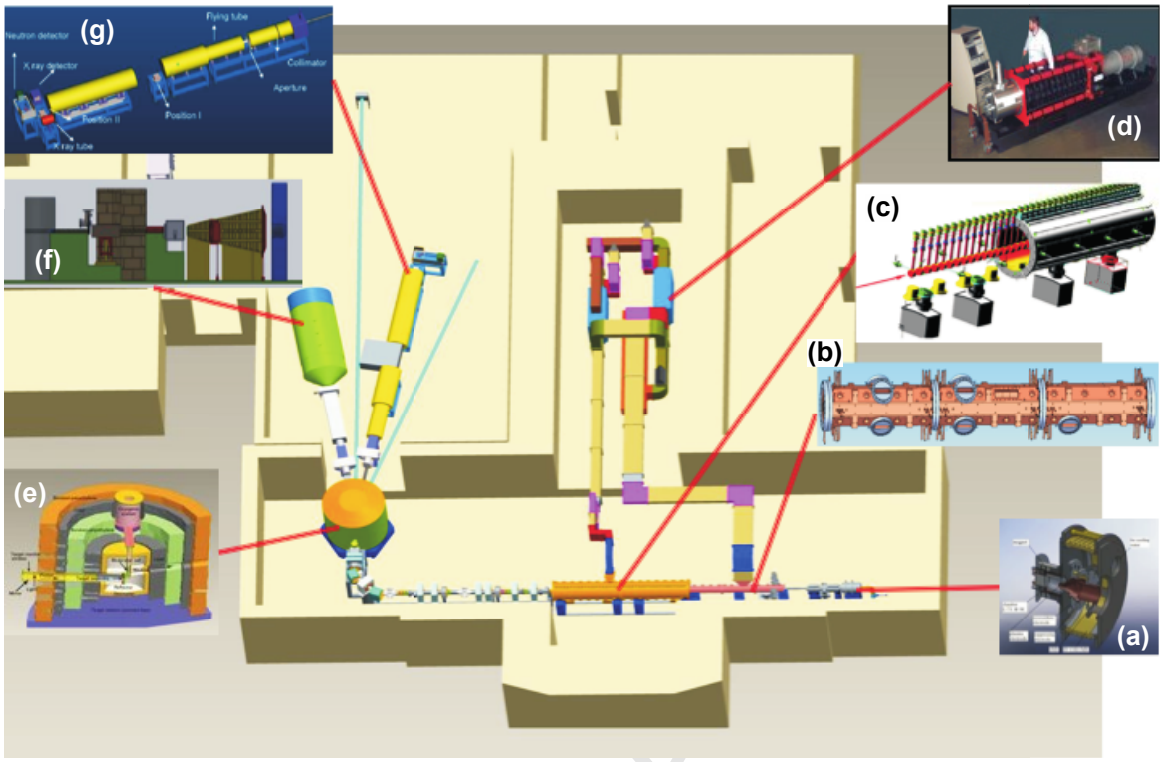

Figure 4.1.2 A schematic layout of the CPHS neutron source. (a) Ion source, (b) radio frequency quadrupole, (c) drift tube linac, (d) radio frequency power, (e) target station, (f) small-angle neutron scattering beam line, (g) imaging beam line.

4.1.3 The quasi-monoenergetic neutron beam facility at CYRIC

A high-intensity fast neutron beam facility was located downstream from a straight proton beam line of the 110-MeV azimuthal varying field cyclotron at CYRIC (Cyclotron and Radioisotope Center) [26], which has been in operation at the Tohoku University in Japan since 2004. [27] The proton beam used for neutron production has a selectable energy ranging from 14 to 80 MeV. The facility is mainly used for cross section measurements for nuclear physics, testing of semiconductors for single-event effects, and dosimetry development. Figure 4.1.3 shows the schematic view of the neutron source. The quasi-monoenergetic neutron beam is produced using the ^{7}Li(p,n)^{7}Be reaction. The primary proton beam bombards a water-cooled, neutron-producing lithium target. After penetrating the target, the proton beam is bent in the clearing magnet by 25° and stopped in the water-cooled beam dump, which consists of a carbon block shielded by copper and iron blocks.

The typical neutron beam intensity is about 10^{10} n/sr/s/μA with a beam spread of about 5% for the beam energy and ± 2° for the horizontal and vertical directions. The neutron beam is collimated by iron blocks 595 mm thick and of a sufficiently low background at the off-axis position. The available flux of the neutron beam is about 10^{6} n/cm^{2}/s/μA at the sample position, which is located about 1.2 m downstream of the production target. The thermal neutron flux at the sample position is about 2×10^{4} n/cm^{2}/s, which was measured by a method combining foil activation and imaging. At present, this neutron beam is used extensively to study the radiation damage effects on semiconductors and many types of functional materials, such as high-temperature superconducting coils. The design also enables the moderator and target systems to obtain thermal neutrons to study boron neutron capture therapy, and development of neutron imaging is in progress.

Table 4.1.3 Parameters of the quasi-monoenergetic neutron beam facility at CYRIC

Azimuthal varying field cyclotron	**Target station**	**Major activities**
70 MeV, 1 μA < 0.1kW	Li(p, n) 10^6 n/cm^2/sec/μA at 1.2 m downstream from the production target	Radiation damage effects on semiconductors Detector/optics/moderator R&D Education

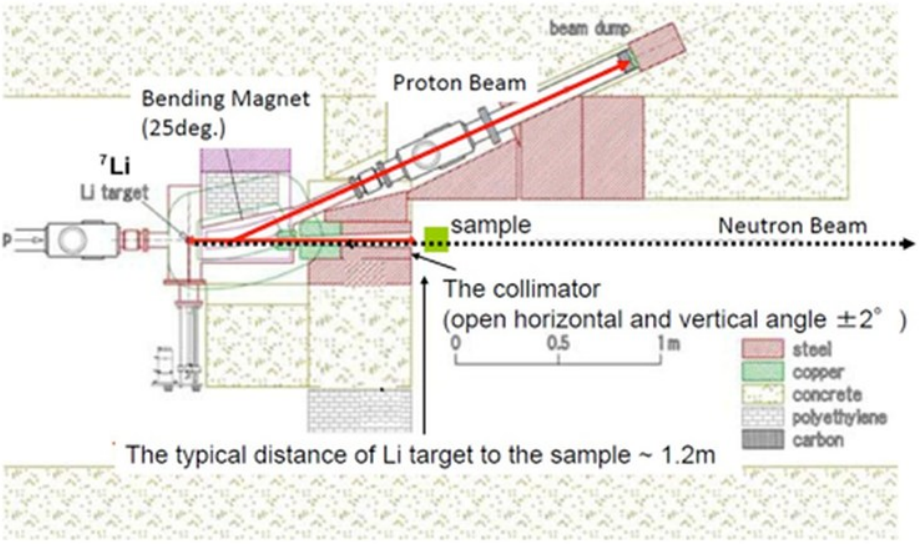

Figure 4.1.3. Schematic layout of the CYRIC neutron facility.

4.1.4 The Frascati Neutron Generator

The Frascati Neutron Generator (FNG) is a linear electrostatic accelerator-driven neutron source in which D^+ ions are accelerated up to about 300 keV at a current of about 1 mA and directed onto a target containing tritium and deuterium, where neutrons are produced by means of fusion reactions. FNG started operation in November 1992 at the ENEA Laboratory (Fusion Division) in Frascati, Italy [28]. It produces a flux of 14-MeV neutrons at a medium intensity (10^{11}n/s) used by the European fusion community for neutronics experiments, database and code improvement, and development of (new) experimental techniques and detectors, as well as benchmarks or mock-up experiments of interest to fusion research. Additional tests are also carried out in chip irradiation for avionics and aerospace, radiobiology, and aging tests of electronics and components for experiments at large-scale accelerators such as those at CERN and Jefferson Laboratory.

Table 4.1.4 Parameters of the FNG

Deuteron electrostatic accelerator	Target station	Major activities
300 keV, 1 mA (average) 300 W continuous	d(d,n) ^{4}He and D(d,n) ^{3}He No moderators 10^{11} n/s (DT) 10^9 n/s (DD)	Radiation effects, nuclear data and codes validation Detector R&D Training and education

Figure 4.1.4: (left) Photo of the FNG; (right) photo of the FNG target.

4.1.5 Gaerttner Linear Accelerator at Rensselaer Polytechnic Institute

The Gaerttner Linear Accelerator (linac) Facility (United States) at the Rensselaer Polytechnic Institute (Troy, NY, USA) [29] began construction in 1958 with funding from the Atomic Energy Commission, and the facility became operational in December 1961. It was designed to produce electrons, x-ray photons, and neutrons, thus serving a large number of research applications involving nuclear engineering, nuclear physics, radiation effects in electronics, nondestructive testing, radiation processing of materials, computed tomography, and other industrial processes. Current areas of research at the linac include reactor physics, photoneutron reactions, assay of used nuclear fuel, neutron cross sections, radiation effects on electronics, and production of medical isotopes. [30, 31] In 1997, the linac was designated as a Nuclear Historic Landmark by the American Nuclear Society. According to the declaration, "This was one of the first laboratories, utilizing a high-power electron linear accelerator that generated accurate nuclear data for the design of safe and efficient nuclear power reactors."

Table 4.1.5 Parameters of the Gaerttner Linear Accelerator at Rensselaer Polytechnic Institute

Electron linac	Target station	Major activities
60 MeV, 8 μA, 12 kW Short pulse, width 5 ns, 400 Hz	Tantalum plates target Evaporation spectrum/ water-graphite moderators 10^{12} n/s	Nuclear data Total and partial cross section measurements Neutron resonance analysis

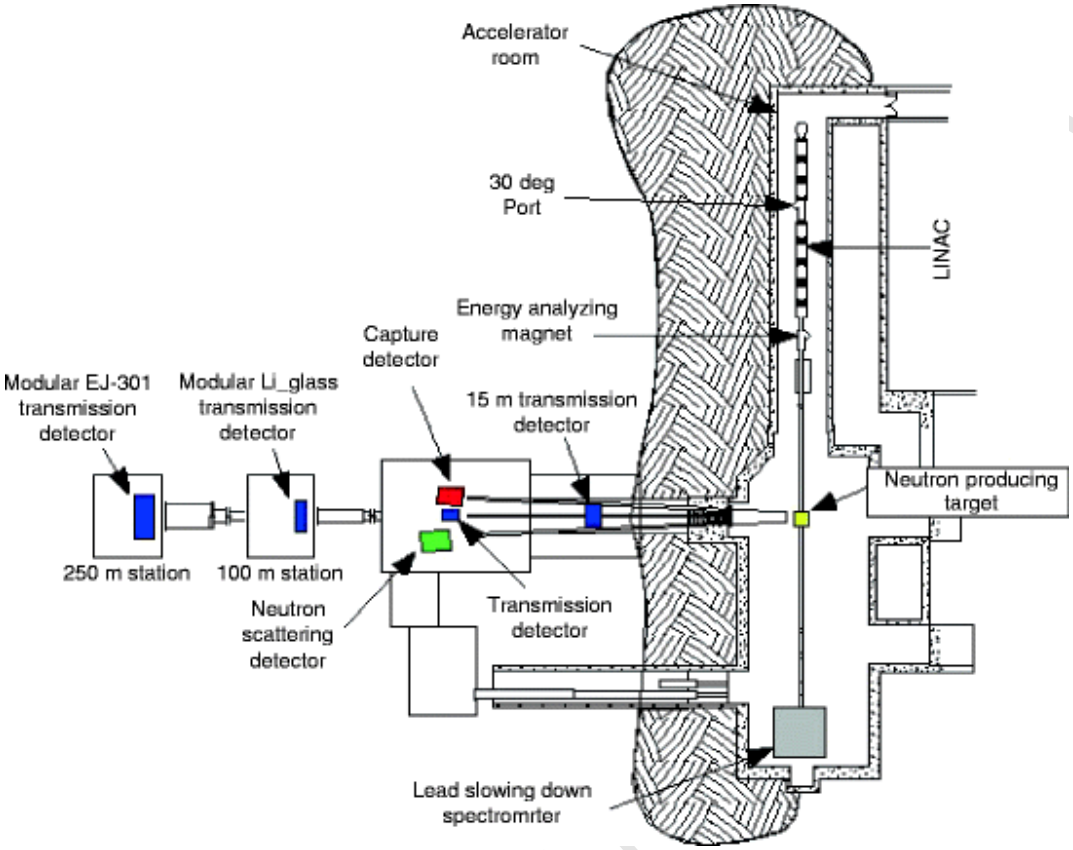

Figure 4.1.5: Schematics of the Gaerttner Linear Accelerator and neutron producing targets at Rensselaer Polytechnic Institute. [32]

4.1.6 GELINA—The Geel Electron Linear Accelerator Facility

The Institute for Reference Materials and Measurements (IRMM) of the Joint Research Centre of the European Commission (EC-JRC), located in Geel, Belgium, is a nuclear research infrastructure dedicated to the measurement of accurate nuclear data for nuclear energy safety [33]. IRMM encompasses a 150-MeV linear electron accelerator (GELINA) with a high-resolution neutron TOF facility and a 7-MV Van de Graaff facility for the production of continuous and pulsed proton, deuteron, and helium ion beams. It serves as a source of well-characterized quasi-monoenergetic neutrons.

GELINA is a white neutron source in which the TOF method is used to determine the energy of the interacting neutrons in the energy range covering 10 decades (10–20 MeV). [34] The facility, shown in Figure 4.1.6a, was designed and built for high-resolution cross section measurements in the resonance region. [35] GELINA is based on a linear electron accelerator producing electron beams with a typical beam operation mode characterized by a 100-MeV average energy, 10-ns pulse length, 800-Hz repetition rate, and 75 μA average current. Using a post-acceleration pulse compression system, the electron pulse width can be reduced to less than 2 ns (full width at half maximum) while preserving the current. [36] The accelerated electrons produce Bremsstrahlung in a uranium target, which in turn, by photonuclear reactions, produces neutrons. Within a 1 ns pulse, a peak neutron production of 4.3×10^{10} neutrons is achieved (average flux of 2.5×10^{13} neutrons/s).

The neutron energy distribution ranges from subthermal to about 20 MeV, with a peak at 1–2 MeV. To provide a significant number of neutrons in the energy range below 100 keV, a hydrogen-rich moderator

is added (Figure 4.1.6b. The energy distribution of the partially moderated neutrons has approximate 1/E energy dependence plus a Maxwellian peak at thermal energy. By using collimators and shadow bars, moderated or unmoderated neutron beams are selected. Further tailoring of the spectral shape is obtained with filters. GELINA serves ten neutron flight paths simultaneously. The flight paths, up to 400 m long, which point radially to the uranium target, lead to experiment stations at distances of 10, 30, 50, 60, 100, 200, 300 and 400 m. These experiment stations are equipped with a wide variety of sophisticated detectors and data acquisition and analysis systems especially designed for neutron-induced cross-section measurements with an exceptional accuracy and energy-resolving power. Modern detection techniques are in use, such as advanced HPGe Compton-suppressed detectors and data acquisition systems based on fast signal digitizers. TOF measurements are possible at GELINA at up to about 10 MeV, or in favorable cases at up to 20 MeV. The facility is operated in shifts on a 24 hour/day basis for about 100 hours per week. [37]

Table 4.1.6 Parameters of GELINA, the Geel Electron Linear Accelerator Facility

Electron linac	**Target station**	**Major activities**
140 MeV, 4.7–75 μA Short pulse, width 1ns, 50-800 Hz	Rotating uranium target Water moderator $1.6\times10^{12} – 2.5\times10^{13}$ n/s	Nuclear data Total and partial cross section measurements Neutron resonance analysis

Figure 4.1.6. (a) Photograph of the time-of-flight facility GELINA of the EC-JRC-IRMM in Geel, Belgium.

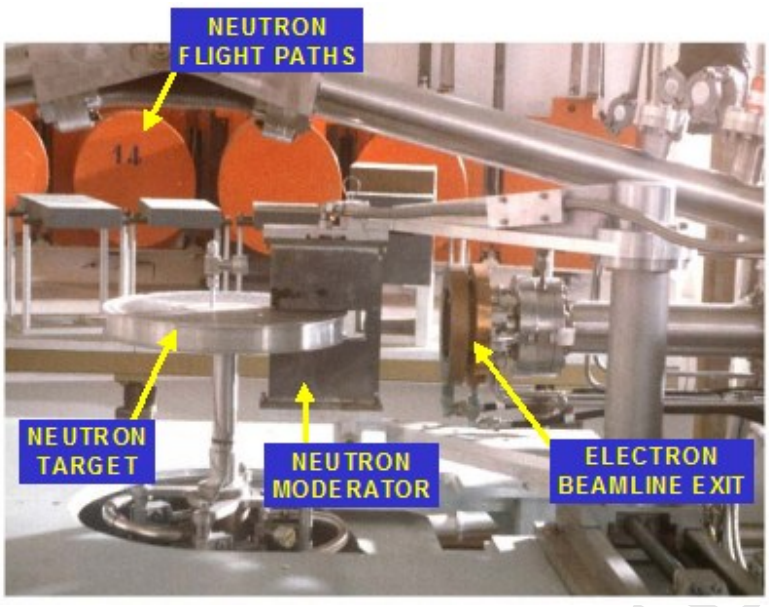

Figure 4.1.6 (b): The neutron target-moderator system at GELINA.

4.1.7 HUNS—The Hokkaido University Neutron Source

HUNS is an accelerator-driven neutron source at Hokkaido University (Japan) [38]. Since starting operation in 1974, HUNS, over a long history, has made steady contributions to the R&D of neutronics. These include the first measurements of cold-neutron spectra of ice, ethane, and solid methane, device evaluation (e.g, scintillation detectors, magnetic lenses), and neutron-scattering instrumentation (e.g., small-angle neutron scattering (SANS), imaging). Recent developments include materials testing with industrial applications. On the nuclear physics side, research interests include nuclear astrophysics (e.g., [γ, n] and [n, γ] reaction rates in p-processes and s-/r processes, respectively) and nuclear data for accelerator-driven systems. The recent development of neutron devices has led to many novel applications. For example, the use of a beam-focusing device enables the setup of a very compact small-angle scattering instrument, i.e., mini-focusing SANS, which has demonstrated the collection of high-quality data. [39]

Table 4.1.7 Parameters of HUNS, the Hokkaido University Neutron Source

Electron linac	Target station	Major activities
35 MeV, 30 μA (50 pps) 1 kW Short pulse, width 10 ns–3μs 50 or 100 Hz	(e, X), (X,n) Water/coupled methane 1.6×10^{12} n/s	Radiation effects, imaging, SANS Detector/device/moderator research and development Education Astrophysics, nuclear transmutation

Figure 4.1 7. The HUNS facility: (left) electron linac, (right) experiment hall.

4.1.8 iThemba in South Africa

Quasi-monoenergetic and white neutron beams with a maximum energy of 200 MeV are produced at the neutron beam facility of the iThemba Laboratory (iTL) in Somerset West, South Africa for accelerator-driven sciences through (p, n) reactions on Li, Be, and C targets. [40] The iTL separated-sector cyclotron can accelerate protons from 25 to 200 MeV. TOF measurements can be carried out by increasing the time separation between proton bunches up to 500 ns with a beam pulse selector. Dosimeter calibrations, irradiation of samples, and cross section measurements can be performed at the iTL neutron facility with reliable monitoring and a neutron beam characterization traceable to Physikalisch-Technische Bundesanstalt standards. The iTL facility has been used for detector development, cross section measurements, and radiation biology experiments. [41]

Table 4.1.8 Parameters of the iThemba neutron facility

Proton cyclotron	**Target station**	**Major activities**
Proton energy ranging between 25 and 200 MeV 200 MeV, 300 nA (selected mode at 26 MHz) 100 MeV, 5 μA (unselected mode) Short pulse, width 1 ns	^{7}Li(p,n)^{7}Be or ^{9}Be(p,n)^{9}B Quasimonoenergetic spectra 1.0×10^{4} n/s/cm^{2} at irradiation positions	Nuclear physics Medical radiation Neutron metrology

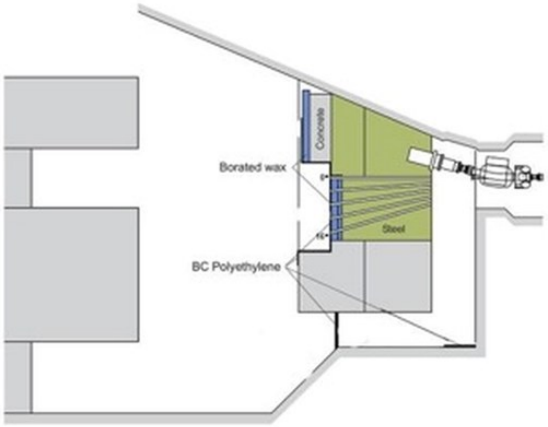

Figure 4.1.8 Layout of the iThemba Laboratory neutron vault.

4.1.9 KOMAC-NST, KIRAMS-MC-50, and PAL-PNF facilities in Korea

The Tandem Van de Graff— Korea Institute of Geoscience and Mineral Resources (KIGAM) in Pohang, Korea [42] is dedicated chiefly to the measurement of MeV-energy neutron capture and total cross section using TOF and a prompt gamma ray detection system, i.e., for fast neutron capture and elastic cross section measurements. In 2015 the facility was moved to the Korea Multi-purpose Accelerator Complex (KOMAC), and restart of operation is pending in 2016. The MC-50 cyclotron at the Korea Institute of Radiological and Medical Sciences (KIRAMS) is generally used for fast neutron irradiation, therapy, and cross section measurements. The Pohang Accelerator Laboratory (PAL) operates with an electron linear accelerator for a pulsed neutron source. The linac has two operating modes: one for short-pulse mode with pulse lengths of 2–100 ns and the other for long-pulse mode with a 1 μs pulse length. The Pohang Neutron Facility consists of a 100-MeV electron linac, a photoneutron target, and at least three different TOF paths. It began operating in January 2000 [43]. The main parameters of the three facilities are reported in Tables 4.1.9 a), b) and c), respectively.

Table 4.1.9 a) Parameters of the KOMAC-NST facility.

Proton tandem accelerator	**Target station**	**Major activities**
1.7 MV tandem accelerator Short pulse, width 1–2 ns	$^{3}H(p,n)^{3}He$: selective mono-energies 0.144–2.5 MeV 10^{2}–10^{3} n/cm^{2}/s	Fast neutron capture and elastic cross section measurements research and development

Table 4.1.9 b) Parameters of the KIRAMS-MC-50 facility.

Proton/deuteron cyclotron	**Target station**	**Major activities**
Protons : 20–51 MeV; 60 μA Deuteron : 10–25 MeV; 30 μA	$^{9}Be(p,n)^{9}B$	Fast neutron irradiation Neutron irradiation therapy Cross sections measurements

Table 4.1.9 c) Parameters of thePAL-PNF facilitiy

Electron linac	Target station	Major activities
80 MeV 30–60 mA (peak) Short pulse: width 1–2 μs, 30 Hz	Water-cooled tantalum target ~2×10^{12} n/s (calc.)	Cross sections measurements Education

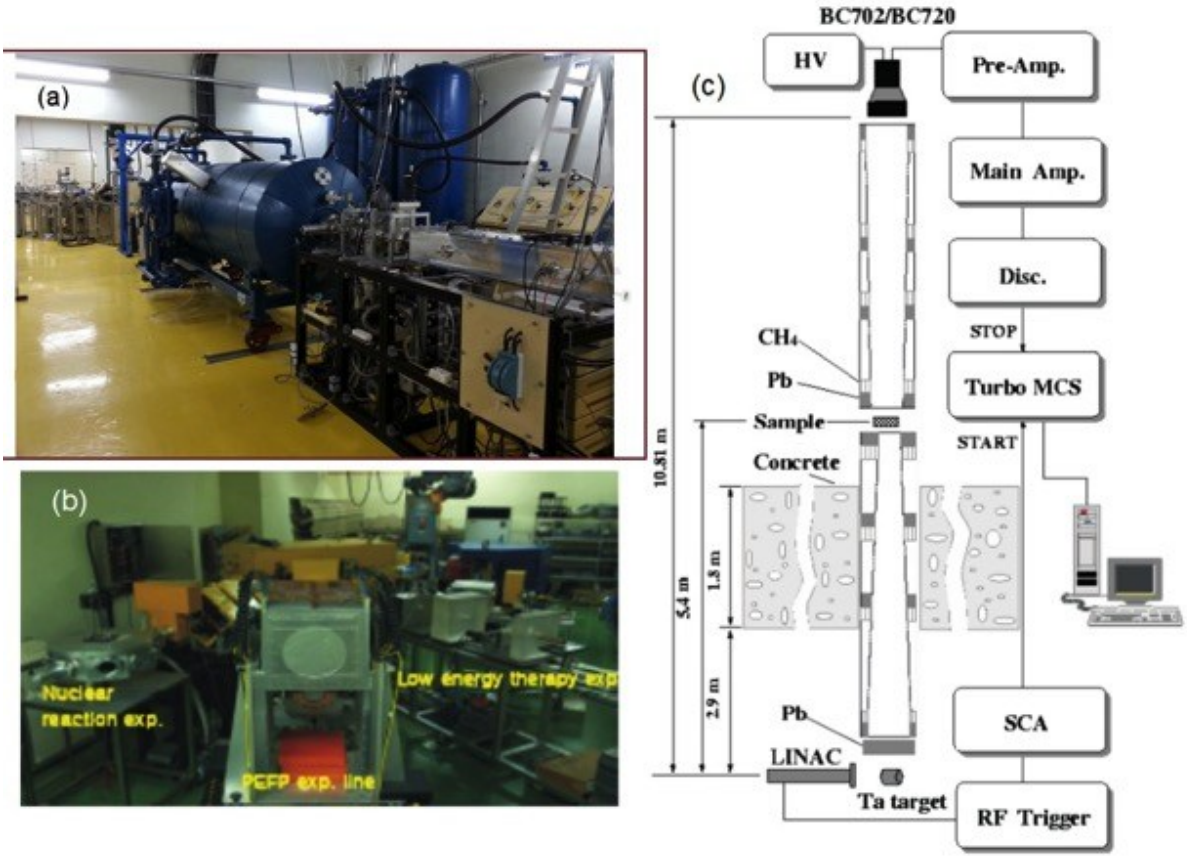

Figure 4.1.9 (a) The tandem accelerator and beam lines of the KOMAC-NST facility. (b) The beam utilization experiment hall of the MC-50 facility. (c) The neutron TOF instrument at the Pohang Neutron Facility (PAL-PNF).

4.1.10 KUANS—The Kyoto University Accelerator-driven Neutron Source

The Kyoto University Accelerator driven Neutron Source (KUANS) in Kyoto, Japan [44], employs a compact, commercial proton linac (AccSys Technology Inc.) and a beryllium target in conjunction with polyethylene moderator, a carbon reflector, and concrete shielding for neutron production. The relatively low neutron flux of KUANS entails high-efficiency instrumentation. For example, by employing a time-resolved imaging of typical samples using ZnS-based scintillators and a position-sensitive photomultiplier tube, imaging data collection can be achieved with 10 minutes of exposure. [45]

Table 4.1.10 Parameters of KUANS, the Kyoto University Accelerator-driven Neutron Source

Proton radio frequency quadrupole (AccSys Technology)	Target station	Major activities
3.5 MeV, 16 kW 10 mA (peak), 100 μA (average) Long pulse, width 0.03–0.2 ms, 20–200 Hz	Be(p, n) PE, ambient ~1×10^{11} n/s (calc.)	Imaging Detector development Education

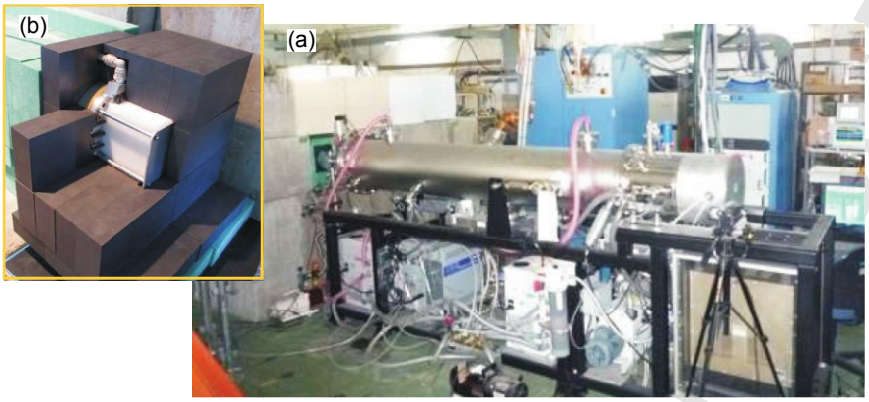

Figure 4.1.10. The accelerator system (a) and the target assembly (b) of the KUANS facility.

4.1.11 KURRI-LINAC—The Kyoto University Research Reactor Institute–Electron Linear Accelerator

The KURRI-LINAC facility Kyoto, Japan [46], has been used as a pulsed neutron, electron, and photon source for research in nuclear data measurement, low-temperature electron irradiation, isotope production by photoreactions, and spectroscopy with coherent THz radiation. About a third of the operation time was spent on nuclear data measurements and nondestructive nuclear material assays with the neutron TOF method and a lead slowing-down spectrometer. The linac is an L-band electron accelerator that produces an electron beam with a maximum power of 6 kW and an energy of 30 MeV. The maximum energy is 46 MeV with no load. It consists of an electron gun, a radio frequency source, a pre-buncher, 2.000- and 1.845-m-long accelerator tubes, and a beam transport system. It uses a water-cooled tantalum target assembly coupled with a light water moderator in an aluminum can as a pulsed neutron source. The facility offers white neutrons in the energy range from the thermal to the MeV region. There are three flight paths of 10, 12, and 22 m for TOF measurements, as shown in Figure 4.1.11. The 10- and 22-m measuring stations are available for measurement of nuclear data such as neutron capture or total cross sections. The 12-m beam line is under reconstruction for nondestructive assay by neutron resonance transmission analysis, neutron resonance capture analysis, and pulsed neutron imaging. [47] A neutron moderator to enhance neutrons in the epithermal energy region is also under development.

Table 4.1.11 Parameters of KURRI-LINAC, Kyoto University Research Reactor Institute–Electron Linear Accelerator

L-band electron linear accelerator	**Target station**	**Major activities**
30 MeV, 1 μA 6 kW	Tantalum Water moderator 3×10^{11} n/s/cm^2	Neutron resonance transmission analysis Neutron resonance capture analysis Pulsed neutron imaging

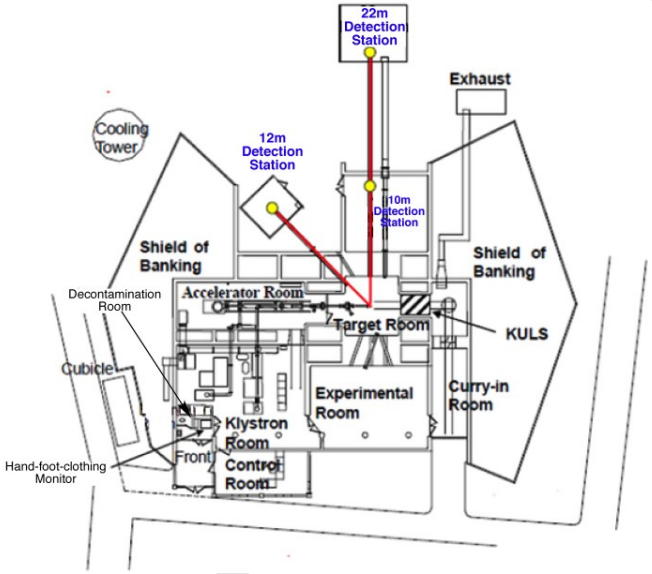

Figure 4.1.11. A schematic layout of the KURRI-LINAC facility.

4.1.12 LENS—The Low-Energy Neutron Source

The Low-Energy Neutron Source (LENS) at Indiana University (Bloomington, IN, United States) [48] is a small pulsed neutron source dedicated to materials research, development of neutron instrumentation, and education. [49, 50] The facility offers unique capabilities for research on neutron moderators and rapid testing of novel instrumentation ideas. The neutron scattering instruments are fed by a cryogenic methane moderator, and two of these are devoted to studies of large-scale structure through SANS and SESAME (spin-echo scattering angle measurement). A third instrument was implemented for moderator studies (the Moderator Imaging Station), but this line has also been used extensively for testing various neutron detectors and is also now used to measure the neutron albedos of materials. A Neutron Radiation Effects Facility is also available at a second target assembly for commercial users interested in the effects of neutron radiation on electronics. Insertion of various moderators allows this facility to investigate effects from fast neutrons (up to 11 MeV) and thermal neutrons. This second target is also used for neutron radiography and tomography.

Table 4.1.12 Parameters of LENS, the Low-Energy Neutron Source

Proton radio frequency quadrupole + two linacs	**Target station 1**	**Target station 2**	**Major activities**
13 MeV, 25 mA (peak) < ~4 kW Short pulse, width 10 μs Long pulse, width 0.6 ms 20 Hz	Be(p, n) Methane 4K ~2×10^{10} n/cm^2/s	Be(p, n) PE/PE w Cd/none ~1×10^{13} n/s	TS1: SANS, spin polarized reflectometry Detector/optics/moderator research and development Education TS2: radiation effects, imaging

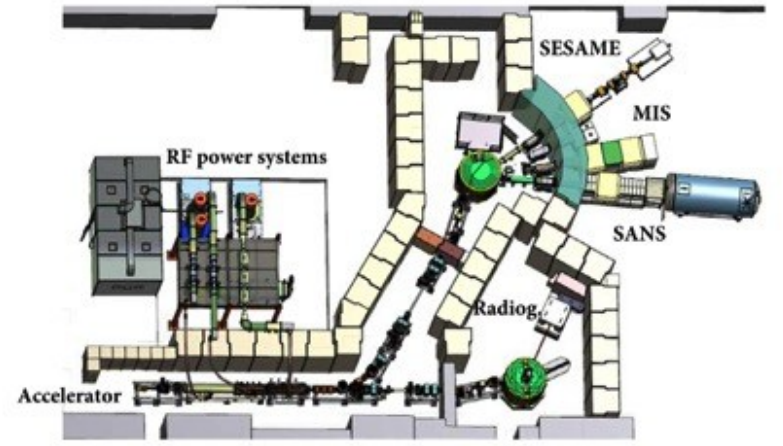

Figure 4.1.12. The current floor plan of the LENS facility. The linac and its associated radio frequency systems are visible on the left and the two target stations are visible as the green circular structures near the center of the figure. The cold-neutron instruments, which include SANS, SESAME, and a Moderator Imaging Station, are served by the upper target station; and the radiography and neutron irradiation facility are served by the lower target station. The two target stations may not be run simultaneously, but operations can be switched from one to the other in less than a few hours.

4.1.13 PKUNIFTY—Peking University Neutron Imaging Facility

PKUNIFTY is a neutron imaging facility based on a compact accelerator-driven neutron source located at Peking University in Beijing, China. [51] An RFQ linac accelerates deuteron ions to an energy of 2 MeV. The accelerator works in pulsed mode with a frequency of 100 Hz. The pulse width can be adjusted from 0.2 to 1 ms, and the peak current can reach 40 mA. A beryllium target is bombarded by a deuteron beam, and a total fast neutron yield of 3×10^{12} n/s can be obtained. The target-moderator-reflector assembly is mounted inside a cylindrical vessel made of aluminum. The moderator material is polyethylene and the reflector material is light water. There are two layers of shielding materials outside the aluminum vessel. The inner lead layer and the outer boron-doped polyethylene layer are used for shielding γ ray and neutrons, respectively. The thermal neutron beam is emitted from a moderator through a collimator. The thermal neutron flux on the imaging plane can be 5×10^5 n/cm^2/s with the collimation ratio L/D = 50, and the n/γ ratio is 1.6×10^{10} n/cm^2/Sv. The field of view is 20×20 cm at a distance of 200 cm from the collimator entrance aperture. The non-uniformity of the thermal neutron flux at the imaging plane is less than 7%. The length of the RFQ cavity is about 3 m, and the total linear dimension of the entire facility is less than 10 m.

Table 4.1.13 Parameters of the PKUNIFTY, Peking University Neutron Imaging Facility

RFQ linac	Target station	Major activities
Deuterons, 2 MeV, 40mA (peak) Long pulse, width 0.015–0.8 ms for <10–40 Hz Normal operation 20 Hz, width 0.6ms	Be(d,n) PE + H_2O 3–10^{12} n/s	Imaging, cross section measurements Education

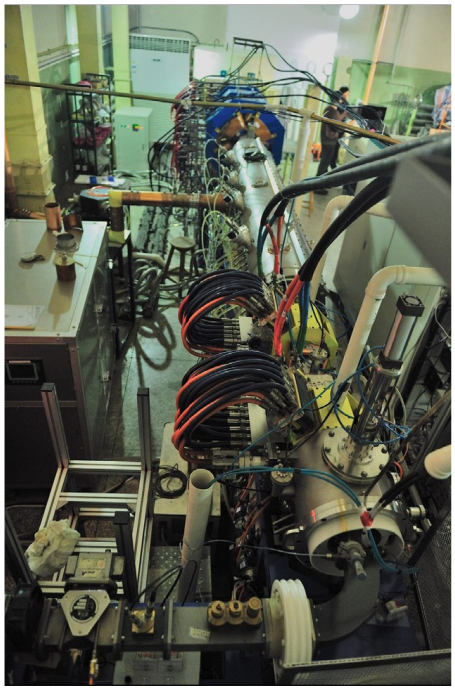

Figure 4.1.13 A bird's-eye view of the PKUNIFTY facility.

4.1.14 RANS—RIKEN Accelerator-driven Neutron Source

The RIKEN Accelerator-driven Neutron Source (RANS) is a new (operation began in January 2013) small neutron source specialized for industrial products characterization at the RIKEN institute in Japan [52]. One of RANS' missions is neutron interrogation of manufacturing treatments of materials consisting of metallic and light-element components. The facility also conducts R&D in fast neutron imaging, detectors, visualization and analysis techniques of nondestructive inspection of physical quantities such as 3-dimentional magnetic field distributions, thermal distribution inside materials, and the deformation of metals. [53]

Table 4.1.14 Parameters of RANS, RIKEN Accelerator-driven Neutron Source

Proton RFQ + 1 linac	Target station	Major activities
7 MeV, 16KW 10 mA (peak), 100 μA (average) Long pulse, width 0.5 ms, 20 Hz	Be(p, n) PE(initial), cold mesitylene (final) ~1×10^{12} n/s	Imaging, industrial applications Fast neutron interrogation

Figure 4.1.14 RIKEN Accelerator-driven Neutron Source.

4.1.15 The Svedberg Laboratory neutron facility

The quasi-monoenergetic neutron beam facility at the Svedberg Laboratory (TSL) in Uppsala, Sweden, uses the ^{7}Li(p,n) ^{7}Be reaction to produce a quasi-monoenergetic neutron beam [54]. Two kinds of beams from the Gustaf Werner cyclotron are used for neutron production: a proton beam with an energy variable in the 20–180 MeV range and a beam of H_2^+ ions with an energy of about 13 MeV. The energy peak of the produced neutrons is selectable within the 11–175 MeV range. [55] Recently, a high-flux irradiation position (close user position) was constructed and put into operation at the ANITA facility at the TSL for accelerated testing of single-event effects. The energy-integrated neutron flux above 10 MeV amounts to more than 10^7 cm^2 s^{-1} with an atmospheric-like spectrum. Characterization measurements have confirmed that the availability of the neutron flux is currently the highest among the facilities of the same class [56].

Table 4.1.15 Parameters of the TSL neutron facility

Proton and H_2^+ cyclotron	**Target station**	**Major activities**
Protons, 11–175 MeV Energy-dependent proton beam current between 10 μA and 0.5 μA Energy-dependent pulse duration : 4 ns (11–174 MeV); 0.7 ms (>100 MeV)	Lithium target ~4.6×10^5 n/s/cm^2 at the entrance of the beam line to the user area	Accelerated testing of components and systems for single-event effects

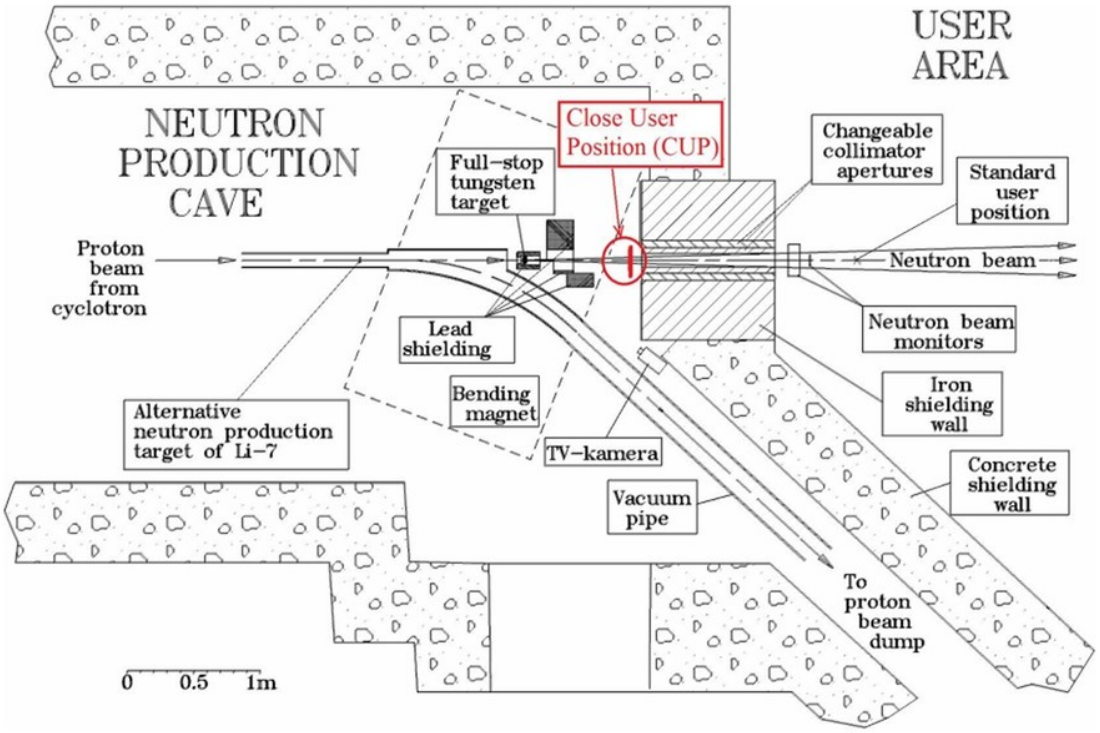

Figure 4.1.15. Layout of the neutron source at the TSL facility with indication of the new close-user irradiation position.

4.2 CANS under Development

4.2.1 The ESS-Bilbao Project, Spain

The ESS-Bilbao (ESSB) located in Bilbao (Spain) [57] is a multipurpose machine based on a light-ion linear accelerator.[58] The facility aims to develop capabilities needed to support Spanish participation in accelerator projects worldwide (e.g., IFMIF/EVEDA, LINAC4/SPL, FAIR, XFEL, ESRF upgrades, and ISIS-FETS). The multipurpose accelerator design is modular and should serve as a benchmark for components and subsystems relevant to the ESS project and as a resource of expertise. Industrial involvement in ESSB activities is welcome. Both proton and neutron beams are expected to be used by a local user community interested in physical and biomedical sciences.

Table 4.2.1 Parameters of the ESS-Bilbao project

Proton linac	**Target station**	**Major activities**
50 MeV, 16 kW 2.25 mA (average), 20 Hz Long pulse, width 1.5 ms	Be(p, n) Solid methane with water premoderator ~1×10^{15} n/s (calc.)	SANS, moderator and neutron-scattering component testing

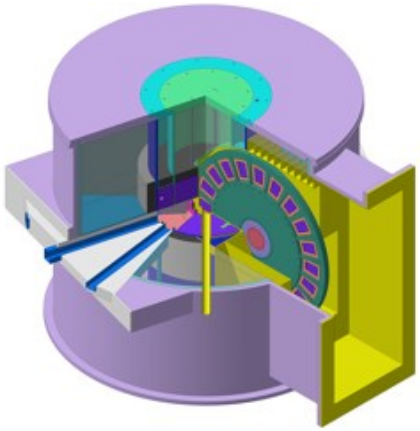

Figure 4.2.1 A layout of the target station at the ESS-Bilbao facility in Spain.

4.2.2 The Frankfurt Neutron Source at the Stern-Gerlach-Zentrum (FRANZ), Germany

The Frankfurt Neutron Source (FRANZ) facility is currently under development at the Stern-Gerlach-Zentrum FRANZ in Frankfurt (Germany) [59]. It will use a 2-MeV proton beam to produce a quasi-Maxwellian neutron spectrum of around 30 keV by the ^{7}Li(p,n)^{7}Be-reaction. The neutron beam will be tunable between 10 and 400 keV by changing the primary proton beam energy between 1.8 and 2.2 MeV. [60] Initially, the facility is expected to operate in the activation mode, driven by a continuous wave (cw) proton beam using a level of current of a few mA. In a second stage, a bunch compressor will be realized. The research program at FRANZ is focused on nuclear astrophysics, but it also allows investigations in many other fields. [61]

Table 4.2.2 Parameters of the Frankfurt Neutron Source at the Stern-Gerlach-Zentrum (FRANZ).

Proton linac	**Target station**	**Major activities**
1.87–2.1 MeV, 16KW 200 mA macro pulse, 250 kHz Short micro pulse, width 1 ns	Li(p, n) Neutron energies 1–200 keV Pulsed beam ~10^{7} n/cm^{2}/s @ 0.8m Straight beam ~10^{9} n/cm^{2}/s	Nuclear astrophysics Materials research, radiography Detector development Education

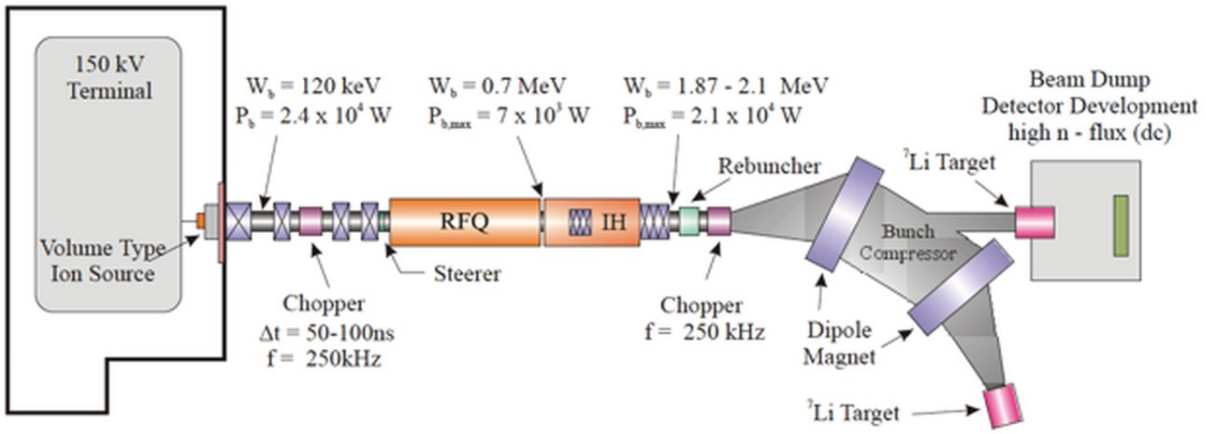

Figure 4.2.2 An overview of the FRANZ layout.

4.2.3 LENOS—The Legnaro Neutron Source, Italy

The Legnaro Neutron Source (LENOS) at the Laboratori Nazionali di Legnaro (Italy) [62] is an irradiation facility that will deliver a high-flux neutron beam with a Maxwell-Boltzmann (MB) energy spectrum of a tunable temperature. The main goal of the facility is to provide new and more accurate neutron cross section data by measuring integral nuclear data with very well characterized MB energy neutron beams. This is also very important for benchmarking available nuclear data. LENOS will meet the needs of a large national and international community for cross-disciplinary studies, from nuclear astrophysics to bio-medicine, and applied research, from development of new detectors to materials relevant to fusion technology.

Table 4.2.3 Parameters of the Legnaro Neutron Source

Proton RFQ	Target station	Major activities
5 MeV, 250 KW 50 mA, 325 MHz CW (first phase), pulsed second phase) Width 2 ns, 125 kHz	Li(p, n) Moderated and not 10^{11}–10^{15} n/s (c+alc.)	Nuclear astrophysics, nuclear data Neutron activation Imaging

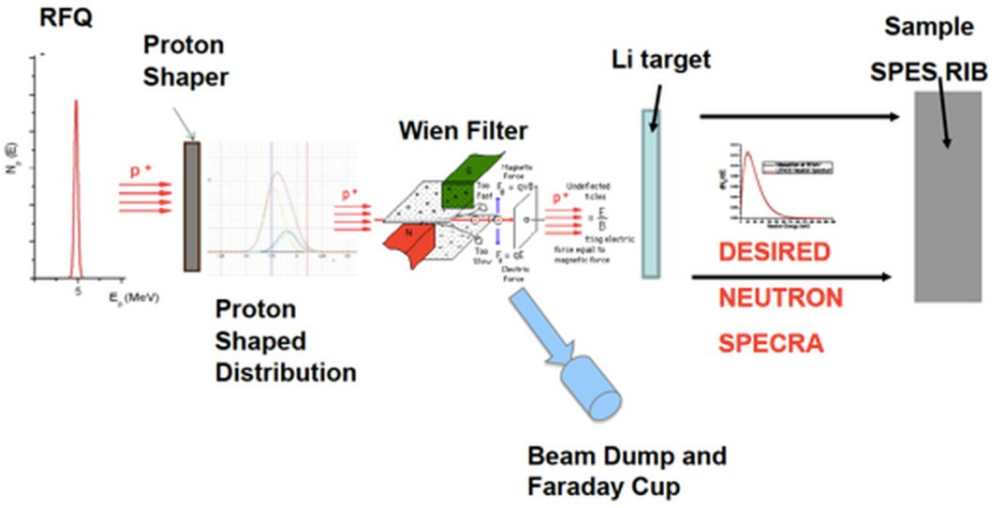

Figure 4.2.3 A schematic view of the Legnaro Neutron Source facility.

4.2.4 n@BTF, The Frascati electron-driven source

n@BTF is a small neutron source being developed since 2008 at the electron facility of the Frascati LINAC (BTF, beam-test facility) at the Laboratori Nazionali di Frascati (Italy) [63]. This source is mainly meant for calibration, metrology and training and possibly also applications from historical heritage to electronics and material studies, biology and bio-technology [64]. The possibility of optimizing the source for thermal neutrons will open also the industrial application field. It is driven by a up to 49 Hz (currently

2 Hz), 510 MeV, up to $3 \cdot 10^{10}$ electron/s beam onto an optimized tungsten target (70 mm diameter, 60 mm long), enclosed in a lead/polyethylene shielding optimized to reduce the gamma/neutron ratio. A Maxwellian peak of 1 MeV neutron is produced, with an expected and measured yield of $8 \cdot 10^{-7}$ n/cm^2/primary at 1.5 m distance. The primary beam energy and intensity are to be upgraded within the framework of an extensive improvement of the n@BTF, including the addition of beam-line splitting, a new experimental hall, improved diagnostics, etc.

Table 4.2.4 Parameters of Frascati electron-driven neutron source, n@BTF.

Electron linac	Target station	Major activities
510 MeV, 0.04 KW Pulse-width 0.5-40 ns, 50 Hz	Tungsten Lead/Polyethylene shielding ~8 10^{-7} n/cm^2/primary	Calibration, metrology, training

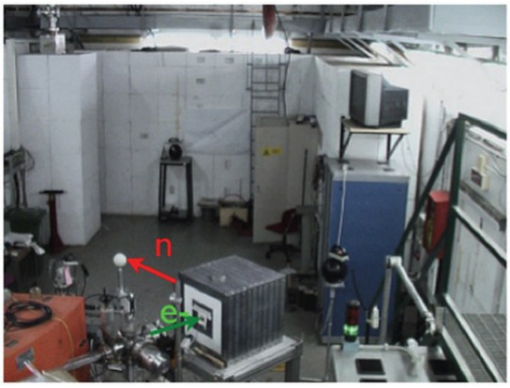

Figure 4.2.4 View of the Frascati BTF neutron source (n@BTF) showing primary electron beam and the outgoing neutron beam directions.

4.2.5 The nELBE Time-of-flight Facility at the Helmholtz-Zentrum Dresden-Rossendorf

The compact neutron-TOF facility nELBE, at the superconducting electron accelerator ELBE of Helmholtz-Zentrum Dresden-Rossendorf (Germany) [65] is being rebuilt and extended with a low-background experimental hall. The neutron radiator consists of a liquid lead circuit without additional neutron moderators. The useful neutron spectrum extends from some tens of keV to about 10 MeV. nELBE is intended to deliver cross section data of fast-neutron nuclear interactions, [66] e.g., for the transmutation of nuclear waste and improvement of neutron physical simulations of innovative nuclear systems.

Table 4.2.5. Parameters of the nELBE Time-of-flight facility at the Helmholtz-Zentrum Dresden-Rossendorf

Superconducting electron accelerator	Target station	Major activities
40 MeV 1 mA, 100 kHz to 13 MHz width 5 ps	Liquid lead circuit 10^{13}n/s (calc.)	Transmutation of nuclear waste and improvement of neutron physical simulations of innovative nuclear systems

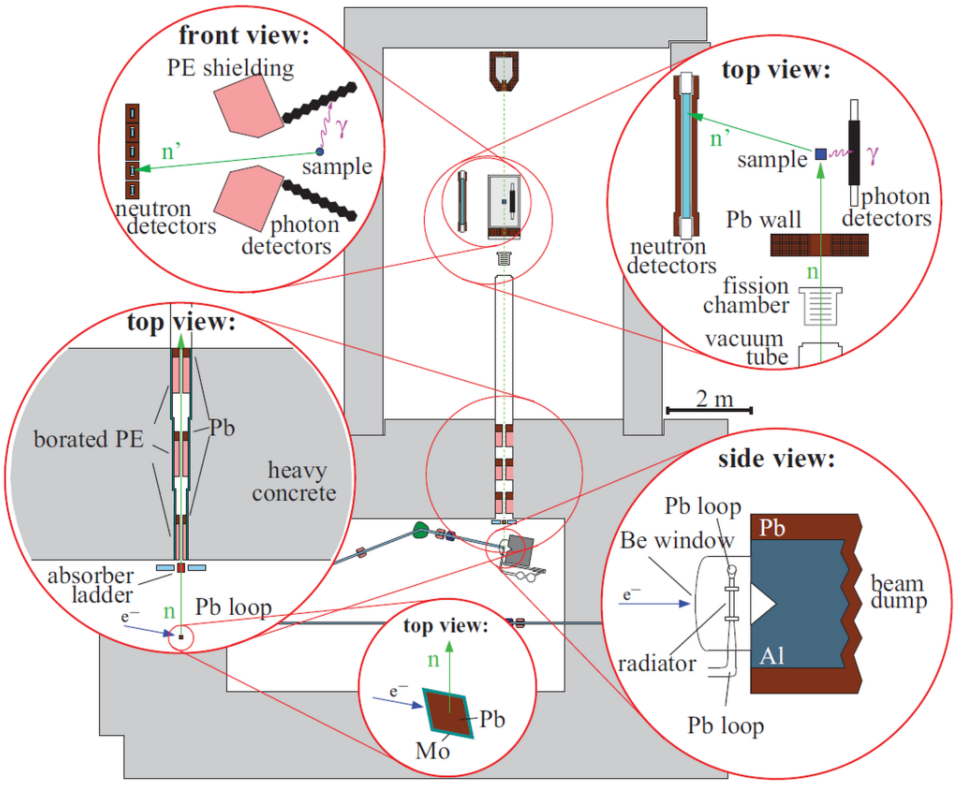

Figure 4.2.5. Floor plan of the new nELBE neutron source and low-background experimental hall.

4.2.6 NEPIR facility at the SPES source of the Laboratori Nazionali di Legnaro

The NEPIR (NEutron and Proton IRradiation) CANS facility has been proposed at the Laboratori Nazionali di Legnaro (Italy) [62] to produce both discrete and continuous energy neutrons, within the prospect of a high flux neutron irradiation facility. A direct proton beam line has also been conceived.

Presently the NEPIR project foresees three different tools:

1. An intense beam of quasi mono-energetic neutrons (QMN) with a controllable energy peak in the 35–70 MeV energy range (by degrading the minimum 35-MeV energy protons, the neutron peak energy can be lowered to 20 MeV) [67]
2. An intense beam of fast neutrons (E_n > 1 MeV)with a continuous energy distribution similar to that of neutrons found at flight altitudes and at sea level (the Atmospheric Neutron Emulator, ANEM) in the accessible energy range
3. An independent direct low-current proton beam line (PROTON)

The NEPIR project is at the design level, while the building to host the full facility has already been constructed. The schematic layout of NEPIR is shown in Figure 4.2.6. The QMN and the ANEM lines coincide (hall A9); the two complementary systems are designed to enable exchanging modes of operation. ANEM is a specialized neutron production target capable of producing neutrons with a continuous energy distribution similar to that of atmospheric neutrons in the 1–70 MeV energy range.

The design and thermal-mechanical finite-element modelling of the ANEM target system are in an advanced stage. The model will be validated by applying thermo-structural tests to a realistic prototype system.

The direct proton beam line will be developed once the first phase of NEPIR (QMN+ANEM) is financed and completely designed.

A very-high-flux slow-neutron line (SLOWNE) will also be developed in the future. It will be based on a thick tungsten high-power target developed for the FARETRA, a next-generation reactor simulator for transmutation studies. A tailored system of moderators and reflectors will then shift the energy of the produced neutrons to deliver neutrons with the energy spectrum of interest for measurements on the floor. This high-intensity slow-neutron beam line could be used to perform neutron imaging or prompt gamma activation analysis of materials and industrial and cultural/archeological artifacts.

Table 4.2.6 Parameters of the NEPIR facility at the SPES source of Laboratori Nazionali di Legnaro

Proton cyclotron	**Target station**	**Major activities**
35–70 MeV, Up to 500 μA on target (lower proton energies, too, by using degraders) Continuous wave (can be converted to pulsed mode)	X(p,n), X=Li, Be, W Slow neutron energies 1–200 keV 10^{13} – 10^{14} n/s 4π Fast neutrons up to ~ 70 MeV 10^{5} – 10^{7} n/cm^2/s	Fast neutron irradiation for SEE tests Cross section measurements Nuclear data for ADS Imaging, materials analysis

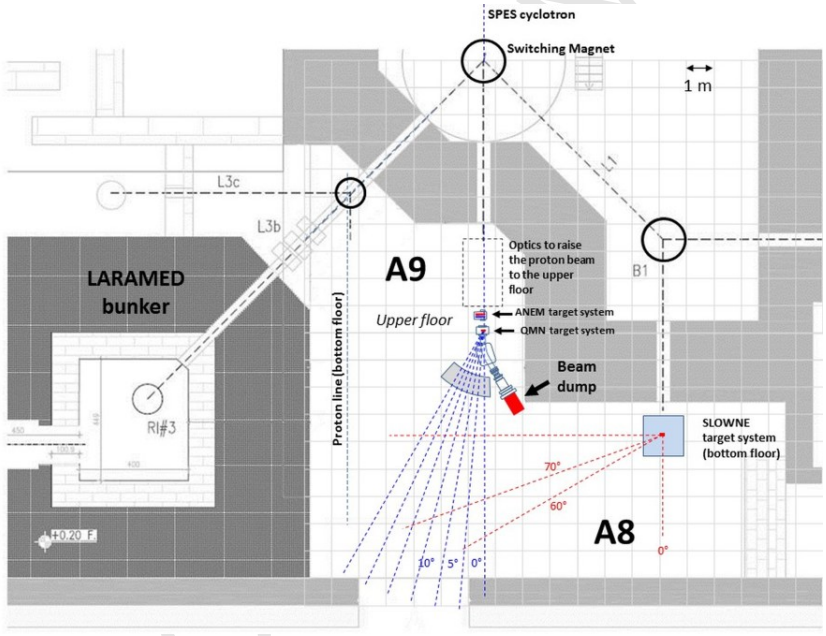

Figure 4.2.6 Conceptual floor plan of the NEPIR facility at SPES (overlaid on 1 m^2 grid). The supplementary shielding is not shown. The QMN and ANEM beam lines in hall A9 coincide and are raised by a magnetic chicane to be near the midsection of the hall. A fixed multi-angle collimator system will allow measurements in the range 5–30°. A direct proton line is also in hall A9. The eventual SLOWNE target system would be installed in hall A8 (serviced by the B1 bending magnet). The LARAMED bunker on the lower left is dedicated to the production of radioisotopes for medical applications.

4.2.7 The Nagoya University Accelerator-driven Neutron Source (NUANS)

Development of a compact neutron source, driven by a low-energy, high-current DC proton accelerator [68, 69], has been underway in Nagoya University (Japan) for BNCT application (beam line 1), and for fundamental physics experiments and industry uses (beam line 2). The accelerator, a Dynamitron, delivers a 2.8-MeV, 15-mA proton beam and neutrons are to be produced by the ^{7}Li(p,n)^{7}Be reaction. The resulting neutron flux will be moderated using a compact beam shaping assembly (BSA). The use of low-energy protons incident on a lithium target is one of the most suitable reactions for accelerator-driven BNCT to obtain high neutron production rates and useful thermal-to-epithermal neutrons. However, a lithium target has several difficulties (low melting point, high chemical activity, and ^{7}Be production). A new design of a sealed lithium target and the associated BSA, together with a plan for evaluation of the expected performance using the Dynamitron's proton beam are currently under consideration as a part of the compact neutron source project for BNCT.

Table 4.2.7 Parameters of the Nagoya University Accelerator-driven Neutron Source

DC accelerator (Dynamitron)	**Target station**	**Major activities**
Protons, 1.9–2.8 MeV (variable), maximum 42 kW	Li(p, n)	Compact neutron source R&D for BNCT Engineering applications (neutron imaging)
15 mA	MgF_2	
DC	Epithermal neutron flux ~ 1×10^{9} n/cm^2 s	

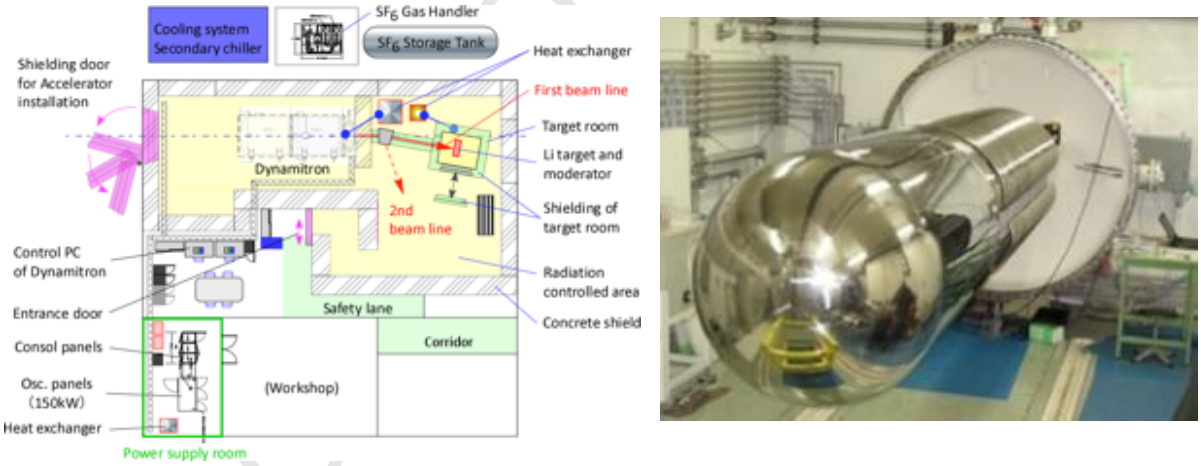

Figure 4.2.7 A schematic layout and photograph of the NUANS facility and Dynamitron proton accelerator in NUANS.

4.2.8 UTCANS—U-Tokyo

The UTCANS facility at the University of Tokyo (Japan) will consist of 35-MeV and 3.95-MeV electron linac sources, the latter being studied as a mobile neutron source.

The 30-MeV X-band (11.424 GHz) electron linac is originally designed and operated as a Compton scattering monochromatic x-ray source. This Compton scattering x-ray source consists of the 3-MeV thermionic radio frequency gun, solenoid magnet for focusing, α magnet as an energy filter, 700-mm accelerating tube, 50-MW X-band klystron, and 500-kV, 1-μs modulator. These components provide a very low emittance beam with a YAG laser. However, it is not the emittance but the high average current that is crucial to a neutron source. Therefore, the low-energy part is replaced with a 100-keV thermionic gun that can emit a beam of up to 500 mA at 100 kV. The capture efficiency of the accelerator, now attainable to 35 MeV, is about 25-33%.

35-MeV X-band (11.424 GHz) electron linac–driven neutron source

Table 4.2.8. Parameters of the 35-MeV X-band (11.424 GHz) electron linac–driven neutron source

Electron linac	Target station	Major activities
Electrons, 35 MeV, 0.375 KW 250 mA (peak), 50 Hz Short pulse, width 0.1–1 μs	W(γ, n) Polyethylene moderator ~8×10^{11} n/s	Nuclear data acquisition of nuclear materials

The main goal of this neutron source is nuclear data acquisition of nuclear materials using a 5m-long neutrons TOF beamline. The requirement for the target and moderator is to generate as many neutrons as possible with a pulse width as short as 100 ns. The Monte Carlo simulation code PHITS[70] is used to optimize the target-moderator design and production of short-pulse neutrons. Design of the shielding and cooling system has been completed using Monte Carlo simulations.

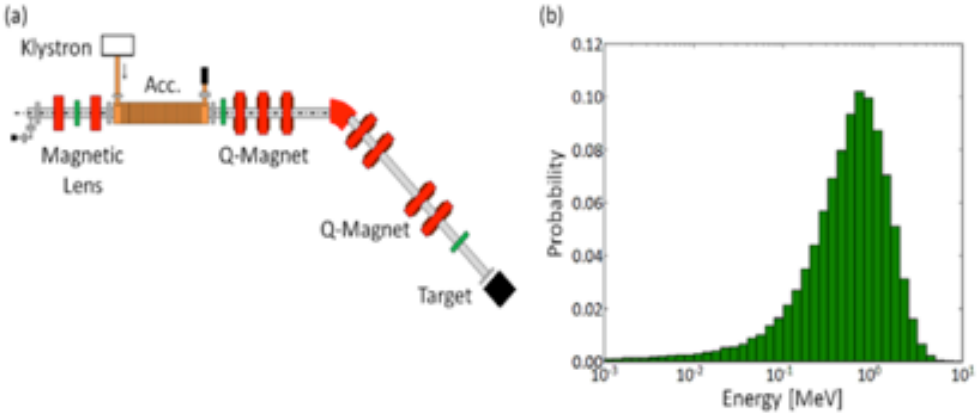

Figure 4.2.8 (a) Schematic view of 35-MeV X-band electron linac neutron source. (b) Energy spectrum of neutrons from tungsten target.

3.95 MeV X-band (9.3 GHz) electron linac–driven neutron source

A 3.95-MeV X-band (9.3-GHz) electron linac–driven mobile x-ray source for nondestructive inspection of infrastructures, including bridges, motoring roads, and tunnels, has been developed. Outdoor operation of the x-ray source has been successfully demonstrated by transmission imaging of a 400-mm thick concrete structure cut from a deteriorated bridge.

The applications of the mobile x-ray source will be complemented by a mobile neutron source. This will be realized by using the photonuclear reaction of beryllium with a low energy threshold of 1.66 MeV. The expected flux of 1.6×10^7 n/s/cm^2 just behind the target, obtained by Monte Carlo simulation with the PHITS code using a 5-cm thick beryllium target, is sufficient for nondestructive inspection of infrastructures (especially for moisture detection) and on-site measurement of nuclear materials in fuel debris, for example, at the decommissioned Fukushima nuclear plants. This project would also pave the way to more mobile x-ray/neutron hybrid source systems in the future.

Table 4.2.9 Parameters of the 3.95-MeV X-band (9.3 GHz) electron linac–driven neutron source

Electron linac	**Target station**	**Major activities**
Electrons, 3.95 MeV, 0.300 kW 95 mA (peak), 200 Hz Short pulse, width 2–4 μs	W(γ, n)+Be(γ, n) Polyethylene moderator ~2×10^9 n/s	On-site nondestructive inspection of infrastructures and nuclear materials in fuel debris for decommissioned Fukushima reactor

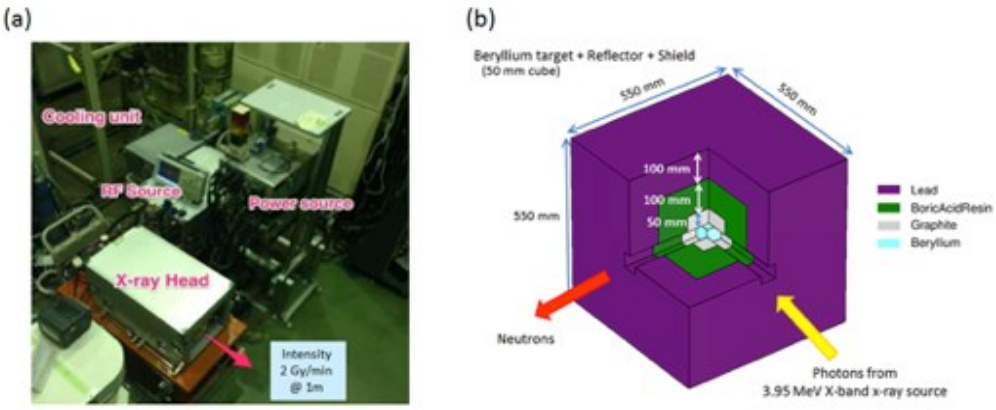

Figure 4.2.9. (a) 3.95-MeV X-band electron linac–driven mobile x-ray source. (b) Design of neutron target station.

4.2.9 Van de Graaff facility at the Institute for Reference Materials and Measurements of the Joint Research Centre of the European Commission in Geel, Belgium.

At the Van de Graaff facility of the IRMM, in Geel (Belgium) [71], quasi mono-energetic beams of neutrons are produced in an energy range of up to 24 MeV. Especially in the MeV neutron energy domain, where the rich resonance structure of the cross-sections is averaged out for insufficient energy resolution, the high-resolution measurements at GELINA can be complemented by measurements at the Van de Graaff, where the experimental conditions are more favorable for weak cross sections and low sample quantities.

The Van de Graaff facility is a 7-MV electrostatic accelerator for the production of continuous and pulsed proton, deuteron, and helium ion beams. Ion beams can be produced with a current of up to 60 μA on a target in DC mode and up to 5 μA in pulsed mode. The pulse repetition rates are 2.5, 1.25, or 0.625 MHz and the ion pulse lengths are 2.50–1.25 ns full width half maximum, depending on the ion energy. The energy of the mono-energetic neutrons is defined by the selection of lithium, deuterium or tritium targets and the appropriate emission angles. Depending on the neutron energy, up to 10^8 neutrons/s can be

obtained. Experimental setups for activation, fission, and scattering experiments are attached to the accelerator. In contrast to GELINA, here, only one setup can be used at a time. In fall 2016, the 38-year-old Van de Graaff accelerator will be replaced by a new tandem accelerator delivering proton, deuteron, and helium ion beams with similar characteristics. Replacement of the Van de Graaff will lead to increased reliability, stability, and reproducibility. This machine will have major critical components at mass potential, which has the advantage that a more sophisticated and flexible particle injector can be used so that a greater variety of experimental conditions can be offered.

4.3 Preferred Characteristics of CANS Applications

The inherent versatility and diversity of CANS is both an asset and a potential drawback: not every source type is suitable for every potential application; hence sources tend to be designed with specific applications in mind. In Section 6, the typical applications of CANS are described in more detail. In Table 4.3, we outline some of the generally preferred source characteristics for different applications.

Table 4.3 Preferred characteristics of CANS for specific applications. The underlined items represent the preferred configurations

Applications	**Neutron-matter reactions**		**Accelerator systems**	**Neutronics and energies**	**Remarks**
Interrogation of materials/structures	(n,γ)	PGAA	<u>P</u>, CW	Cold, thermal	Compact, rugged, transportable (portable for landmine detection and well logging), minimal innate γ background, and large, scannable beams
		DGAA	<u>P</u>, CW	Cold, thermal	
		NRCA	<u>P</u>, CW	Epithermal	
		FNAA	<u>P</u>, CW	Fast	
		APT	P (ns)	$D(T,\alpha)$n, E_n=14MeV	
Radiography and imaging	(n,γ)	+ PGAA	<u>P</u>, CW	Cold, thermal	Combined tomographic and activation analysis techniques, neutron polarization analysis of magnetic materials
		+ NRCA	<u>P</u>, CW	Epithermal	
		+ FNAA	<u>P</u>, CW	Fast	
		RITS	P	Thermal	
		polarization	<u>P</u>, CW	Cold, polarized	
Irradiation effects on electronics	Neutron-induced soft errors (SEU)		<u>P</u>, CW	Fast, selective	High flux to speed up testing/certifying processes, matching test and environmental spectra
Neutron capture therapy	Boron neutron capture therapy		P, <u>CW</u>	Epithermal	Compact and suitable for operation in hospitals, good flux and clean beam, development of boron-bearing pharmaceuticals
Isotope production	$^{N}X(n,\gamma)X^{N+1}*$		CW	Selective	Compact, prevalently located near isotope processing and generation facilities
Nuclear data and cross section measurements	Reaction and scattering		<u>P</u>, CW	All	Flexible and multi-purpose beamline and endstations
Nuclear astrophysics	n-capture, β-decay, (n,γ) decay rate, calorimetry		<u>P</u>, CW	Fast	High-intensity beams needed for microgram samples
ADS science and technology	Subcritical fission, transmutation		P	Thermal to epithermal	Intense beams and reliable operation

CW = continuous wave; P = pulsed

5. Neutron Interactions

In this section, we discuss the interactions that neutrons may have with matter that are of relevance to the applications of CANS described in Section 6.

Neutrons have no charge, and their electric dipole moment is either zero or too small to be measured. Hence, neutrons interact with matter principally via nuclear rather than electrical forces, and nuclear

forces are very short in range. Hence, as far as the neutron is concerned, solid matter is not very dense and interaction probabilities are low.

Neutrons do, however, possess a magnetic moment and so can experience a force of magnetic origin when it moves in a field. A good example is the field produced by unpaired electrons in matter. Magnetic moments in solids can therefore give rise to magnetic scattering of neutrons, much the same as the nuclear interactions and x-ray atomic electron interactions. The magnetic interaction, unlike the nuclear interaction, is not isotropic; it is dipolar and depends on the relative orientations of the neutron moment, and hence its spin, and the scattering moment. Neutron scattering is therefore sensitive to the spatial distribution of both the direction and magnitude of magnetization in a material. The magnetic forces can also be used effectively to steer neutron beams, even though the forces are in general weak.

Neutron-nucleus interactions

In all matters that we discuss here, neutrons are nonrelativistic: their kinetic energy is far below the rest energies of the particles. There are several types of neutron-nucleus interactions, as portrayed in Figure 5.1.

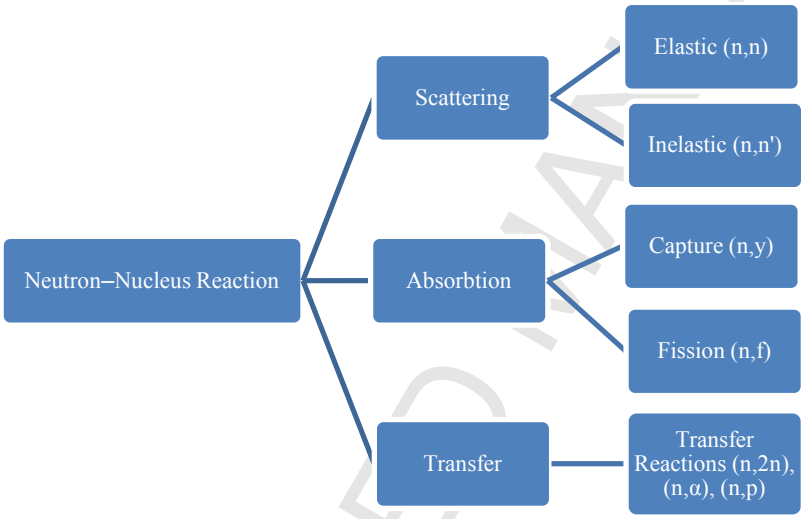

Figure 5.1 Neutron-nucleus interactions.

- **Nuclear elastic reaction.** The nucleus is left in the same internal quantum state after interaction as before, but it may gain laboratory kinetic energy while the neutron loses kinetic energy. Neutron–nuclear elastic scattering is the main basis of neutron scattering measurements, in which the cross sections are usually independent of neutron energy. Cross sections in many cases depend on the relative orientation of nuclear spin and neutron spin: usually, samples or neutron beams are not spin-polarized, and cross sections are then the average over relative spin orientations.
- **Nuclear inelastic reactions**. The nucleus absorbs energy from the neutron and is left in a different internal quantum state after the interaction than before. The struck nucleus decays by photon (gamma-ray) emission, and the neutron emerges with lower energy than before colliding. The cross section typically exhibits a threshold energy below which inelastic reactions cannot occur.
- **Absorption**. The neutron disappears into the nucleus, forming a compound nucleus that is in an excited state—one mass unit heavier than the original—that decays by emitting lighter particles or

electrons. Usually, the formation of a compound nucleus is promptly accompanied by the emission of gamma rays. In many instances, a massive charged particle emerges from the reaction, and the products carry substantial kinetic energy. The residual nucleus may have a long lifetime (this is neutron activation) and beta decay may be followed by emission of characteristic gamma rays. The absorption cross sections for some isotopes are spin-dependent, that is, they depend on the relative orientation of the nucleus and the neutron spin.

- **Fission**. The neutron disappears into the nucleus, momentarily leaving it in a highly excited state from which the nucleus (it must be a heavy nucleus, Z >80) splits into two roughly equal fragments and a few light particles, almost always neutrons. Fission fragments carry about 180 MeV of energy, which appears as ionizing particles and heat in the surroundings.
- **Capture**. The neutron disappears into the nucleus regardless of what happens afterward (therefore, capture includes absorption and fission). Capture cross sections for low-energy neutrons are usually proportional to the neutron wavelength.
- **Transfer**. The neutron collides directly with the nucleus and emits nucleons.

The probability of occurrence of a certain type of interaction is described by its cross section. The product of this probability and the neutron flux is called the reaction rate—the number of reactions per unit of volume per unit of time. The total cross section, σ_t, is the sum of the cross sections of the neutron–nucleus interactions discussed above. The experimental determination of the total cross section over a broad range of neutron energies is well-suited to the mission of the CANS. Ideally, measurements should be done under the conditions relevant to the application.

5.1.1 Condensed matter scattering of slow neutrons

The energies of slow neutrons are too small to alter the chemical or electronic structure of condensed matter. Here, the strength of neutron scattering is characterized by a scalar that is denoted as the neutron *scattering length, b*, of the nucleus. Nuclei are pointlike with dimensions of the order of 10^{-14} m. As a consequence, the scattering is purely isotropic; i.e., mathematically, one deals with pure *s*-wave scattering [72]. The physical quantity *b* is generally a complex number: $b = b' + ib''$ where the imaginary part of *b* describes the absorption of neutrons by the nucleus and varies from nucleus to nucleus: isotopes, elements, nuclear spin direction. With few exceptions, it is independent of wavelength for low-energy neutrons. Values of *b* used in neutron scattering are experimentally determined and tabulated [73] [72, 74]

The scattering length *b* depends on the spin channel through which the scattering takes place. For each isotope, except for spin-zero nuclei, there are two scattering lengths—one denoted as b^+, associated with the $2I+2$ states of spin $I+1/2$, and one denoted as b^-, associated with the $2I$ states of spin $I-1/2$—according to whether the spins of the neutron and of the nucleus align or anti-align. One assumes that *b* at site *j* is stochastic: $b_j = \langle b_j \rangle + \delta b_j, \langle \delta b_j \rangle = 0$ and $\langle \delta b_j \delta b_j \rangle = 0$, where $\langle b_j b_j \rangle = \langle b_j \rangle \langle b_j \rangle = \langle b \rangle^2$, $i \neq I$, and $\langle b_j b_j \rangle = \langle b_j \rangle^2 = \langle b^2 \rangle, i = j$.

In practice, which almost always involves unpolarized neutrons and/or nuclei, there are two statistical averages—with respect to the numbers of possible relative neutron and nuclear spin states—of scattering lengths: *coherent*, due to the interference between waves scattered from distinct pairs of centers, and *incoherent*, in which a scattered wave cannot interfere with others, but only with itself, and describes single-nucleus scattering:

$$\sigma_{coh} = 4\pi\langle b\rangle^2, \quad \sigma_{inc} = 4\pi(\langle b\rangle^2 - \langle b\rangle^2) \ . \tag{5.1}$$

These microscopic cross-sections can be interpreted as the effective target area presented by the nucleus to the incident neutron. The standard unit for the cross-section is the barn, which is equal to 10^{-28} m^2. Furthermore, scattering from elements consisting of mixtures of isotopes involves the average over isotopic composition, the *isotope average*. That composition is usually the known natural mix of isotopes. In important cases, the isotope composition differs from the natural one, sometimes by design, sometimes by default: nominal heavy water, D_2O, often contains significant light hydrogen, often in purposely designed H/D mixes; commercial lithium may be depleted in ^{6}Li; nominal depleted uranium, ^{238}U, contains a variable amount of ^{235}U; the composition of plutonium, which does not occur in nature, varies according to processing.

In condensed matter, "macroscopic" cross sections characterize interaction probabilities on a laboratory scale, on a per-unit-length scale, $\Sigma = n\sigma$, where *n* is the atomic number density. The usual unit for expressing Σ is an inverse length, cm^{-1}. In a monatomic material, $n = \rho N_A / M$, where ρ is the mass density, N_A is Avogadro's number, and M is the mass of the atoms.

Transmission

In a condensed matter sample, on a laboratory scale, neutrons interact at a rate □ per unit distance. Passing through a sample of thickness *d,* a neutron ray or beam attenuates exponentially, and the probability of transmission is

$$T_r = \exp(-\Sigma_t d) = \exp(-n\sigma_t d) \ . \tag{5.2}$$

The subscript *t* denotes total cross sections. This equation serves as the basis of *conventional* transmission imaging, including radiography and computed tomography. Most recent developments in Europe on phase contrast imaging [75] and in Japan [76] on Bragg-edge contrast imaging are also transmission techniques, but less directly tied to equation 5.2. In practice, the measured quantity is the transmitted intensity of neutrons at energy *E*, $I(E)$, relative to the intensity without the sample, $I_0(E)$, i.e.,

$$\frac{I(E)}{I_0(E)} = \exp\left[-\int_0^d \Sigma_t(x,E)\,dx\right], \tag{5.3}$$

where $\Sigma_t(x,E)$ is the total cross section at distance *x* within the sample for source energy *E*. Thus the material difference along the beam path, if any, cannot be detected. If the material is homogeneous and the cross section is known, Eq. (5.3) is useful to obtain the thickness *d*.

Elastic scattering: small-to-wide-angle diffraction

Coherent elastic scattering of neutrons from a condensed system—a fluid, solid, or soft matter—senses the time-averaged spatial variation of the nuclear scattering lengths of the constituent atoms (or many-atom particles) over a length scale from interatomic distances (diffraction) to local deviations (diffuse scattering) to inter-particle distances (small-angle scattering). In practice, elastic scattering is approximated by total scattering measurements. For fluids, the time-averaged structure does not correspond to the static structure (non-ergodicity); the result represents a snapshot of the instantaneous structure. Broadly speaking, coherent scattering depends on the contrast of coherent scattering-length

density over the length scale of interest. Neutron scattering has an advantage over its x-ray counterpart in its ability to detect light atoms (e.g., deuterium that replaces hydrogen) and differentiate elements/isotopes with nearly the same mass numbers within a multicomponent system.

Neutron powder diffraction and SANS are two well-developed areas of CANS, serving education and precursory research for users. Figure 5.1.1 depicts a generic pulsed-source time-of-flight diffractometer. The relation of $\vec{Q} = \vec{k}_0 - \vec{k}_1$ is called the scattering triangle, where $\hbar\vec{Q}$ is the neutron momentum transfer, $\vec{k}_0$ and $\vec{k}_1$ are the incoming and outgoing neutron wave vectors, respectively. For diffraction, $|\vec{k}_0| = |\vec{k}_1|$, and 2θ is the scattering angle. In general, experiments at CANS focus on problems that do not require high neutron flux and high resolution, for example, by choosing samples that have strong intrinsic scattering-length density contrast for SANS measurements.

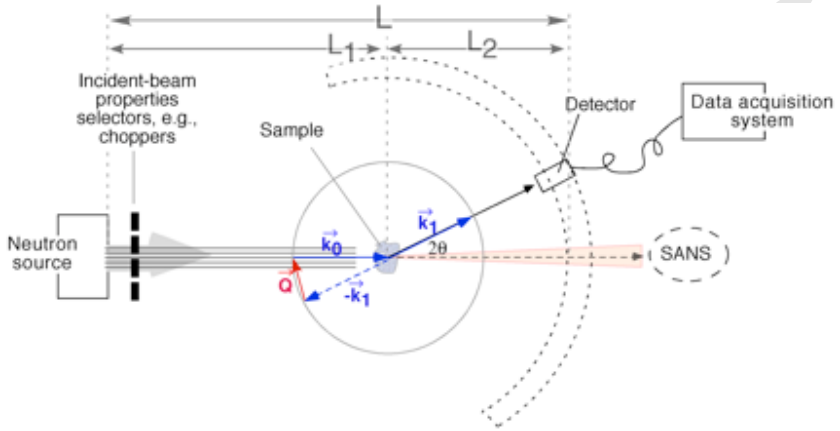

Figure 5.1.1 Schematic layout of a generic pulsed-source time-of-flight neutron diffractometer.

An alternation from traditional powder diffraction, *i.e.*, analyzing the Bragg-edge transmission intensity via a 2-dimensional imaging technique rather than treating the diffraction data, is well suited for CANS, as successfully demonstrated at HUNS. Sato *et al*. [76] and Steuwer *et al*. [77] have developed a method to evaluate the properties of polycrystalline materials with a relatively simple crystallographic structure but complex texture and/or microstructure of practical interest. Figure 5.1.2 shows the experimental setup and the expected data. By carrying out a goodness-of-fit analysis called Rietveld imaging transmission spectra (RITS) of the pixel-by-pixel intensity profile of Eq. (5.3), Sato et al. [76] extract information regarding the preferred orientation of the crystalline grains, crystallite size, and internal strain in a bulk material.

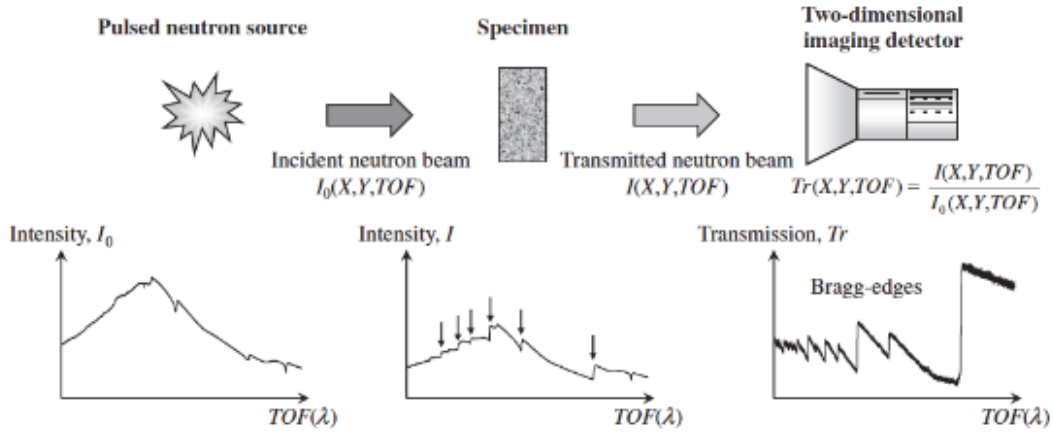

Figure 5.1.2 Schematic layout of transmission 2-dimensional–imaging measurements (top row), and the incident and transmitted time-of-flight intensity profiles and the Bragg-edge profile (bottom row). From Sato et al. [76].

Inelastic scattering: spectroscopy

In lattice dynamics $\left|\vec{k}_0\right| > \left|\vec{k}_1\right|$ and $\left|\vec{k}_0\right| < \left|\vec{k}_1\right|$ of the scattering triangle correspond to phonon creation and phonon annihilation, respectively. The scattering vector is expressed as $\vec{Q} = \vec{\tau} + \vec{q}$, where $\vec{\tau}$ is a reciprocal lattice vector and $\vec{q}$ is the reduced wave vector of a phonon with respect to the Brillouin-zone center. This 1-phonon inelastic scattering can be extended to higher-order multiphonon processes. Thus far pulsed-source spectrometers designed for the measurement of phonon dispersion relations or phonon density of states are typically found only at high-power neutron sources because of the demand for high neutron flux and complicated instrumentation.

Of relevance to CANS applications that detect specific gamma rays emitted by neutron-induced resonances in a metallic foil is the broadening of the resonance peak due to nuclear motion (phonons). The measured cross section of a neutron–nucleus reaction is the sum of contributions from individual neutron–nucleus interactions. Therefore, thermal motion of atoms (nuclei) in the sample will give rise to the nuclear Doppler effect, leading to the broadening of the resonance width of the gamma emission corresponding to a $\left(\mathrm{n},\gamma\right)$ reaction (see below). As vibrational amplitudes of atoms vary with temperature, resolution can be improved by keeping the foil at a low temperature. Conversely, precise measurements of the resonance widths would probe the temperature of the nuclei in condensed matter.

At high energies, the scattering process happens in such a short time that the neutron does not “see” the interaction of the impacted atom with its neighbors, and the scattering is as if from a free atom. In this impulse approximation, there is no difference between self and collective motion or between coherent and incoherent scattering. Here we enter the regime of DINS. A recoil peak in the inelastic spectrum is observed, centered at the recoil energy, which is inversely proportional to the mass of the scattering atom. The profile of this peak carries information regarding the initial momentum distribution of the atoms imposed by many-body interactions in the medium. DINS is well suited for research at CANS by virtue of the sources’ rich epithermal neutron flux. In particular electron-driven CANS facilities in principle are best suited to DINS experiments due to the normal short pulse widths of the e-linac whereas typical proton-driven CANS would sacrifice too much intensity for short-pulse operation.

Refraction

In dense materials, neuron waves propagate with a slightly different wave vector, k_1, than in vacuum, k_0. The ratio $k_1/k_0=\eta$, where η is the index of refraction of the material, is familiar in the optics of ordinary light. The refractive index is

$$\eta = 1 - \frac{1}{2\pi} n_d \lambda^2 \langle b \rangle, \tag{5.4}$$

where $\langle b \rangle$ is the average coherent scattering length and n_d is the atomic number density. For most materials, $\langle b \rangle$ is a positive number, so the refractive index is usually less than 1.0 with a residual proportional to the square of the wavelength. Refraction of the beam is always very small; nevertheless, material compound lenses have been developed to focus a beam of long-wavelength neutrons [78].

Surface reflection

When neutrons impinge onto a surface, they reflect as from a mirror (specular reflection, angle of incidence = angle of reflection). For neutrons incident from vacuum at grazing angle ϑ_o and transmitted at angle ϑ_T, the angles are related by Snell's law, $\cos\vartheta_o = \eta\cos\vartheta_T$. Because, usually, $\eta < 1$, neutrons are usually reflected back into the vacuum. If $\vartheta_T \to 0$, the transmitted wave simply travels along the surface, no neutrons penetrate the material, and the incident neutrons are totally, that is, 100% reflected. The corresponding incident grazing angle is then the "critical angle",

$$\vartheta_o^{crit} \approx \sqrt{\frac{1}{\pi}\lambda^2 n_d \langle b \rangle}\ , \tag{5.5}$$

which is proportional to the wavelength.

For example, the critical angle for 2 Å neutrons on natural nickel, ($\langle b \rangle = 10.3$ fm, atomic density $n_d = 9.1\times10^{22}$ atoms/cm^3, and $n_d\langle b \rangle = 9.4\times10^{11}\,\mathrm{cm}^{-2}$), $\vartheta_o^{crit} \approx 1.09\times10^{-2}$ radians $= 0.62°$. For angles less than ϑ_o^{crit}, the reflectivity remains 100%; for angles greater than ϑ_o^{crit}, reflectivity is less than 100% and some neutrons travel into the bulk. Hence, neutron reflectivity measurements as a function of the incident grazing angle reveal the variation of the (scattering length) density normal to the surface. They are useful to study thin films and interfaces.

5.1.2 Non-scattering interactions

The cross sections of reactions such as $(\mathrm{n},\gamma),(\mathrm{n},\mathrm{p}),(\mathrm{n},\alpha),(\mathrm{n},2\mathrm{n})$ are treated within the framework of the compound-nucleus model first proposed by Niels Bohr in 1936. Only *s*-wave neutrons are needed for applications pertinent to CANS. The low energy of the *s*-wave neutrons also implies a well-defined surface of the target nucleus characterized by the nucleus radius R_X. For simplicity, we assume the spin of the target nucleus is zero.

The scattering amplitude can be expressed as

$$f = -k_0 R_X \tan\left(k_0 R_X + \delta' + i\delta''\right) , \tag{5.6}$$

where δ' and δ'' are the real and imaginary part, respectively, of the neutron-energy-dependent phase shift, δ. In general, the scattering cross section is composed of the potential scattering $\left(A_{pot}\right)$ and resonance scattering $\left(A_{res}\right)$ components:

$$\sigma_s = \frac{\pi}{k_0^2}\left|A_{res} + A_{pot}\right|^2 , \tag{5.7}$$

where

$$A_{res} = \frac{-2ik_0 R_X}{f - ik_0 R_X}, \tag{5.8}$$

and

$$A_{pot} = \exp\left(2ik_0 R_X - 1\right). \tag{5.9}$$

The reaction cross section is

$$\sigma_r = \frac{\pi}{k_0^2}\frac{-4k_0 R_X \,\mathrm{Im}\, f}{\left(\mathrm{Re}\, f\right)^2 + \left(\mathrm{Im}\, f - k_0 R_X\right)^2}. \tag{5.10}$$

From Eq. (5.8), A_{res} is the maximum when $f = 0$, which occurs at a series of resonance energies E_n. By denoting the half-widths of the n^{th} resonance for scattering and reaction by $\Gamma_{s,n}$ and $\Gamma_{r,n}$, respectively, the scattering and reaction cross sections can be expressed in terms of the Breit-Wigner formula as

$$\sigma_s = \frac{\pi}{k_0^2}\left|\frac{i\Gamma_{s,n}}{\left(E - E_n\right) + i\Gamma_{s,n}/2} + 2k_0 R_X\right|^2 , \tag{5.11}$$

and

$$\sigma_r = \frac{\pi}{k_0^2}\frac{\Gamma_{s,n}\Gamma_{r,n}}{\left(E - E_n\right)^2 + \Gamma_n^2/4}, \tag{5.12}$$

where

$$\Gamma_n = \Gamma_{s,n} + \Gamma_{r,n}. \tag{5.13}$$

There are huge numbers of resonances, mostly occurring at higher neutron energies, "*resonance neutrons*."

Figure 5.4 shows the total cross section of Ta-181 in the low-energy range.

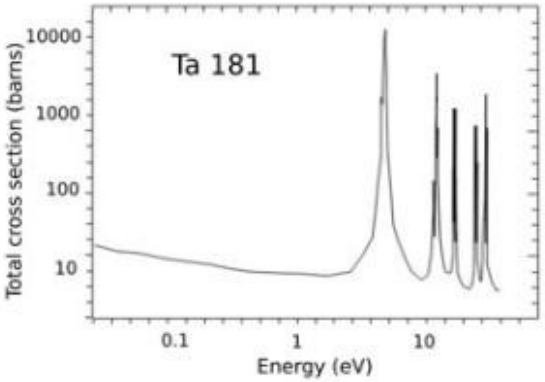

Figure 5.4 The total cross section of Ta-181 as a function of neutron energy.

This formalism relates the resonance widths to the compound-nucleus structure via the logarithmic derivative of the radial wavefunctions, Ψ_0, at the nuclear boundary:

$$D_0 = R_x \left[\frac{d\Psi_0/dr}{\Psi_0} \right]_{r=R_x}, \tag{5.14}$$

where the subscript 0 accentuates the *s*-wave scattering. Furthermore, it can be shown that if D_0 is energy independent and $|D_0| \gg k_0 R_x$, and there is no nearby resonances,

$$\sigma_r \propto \frac{1}{\sqrt{E}} \propto \frac{1}{v}. \tag{5.15}$$

This accounts for the $1/v$ behavior of the neutron absorption cross section that is observed experimentally in general.

If the target nucleus has non-zero spin *I*, the cross section corresponding to a neutron target and the entrance-exit channel configuration of a spin S $\left(S = I + 1/2 \text{ or } I - 1/2\right)$ has to be weighted by the statistical weight of $\frac{2S+1}{2(2I+1)}$.

5.1.3 Neutron capture–induced radiation

Neutron capture almost inevitably is followed by prompt (~10^{-15} s) emission of gamma rays characteristic of the reaction, amounting to the binding energy (several MeV) of the compound nucleus—prompt capture gammas. The residual nucleus may be unstable against beta decay and therefore have long life (seconds, years), the decay emitting an electron or positron and characteristic gamma rays. Energetic, massive charged particles, e.g., α , delayed n, emerge from many reactions (i.e., fission). Some produce spectra of conversion electrons when the capturing nucleus de-excites by knocking out one of the atomic electrons with kinetic energy equal to the decay energy.

Therefore, detecting the fingerprint energies of prompt and delayed gamma radiation emitted from neutron capture provides a suite of neutron-in-gamma-out techniques for examining compositions of the constituent nuclei in materials, including imaging (see Section 6).

One or another of these processes that produce charged particles is always the basis for detecting slow neutrons, which otherwise have insufficient energy to leave an electronically detectable trail.

- Neutron-capture reactions that produce light charged particles commonly used in detecting slow neutrons:

$$n + {}^{3}He \rightarrow {}^{3}H + {}^{1}H + 0.764\ \text{MeV}, \tag{5.16}$$

$$n + {}^{6}Li \rightarrow {}^{4}He + {}^{3}H + 4.79\ \text{MeV}, \tag{5.17}$$

$$\begin{aligned} n + {}^{10}B &\rightarrow {}^{7}Li^{*} + {}^{4}He \\ &\rightarrow {}^{7}Li + {}^{4}He + 0.48\ \text{MeV}\ \gamma + 2.3\ \text{MeV}\ (93\%), \\ &\rightarrow {}^{7}Li + {}^{4}He + 2.8\ \text{MeV}\ (\ 7\%), \end{aligned} \tag{5.18}$$

$$n + {}^{14}N \rightarrow {}^{14}C + {}^{1}H + 0.626\ \text{MeV}. \tag{5.19}$$

  The ^{3}He and ^{6}Li capture reactions are notable because there is *no associated gamma radiation*.

  The ^{10}B capture is at the center of BNCT, in which a tumor-specific pharmaceutical molecule carries ^{10}B to a site that is to be attacked; slow-neutron irradiation follows, which releases the high-specific-damage ^{4}He particles locally, kills the tumor cell but producing little damage to nearby tissue (see Section 6).

- Neutron capture that produces *no charged particles*:

$$\begin{aligned} n + {}^{1}H &\rightarrow {}^{2}H \\ &\rightarrow D + 2.2\ \text{MeV}\ \gamma. \end{aligned} \tag{5.20}$$

- Neutron capture reactions that produce prompt electrons:

$$\begin{aligned} n + {}^{155}Gd &\rightarrow Gd^{*} \\ &\rightarrow \gamma\text{-ray spectrum + conversion electrons (}\sim 70\text{-}180\ \text{keV}), \end{aligned} \tag{5.21}$$

$$\begin{aligned} n + {}^{157}Gd &\rightarrow Gd^{*} \\ &\rightarrow \gamma\text{-ray spectrum + conversion electrons (}\sim 70\text{-}180\ \text{keV}), \end{aligned} \tag{5.22}$$

$$\mathrm{n} + {}^{103}\mathrm{Rh}\ (\mathrm{T}_{1/2} = 42.3\ \mathrm{s}) \rightarrow {}^{104}\mathrm{Pd} + \text{decay betas}\ (E_{\max} = 2.44\ \mathrm{MeV}) + \gamma\text{-ray spectrum.} \tag{5.23}$$

The first of these uses the conversion electrons in imaging plate detectors; the last is the basis for reasonably-fast-responding self-powered detectors, all for slow neutrons.

- Prompt capture gammas: These are typically derived from heavy nuclei that happen to have large thermal neutron capture cross sections because of the presence of low-energy resonances. In neutron detection applications, the gamma rays excite a gamma-ray detector (scintillator, solid state device). Examples are

$$\begin{aligned} \mathrm{n} + {}^{113}\mathrm{Cd} &\rightarrow {}^{114}\mathrm{Cd}^{*} \\ &\rightarrow \gamma\text{-ray spectrum (for thermal neutrons),} \end{aligned} \tag{5.24}$$

and similarly for detection at nuclear resonance energies:

$$\begin{aligned} \mathrm{n} + {}^{181}\mathrm{Ta} &\rightarrow {}^{182}\mathrm{Ta}^{*} \\ &\rightarrow \gamma\text{-ray spectrum (for 4.28-eV neutrons),} \end{aligned} \tag{5.25}$$

$$\begin{aligned} \mathrm{n} + {}^{197}\mathrm{Au} &\rightarrow {}^{198}\mathrm{Au}^{*} \\ &\rightarrow \gamma\text{-ray spectrum (for 4.906-eV neutrons),} \end{aligned} \tag{5.26}$$

$$\begin{aligned} \mathrm{n} + {}^{115}\mathrm{In} &\rightarrow {}^{116}\mathrm{In}^{*} \\ &\rightarrow \gamma\text{-ray spectrum (for 1.46-eV neutrons).} \end{aligned} \tag{5.27}$$

$$n^{\frac{1}{2}\uparrow} + {}^{3}He^{\frac{1}{2}\downarrow} \rightarrow \left\{ \begin{array}{c} {}^{1}H^{\frac{1}{2}\uparrow} + {}^{3}H^{\frac{1}{2}\downarrow} \\ or \\ {}^{1}H^{\frac{1}{2}\downarrow} + {}^{3}H^{\frac{1}{2}\uparrow} \end{array} \right\} + 0.764\,MeV. \tag{5.28}$$

5.1.4 Neutron-induced radiation effects

Whereas slow neutrons, by virtue of their low energies, are ideal to probe the physical properties involving low-lying vibrational states associated with atomic/molecular motion and magnetic energy levels near the ground state, typically in thermodynamic equilibrium defined by the sample environment without altering the chemistry or the electronic orbitals of the materials, fast neutrons, upon the bombardment of a solid, are capable of inducing substantial radiation damage. At ~10^{-18} s, a fast neutron transfers a part of its kinetic energy to a primary knock-on atom (PKA), ejecting it from its equilibrium position (e.g., a lattice site). The PKA may displace other atoms—the secondary knock-on atoms—along its recoil trajectory, generating a displacement cascade (in ~10^{-13} s). After recombination, relaxation, and clustering with neighboring atoms in ~10^{-11} to ~10^{-8} s, local defects such as vacancies, Frenkel pairs, and clusters are formed. Additionally, transmutation of atoms may take place, for example, the formation of the hydrogen and helium from nuclear reactions involving protons, neutrons, and deuterons. For structural

materials such as containment vessels of fission and fusion reactors and beam line windows of particle accelerators, a major research area is the manifestation of cumulative radiation damage in the formation of dislocations, voids, bubbles, and other microstructures that are prone to embrittlement, fracture, and creep growth.

5.1.5 Neutron slowing-down and thermalization

The atomic structure and the spectra of atomic vibrational, rotational, and diffusive motions are evidenced in the differential inelastic scattering cross-sections of condensed matter systems. These depend on the detailed thermodynamic state, as well as the chemical composition of the materials. And these are often the object of inelastic scattering studies because they reveal fundamental properties of the materials; they are mostly are carried out using spectrometers at the large neutron sources. In addition, the scattering cross-sections determine the time- and energy-dependent slowing-down (thermalization) properties of materials used as moderators in slow-neutron sources, which is especially important in pulsed sources; the *scattering kernels*, i.e., $\sigma_{ij}\left(E_i \rightarrow E_j, \Omega_i \rightarrow \Omega_j\right)$ for all possible *i* and *j*, are the basis of neutron transport calculations. It is a daunting challenge to derive scattering cross-section (kernels) applicable to the detailed structure and atomic motions in any material, although the capability to do so is very much desired. Here, σ_{ij} includes uniform translation, collisions, continuous slowing down, decay, and introduction from an external source of neutrons, governed by the Boltzmann equation in terms of the angular flux in phase space. An analytic approach is to approximate neutron transport described via the Boltzmann equation by the diffusion equation, using the method of multigrouping—i.e., separating the flux per energy group then solving a system of coupled diffusion equations. Unfortunately, such analytic techniques do not offer closed-form solutions. An alternative approach is the Monte Carlo method, which is based on the use of random sampling to obtain the solution of the Boltzmann equation. This permits a collection of histories of calculated trajectories between numerous events σ_{ij}. The final result is obtained by calculating a statistical average of the histories.

Direct measurement of the neutron spectral output of moderators serves the needs of neutron source and instrument designers. Consequently, such moderator characterization is a major application of CANS, inasmuch as the measurements are most conveniently carried out using neutron sources of moderate intensity. Measurements provide a check on calculations using whatever kernels or approximations exist, in Monte Carlo simulation codes such as MCNP [79], GEANT 4 [80], PHITS [70] which account for macroscopic moderator geometry and surroundings. The combination of such measurements and calculated simulations makes for the most efficient means for source and instrument optimization (see Section 6.1).

The performance of a neutron moderator is often characterized by lethargy. Here, lethargy is defined as

$$u \equiv \ln \frac{E_0}{E}, \tag{5.29}$$

where E_0 is a reference energy, typically the highest reachable energy of the neutron. If neutrons slow down to lower energies, lethargy increases. Thus the efficiency of neutron thermalization and slowing down hinges upon the average gain of lethargy by a scattering event, described by the variable ξ. Good moderator materials, characterized by the moderating power, $\xi \sum_s$, have large scattering cross sections, $\sum_s$ (and small absorption $\sum_a$) and require a small amount of scattering for slowing down. For example, the moderating powers of H_2O and beryllium are 1.35 and 0.162, respectively.

5.1.6 Magnetic interactions

The neutron–electron interactions include the neutron moment–electron charge interaction termed the *Foldy interaction*, the neutron spin–neutron orbit interaction, the diamagnetic interaction, and the neutron magnetic dipole–electron dipole interaction. The last one, abbreviated as dipole-dipole interaction, dominates the rest (accounting for ~99% of the total) cross-section and provides the basis for neutron magnetic scattering studies of magnetism in materials.

Neutron magnetic dipole–electron dipole interactions: Neutrons scatter from unpaired atomic electrons. The magnetic scattering depends on scattering factors that correspond to the magnetization density distribution—spin and orbital contributions—in the magnetic substance, which underlies the physics of magnetism and its applications. Magnetic elastic scattering probes the average (static) magnetic structures—long- or short-range ordered or frustrated configuration of the magnetic moments in crystalline or disordered materials. Magnetic inelastic scattering reveals the excitations (dynamics) of individual or collective magnetic fluctuations in the system. The virtue of magnetic interactions is the neutron's ability to sense the *unpaired* electrons that are the source of magnetism and the associated properties. Reflectivity measurements using polarized neutrons probe the magnetization density profile normal to a surface or buried interfaces at a depth resolution of ~1 nm.

Neutron trajectories under a magnetic-field gradient: Neutron paths bend while passing through inhomogeneous magnetic fields, which are optically birefringent. That is, the energy of the field interaction is opposite for neutron magnetic moments, $\vec{\mu}_n = -\gamma_n \vec{\sigma}$ spins $\vec{\sigma}$ aligned and anti-aligned with the magnetic field. Here, γ_n is the neutron Larmor constant. The potential energy of a neutron in a magnetic field $\vec{B}(\vec{r})$ is $V(\vec{r}) = -\vec{\mu}_n \bullet \vec{B}(\vec{r})$, and the force on the neutron is $\vec{F}(\vec{r}) = -\vec{\nabla}(\vec{\mu}_n \bullet \vec{B}(\vec{r}))$. Neutron magnetic moments and spins precess (in opposite senses) around the magnetic field vector in a magnetic field at the *Larmor frequency*, $\omega_L = \gamma_n \left|\vec{B}\right|$. This treatment forms the basis for the development of neutron focusing lenses, polarizers, and spin-echo spectroscopy.

Polarized neutrons: In some important instances, neutrons in randomly polarized beams can be separated into "up," that is, those with spins parallel to a reference magnetic field direction, and "down," those with spins that are antiparallel [81]. Polarized neutron beams are manipulated to great advantage in some neutron scattering instruments, aiming to provide complete 3-dimensional (3D) polarization analysis [82] of the scattered neutrons. Without polarization analysis, neutrons scattered from and transmitted through magnetic substances always contain superimposed components of nuclear and magnetic interactions. Experimentation using polarized neutrons permits the separation of these components, provided that the

intrinsic nuclear-magnetic coupling is sufficiently small, thereby providing an unambiguous measure of the magnetization distribution at atomic scale (scattering) or as macroscopic images (radiography) within the materials.

5.2 Neutron Detectors

Neutrons are detected through reactions with nuclei resulting in the prompt emission of charged particles and photons. Virtually all types of interactions described earlier can be used in principle in a neutron detector, although those most commonly used are the nuclear reactions that result in prompt energetic charged particles. The detection approach can be conveniently classified according to (1) the neutron interaction process on which it is based and (2) the neutron energy range of interest. For the latter, we distinguish between slow/thermal, epithermal, and fast neutrons. The boundaries between these ranges, in the present context of detector category, differ from those given Table 2.1 in the context of neutron sources and neutron applications. Here, slow/thermal neutrons are those below the cadmium cutoff of 0.5 eV, whereas fast neutrons have energies above, say, 10 keV. The epithermal range falls in between and is characterized by element-specific resonances in the neutron cross section. Fast neutrons can deposit a fraction of their kinetic energy in the detector, which is sufficiently large to be measured accurately and thus provide a basis for fast neutron spectroscopy. On the contrary, in the slow/thermal range the energy that can be deposited in a detector is too small to be useful; and more complex instrumentation (e.g., crystal monochromators) is required for neutron energy measurements.

In recent years, the so-called ^{3}He crisis has motivated new developments in neutron detectors. Tubes filled with ^{3}He gas as a detection medium are the workhorse of thermal neutron detection. They are commercially available (see, e.g., [83]) but have become a scarce resource following the decline in the tritium inventory in the nuclear weapon stockpile. The need for alternatives has triggered a whole new line of detector research toward helium replacement. [84] From the landscape of ongoing developments, a convincing alternative is yet to be found, [85] but some results are promising [86].

For some applications of CANS, the detection of gamma rays is also required. Both neutron and gamma ray detection can be accomplished by adopting/adjusting detection approaches used in other fields. Neutron and gamma-ray detectors are used in many application areas [87-89], and the most authoritative reference in the field is a textbook by the late Prof. G F Knoll. [90] It is usually the case, however, that detectors available from other fields are not optimized for new applications, and further innovation and development is required. [91-93] Whether it is for application in experiments at the CANS itself or as a part of an instrument at a larger neutron sources, a CANS is definitely a suitable environment for testing new detector concepts. For instance, a number of detector technologies were developed over the years at HUNS, including 2D position-sensitive neutron detectors, [94-99] a wavelength-shifting fiber detector, [99] direct-readout pixel-type detectors, [98, 100] a boron-type GEM detector, [101] and a neutron image intensifier. [101] A neutron resonance absorption spectroscopy system is also available at HUNS [102] which uses lithium-glass scintillator pixel-type detectors for neutron absorption spectrum recording and BaF_2 scintillation detectors for prompt gamma-ray measurements.

A comprehensive survey of thermal neutron detection methods for CANS is beyond the scope of this report. The following is a summary list of the main methods.

- **^{3}He gas–filled detectors.** ^{3}He-filled proportional counters feature the highest possible efficiency. This is in part because the neutron absorption cross section is large, and 100% neutron absorption is achieved in a compact detector by raising the gas pressure to 5–10 bar. In addition, detectors can be built so that the energy of the proton and triton produced by the neutron absorption is fully deposited in the ^{3}He gas, with minimal losses to the wall (the "wall effect"). Furthermore a ^{3}He-filled tube is relatively insensitive to gamma rays (gamma ray interactions take place mainly in the metal walls of

the detector). Spatial resolution is achieved by using smaller-diameter tubes (0.5-inch diameter is a typical number but thinner "straw" tubes are also available), usually at the expense of somewhat lower efficiency. The count rate in this type of detector is limited to, say, 30 kHz per detector unit because of the long charge collection time (several μs) associated with an electron drift velocity in the gas of a few cm/μs.

- **Position-sensitive gas detectors filled with ^{3}He.** A multi-wire proportional chamber (MWPC) is the position-sensitive variant of a proportional counter. [103] It consists of a planar array of thin anode wires mounted between two cathode plates with readout strips. The strip orientation on the two cathodes is orthogonal. The spatial resolution across the wires is determined by the wire distance, usually >1 mm. Count rates of 300 kHz per detector are possible because of the shorter charge collection times (1 μs) of MWPCs. Both proportional counters and MWPCs have an additional count rate limitation of 10 kHz/mm^2 due to the slow ion drift motion that results in space charge buildup. Usually these count rate limitations are not a concern for the relatively low neutron fluxes available at a CANS. For even higher count rate capability, micro-pattern gas counters can be used. [104] Micro-strip gas chambers, gas electron multipliers, and micromegas are other recently developed detectors belonging to this class.

- **BF_3 proportional counters.** Boron compounds are usually available for detectors in solid form. An exception is BF_3, which is a gas and can be used as an alternative to He^3. The ^{10}B cross section for neutron absorption is a few times lower than that for ^{3}He, so higher gas pressures are required to reach the same efficiency. BF_3 is toxic.

- **Scintillator detectors.** A scintillator detector is made of scintillating material containing a neutron absorber coupled to a photon detection system. Lithium-6 is a commonly used absorber nucleus. Unlike gas detectors, scintillators are generally sensitive to gamma rays, but satisfactory pulse height separation between neutrons and gamma-rays is achieved in selected scintillators such as Ce-doped ^{6}Li-glass and ^{6}LiF/ZnS films. The charged particle range in a solid is very short (on the order of 10 μm); therefore, scintillators can in principle provide better spatial resolution than gas detectors. Scintillators are also faster, and count rates of MHz/mm^2 are possible, depending on the photon detection system. Using wavelength-shifting scintillating light fibers, [99] the ultraviolet light from a scintillating screen can be converted to green light in a fiber and transported to multi anode photomultiplier tubes. [105] Spatial resolutions of a few mm have recently been achieved with this approach. [106] Much better spatial resolutions (approaching 10 μm) are possible in the case of ^{6}LiF/ZnS films used for neutron radiography/tomography. In that case, the light emitted by the screen is measured by an integrating photon detector, such as a charge-coupled device camera. The thermal neutron detection efficiency of scintillators is typically 20%.

- **^{10}B film detectors.** In this type of detector, ^{10}B coating is used on a gas or solid state detector. Absorption of thermal neutrons in ^{10}B results in the emission of a triton and an ^{4}He particle traveling in opposite directions. Only one of the two particles can leave the ^{10}B layer and be detected (e.g., in the gas) provided its range is longer than the ^{10}B layer thickness. Owing to the range of the triton and ^{4}He particle, which is a few μm, the intrinsic efficiency of a pure ^{10}B layer orthogonal to the neutron beam cannot exceed 6.5% for thermal neutrons. Boron-10–lined tubes have a 10% efficiency because two ^{10}B layers are crossed by each neutron. More complex arrangements of multiple boron layers are needed to achieve higher efficiencies. [86, 107] With >20 layers of ^{10}B oriented orthogonal to the neutron beam the efficiency can exceed 50%. [108] As an alternative, fewer layers with an inclined geometry can achieve a comparable efficiency. [86, 109]

6. Applications

Particle accelerators and neutron sources have evolved from nuclear science and technology as versatile machines because they ultimately manipulate nuclei and isotopes that are constituents of all matter in the universe. CANS have high potential to enable economical, peaceful, and safe applications that affect all aspects of life. In the last two decades, we have witnessed a rapid growth of CANS in various aspects of size, power, and instrumentation, pointing to the diversity in utilization. In the following session we wish to revise some examples of applications which can be exploited with a CANS, without implying their necessary inclusion any of them and some recent important developments and the opportunities of future applications.

6.1 Experimental Neutronics and Device Development

A goal shared by all pulsed neutron sources is to achieve high-brilliance neutron spectra with optimal time structures, a task to be accomplished by neutronic design and engineering of the target–moderator system. Testing and prototyping of design structures are best done at a small source because its relatively simple accelerator, low neutron fluxes, and mild gamma radiation and residual activity can facilitate the work using compact, flexible-to-reconfigure shielding. After the performance parameters are achieved, the design is scaled up according to the power of the source. The Hokkaido e-linac facility and the ZINGP of Argonne were among the first small sources that carried out numerous neutronics experiments and contributed critical design innovations to second-generation neutron sources. This task, to which many CANS have contributed, continues today because of increasing demands for the upgrade of existing facilities and construction of yet newer and bigger sources.

For the development of neutron target–moderator systems, work at CANS includes (a) measurement of scattering kernels of moderator materials; (b) testing and validation of moderator concepts, including moderator geometry, design of premoderators, poisoned decouplers, grooved surfaces, and inhomogeneous structures (e.g., interleaved polyethylene and silicon single crystals); (c) characterization of performance, e.g., the energy spectrum and pulse-width variation of various moderator media (e.g., water, para-to-normal hydrogen, methane, methanol, ethanol, benzene, benzene methanol, mesitylene) under different configurations and operation conditions; and (d) proton heating of the targets and required cooling.

Surrounding the moderator-reflector assembly are beam-extraction optics. Successful engineering of these optic devices relies on the experimental exploitation of neutron thermalization and transportation in the phase space in which slowing-down scattering, reflection, refraction, and absorption take place. In the development of devices and beam line instrumentation, both CANS and reactor sources have contributed to device testing and evaluation. This includes three classes of neutron beam-focusing devices which exploit the neutron's optical and magnetic properties, see Sections 5.1.1 and 5.1.6. The devices are: i) Reflective: super-mirrors; ii) Refractive: compound focusing lenses; and iii) Magnetic: polarizing, and focusing lenses.

CANS are particularly suitable for testing and evaluation of beam line instruments because the open geometry of the flight path can easily accommodate new instrumentation modules with flexible, trial-and-error shielding arrangements. Their contributions in this area include (a) mini-focusing SANS at HUNS, (b) SESAME spin-echo scattering techniques at LENS, and (c) neutron radiology and tomography.

Documentation of the results of experimental neutronics and device development can be found in the Proceedings of ICANS [110-112] and UCANS [107-108].

6.2 Materials Characterization

Many CANS have initiated programs of neutron scattering for materials characterization to complement the work of large neutron scattering facilities in education, user training, demonstrating proof-of-principle experiments, and sharing the load of research problems that are not hindered by low neutron fluxes. Generally, only elastic scattering— i.e., small-angle scattering, reflectometry, and total-scattering measurements—has been pursued at CANS. Short-pulse sources such as electron linac–driven CANS can also carry out TOF powder diffraction. Taking advantage of the cold neutrons usually available at CANS, research programs are in general successful, albeit limited in throughput and Q resolution. Note that most CANS are spin-offs from legacy accelerator projects not previously intended for materials research. Thus investing in competitive neutron scattering instruments was not an viable option.

Recently, prompted by an anticipated reduction in neutron scattering capacity resulting from the concentration of materials research using neutrons at only a few very powerful facilities, the neutron community has begun to contemplate high-brilliant CANS dedicated to materials research. This is an attractive option because not only have the accelerator and neutronics technologies of CANS come a long way, but also realizing these high-brilliant, compact machines is reasonably affordable and expeditious compared with building high-power spallation sources. Novel concepts include versatile accelerator systems that support multiplexing of target–moderator stations and optimized beam extraction optics and instrumentation for neutron scattering. [113]

6.3 Interrogation

The realm of interrogation for civil and safeguards applications is so vast that multitudes of tools and methods with high precision and sensitivity are ever more needed. The neutron as an interrogative probe exhibits several important advantages, including remote detection; nonintrusiveness; high sensitivity of chemical density, including 3D volumetric rendering and element and materials specificity; rapid data collection; and visualization. The flexibility of CANS for portable, on-site deployment and automation adds crucial incentives for wide-ranging applications. A suite of techniques based on the "neutron-in-gamma-out" reactions, including prompt-gamma neutron activation (PGAA) analysis, and delayed (after irradiation) neutron activation analysis, have been established. The systems to be deployed are called (n, γ) devices. Table 6.1 lists the properties of these techniques with examples. Furthermore, energy-dispersed emitted γ-rays can be recorded for element-specific imaging, giving rise to prompt gamma ray activation imaging), neutron resonance capture imaging, neutron resonance transmission imaging (NRTI), and neutron diffraction imaging.

Conventional neutron radiography and computed tomography permit 2D and 3D rendering of an object through analysis of the transmitted intensities of a wide beam. Neutron diffraction and spectroscopy enable characterization of the detailed structures of atomic/molecular organization. These systems employ a CANS that emits neutrons into the object or the environment under interrogation and measures the energy and time distribution of the scattered neutrons; hence they are termed (n, n) devices. The interrogating power increases significantly if the combined technology also uses epithermal and fast neutrons, which are readily supplied by CANS. Moreover, parallel development of complementary detector systems, optics devices, and computer-aided data collection and interpretation schemes is essential to fully exploit the potential of the neutron methodology.

The field of applications includes art and archaeology, mineralogy and geology, environmental protection, industrial product inspection, landmine detection, explosives, nuclear substances and contraband, well logging, medical therapy, basic research, and education. Useful information can be found in recent International Atomic Energy Agency (IAEA) reports on the use of neutron generators [114] and databases for prompt-gamma neutron activation analysis. [115] Excellent reviews in recent

literature include [116-118] on methodology, [119, 120] on archeological and cultural heritage research, and [121] on body composition analysis.

Table 6.1. The properties of "neutron-in-gamma-out" methods and associated neutron activation analyses

Methods	**Examples (cross section σ, yield Y, half-life $\tau_{1/2}$)**
Thermal neutron analysis: An object is irradiated by thermal neutrons, producing characteristic gamma rays corresponding to radiative neutron capture (n,γ) by specific constituent	$n + H^1 \rightarrow H^{2*} \rightarrow H^2 + \gamma(2.232\ \text{MeV})$, $\sigma_{n,\gamma} = 0.332$ b, Y=100% $n + N^{14} \rightarrow H^{16*} \rightarrow H^{15} + \gamma(10.829\ \text{MeV})$, $\sigma_{n,\gamma} = 0.0747$ b, Y=14.12%
Epithermal neutron resonance analysis: An object is irradiated by epithermal neutrons, of which certain energies resonate with the nucleus (with a cross section integrated over the resonance energy, σ_r), producing gamma rays from resonance neutron capture reactions	$n + Ag \rightarrow Ag^{110} + \gamma(657.8\ \&\ 884.7\ \text{keV})$, $\sigma_r = 750$ b, $\tau_{1/2} = 248.8$ d $n + In \rightarrow In^{110} + \gamma(1294\ \&\ 1079\ \text{keV})$, $\sigma_r = 3200$ b, $\tau_{1/2} = 54.2$ min $n + Au \rightarrow Au^{198} + \gamma(411.8\ \text{keV})$, $\sigma_r = 1500$ b, $\tau_{1/2} = 2.694$ d
Fast neutron analysis: An object is irradiated with fast neutrons $E >\sim 8\text{MeV}$, producing characteristic secondary gamma rays corresponding to transmutation of irradiated isotopes and inelastic scattering reactions. Measured gamma rays provide information about the relative concentrations of the nuclei	$^{14}\text{N(n, 2n)}^{13}\text{N} \rightarrow \gamma(5.1\ \text{MeV, Y} = 200\%)$, $\sigma = 19$ mb, $\tau_{1/2} = 9.97$ min $^{16}\text{O(n, p)}^{16}\text{N} \rightarrow \gamma(6.129\ \text{MeV, Y} = 69\%\ \&\ 7.115\ \text{MeV, Y} = 5\%)$, $\sigma = 42$ mb, $\tau_{1/2} = 7.13$ s $^{56}\text{Fe(n, 2n)}^{53}\text{Fe} \rightarrow \gamma(5.11\ \text{MeV, Y} = 196\%\ \&\ 0.378\ \text{MeV, Y} = 30\%)$, $\sigma = 10$ mb, $\tau_{1/2} = 8.51$ min
Pulsed fast neutron analysis: An object is irradiated with fast pulsed neutrons (pulse duration of several ns), permitting measurement of the locations of gamma-ray emissions by neutron time-of-flight techniques	Using collimated incident neutron beams allows determination of the 3D distribution of the emitting nuclei in a large cargo
Pulsed fast and thermal neutron analysis: A combined Fast Neutron Analysis and Thermal Neutron Analysis method.	Dual-energy neutron inspection
Nanosecond neutron analysis/associated particle technique: Using mono-energetic d(t,α) n-type neutron generators to produce 14 MeV neutrons and 3 MeV α particles, each generated pair traveling in opposite directions. A neutron is "tagged" by the associated α particle and, by virtue of TOF techniques, the genuine secondary gamma photons can be identified	Using position-sensitive α detectors in conjunction with neutron TOF techniques enables measurements of the 2D spatial distribution of chemical elements with high signal-to-noise ratio

6.3.1 Civil structures

All civil structures are subject to attack by corrosion reactions with the environment. Corrosion of reinforced concrete structures alone costs about 3–4% of GNP in Western countries. For example, the US Federal Highway Administration estimated the direct cost of corrosion to be $276 billion in that country in 2002[122]. A substantial portion of this expenditure can be avoided if effective diagnostic and

monitoring methods are available for preventive maintenance. Neutrons' strong penetrative power and high sensitivity to moisture and bound water offer an edge in technical diagnostics of civil structures.

Neutron interrogation of civil structures can, in principle, be integrated into a program of nondestructive assessment, which includes monitoring and detection of problems, diagnosis of faults and their causes, and prognosis of future progression. Thus far, the lack of transportable neutron sources and proper instrumentation have hindered such a development. Here, we confine our discussion of interrogation of corrosion to concrete bridge decks to illustrate the potential of CANS for this application.

The maintenance of ~2.8 billion ft^2 of bridge decks in the United States accentuates the scope of detection of structural faults before repair and/or replacement can take place. Four deterioration types are critical: delamination, corrosion, cracking, and concrete degradation. Traditional technologies for fault detection include impact echo (chain-drag/hammer sounding, impulse response), ultrasonic (ultrasonic surface waves, ultrasonic pulse echo), electromagnetic (resistivity, eddy current, galvanostatic pulse, half-cell potential, magnetic flux penetration), radiation (ground-penetrating radar, infrared thermography, microwaves), and chemical methods (chloride concentration, dye penetration). The five important performance measures are accuracy, repeatability, ease of data collection and interpretation, speed of data collection and analysis, and cost. The advantages and limitations of these methods of nondestructive evaluation are well documented. [123, 124].

Given the general ~2-m-thick layered structure of a bridge deck, a CANS optimized for fast-neutron radiography and transmission/backscattering evaluation is a promising complementary nondestructive testing approach. Additionally, other mechanical and chemical properties, such as strain/stress distribution and nature of the water content of drilled-out samples, can be characterized by neutron diffraction and spectroscopic techniques in laboratories. To date, in-the-field examination of bridge desks by CANS has not been realized. Some progress has been made in off-site examination of steel bars in thick concrete slabs using fast neutrons from a CANS. [30]

6.3.2 Cultural heritage

The versatility of neutron methods for structural investigations of materials at the atomic/molecular level benefits cultural heritage applications, generating information of interest to restorers, architects, curators, and the general public. Artifacts are generally made of polycrystalline materials, such as metals, alloys, ceramics, and stone, using ancient technologies. Neutron diffraction provides information in a nondestructive way about chemical composition, crystal structures, strain maps, and micro-pore size distribution over local regions or over an entire object. As anticipated, real objects do not conform to the ideal crystal structure. Therefore, detailed examination of the diffraction profile, phase composition, residual strains, and other imperfections can reveal valuable telltale evidence of manufacture processing, utilization, wear and tear, degradation, and so on. At a length scale beyond interatomic distances, SANS can determine the sizes (from tenths to thousands of nanometers) and shapes of inhomogeneous features such as pores, aggregates, and textures in organic and inorganic matters such as bones, stones, ancient tools, weapons, and so on. [125, 126] A very powerful nondestructive evaluation approach is to combine diffraction, neutron-in-gamma-out techniques with neutron radiography and computed tomography [122-123], (see also Fig. 5.1.2).

The application of the above techniques for a systematic approach to cultural heritage studies was proposed and carried out under the Ancient Charm European project in 2007 [125], using facilities at large neutron sources such as ISIS and PSI. A notable example is an examination of two gilded bronze artifacts that are belong to the monumental doors, The Gates of Paradise and the North Gate, located at the Battistero di Firenze. In this study, the Ghiberti heads, by Lorenzo Ghiberti, were analyzed using the neutron results for a reconstruction of elemental distributions on superficial and interior spots at a

resolution of a few nanometers. [126-127] Another recent example is a study ancient musical instruments. [128]

Although the above studies were carried out using neutron instruments at large facilities, there is no fundamental reasons that prohibit such investigations at CANS, as demonstrated by the analysis of isotope composition of a Scandinavian axe by the NRCA technique at GELINA [123-124] and the imaging of crystalline structural information of 15th-century Japanese swords at HUNS [127]. In fact, the neutron beamlines employed for cultural heritage studies at large facilities are general-purpose diffractometers and imaging instruments. Arguably, CANS are amenable to experimental setup on dedicated instruments for investigations of archeological relics and artifacts, for example, to accommodate special sample environment and safeguard requirements. The complex and costly logistics associated with neutron interrogation of artifacts at faraway neutron sources may represent an onerous hindrance to museum curators, art preservationists and the like, as well as to neutron instrument scientists at large facilities. Programmatic studies organized by the cultural heritage community at regional CANS facilities tailored to fulfill the needs of curators and preservationist is a viable approach as the technology of compact accelerators and neutron instrumentation progresses.

6.3.3 Detection of explosives

The quest for innovative technologies capable of automated, reliable, rapid, and safe inspection of concealed substances for security and law enforcement has intensified in recent years. At the top of the list is detection of explosives and illicit drugs in cargos and luggage.

The goal is to develop a technology, albeit comprising several methods, that is capable of conducting quick, reliable, and safe searches for explosives in containers without the need of entering the containers (nonintrusive) or altering the contents (nondestructive). Current practices such as image reconstruction by x-ray scanning and chemical identification analysis are known for their shortcomings. For example, dual-energy x-ray transmission imaging, by which the cross-section for photoelectric effect varies as Z^4, lacks sensitivity to low-Z elements such as N, O, and C that are the key constituents of explosives. The Z-dependence of the cross section of Compton scattering is less steep. The method becomes less reliable in estimation of Z values when heterogeneity is high, i.e., as the beam passes through overlaid thin, strong absorbers and thick, weak absorbers or composites containing different Z elements. Often the method resorts to detecting explosive-related devices such as detonators, switches, and wires that are made up of high-Z elements.

In the case of neutron interrogation, fast neutron analysis (FNA), pulsed fast and thermal neutron analysis (PFTNA), and thermal neutron analysis (TNA) are effective element-specific techniques for identification of items rich in nitrogen (N), oxygen (O), and carbon (C) that match the characteristic N/C and N/O ratios of many explosives. [128] [129] Regarding the choice of appropriate CANS, neutron generators based on d-d and d-t reactions appear to be the most promising, although the application can be benefited by higher neutron fluxes and narrower pulses than those of currently available commercial sources. TOF PFTNA benefited by the short-pulse structure of electron linac–driven neutron sources has also been considered. [130] [131] Preliminary experimental prototypes and Monte Carlo simulations have demonstrated positive results and the feasibility of the operation. [132-134] Here, improved data analysis schemes and higher-performance gamma-ray detectors are vital to enhance reliability (to achieve sufficiently low false-positive and false-negative rates) and speed to warrant successful commercialization. Note that neutron interrogation is not intended to replace existing inspection methods but rather to augment the overall performance of the present and future systems.

A tabletop laser–driven neutron source, [135] owing, in principle, to its compactness and transportability, high repetition rates, very short pulse structure, and high neutron fluxes in the forward direction, is

another possibility. However, the technology is not yet mature enough to be a viable contender for imminent application.

6.3.4 Detection of antipersonnel landmines

Antipersonnel mines are small devices, carrying ~100 g or less of explosive triggered by a sensitive booster charge, that are housed in nonmetallic casings usually buried (up to ~20 cm deep) in battlefields cluttered with metal pieces. These conditions make de-mining using x-ray imaging or metal detectors very difficult and hazardous. Neutron interrogation permits elemental analysis against the chemical composition of explosives. In addition to useful neutron-in-gamma-out techniques such as TNA (fast neutrons thermalized by the soil and explosive), FNA, PFTNA, and nanosecond neutron analysis/associated particle technique (APT), detection of neutrons that are backscattered (or multiply scattered) by the high-density, low-Z elements of the explosive can be an effective alternate method. In the latter case, a 2D neutron detector is needed. Within the various CANS types, d-d and d-t (for APT method) neutron generators are suitable. Various prototypes have been built and are under testing. [136] [137]

6.3.5 Well-logging and mineralogy

"Well-logging" here means extraction of information regarding potential hydrocarbon (HC) (and to a lesser extent other minerals) reserves in the environment surrounding a well bore. This narrow interpretation fits well with the strength of neutron interrogation of HC content by virtue of the extraordinarily large neutron cross section of hydrogen. Useful cross sections include scattering and absorption of neutrons. This implies (n, n) devices are needed. For example, fast neutrons are thermalized through collision with light elements in water/minerals/HC-containing rock formations and eventually are captured. Therefore, owing to the substantial absorption cross section of chlorine, measurements of the macroscopic thermal neutron absorption cross section by neutron detectors at selected distances from the source provides an effective means to estimate the salinity of water in porous rocks. Moreover, if a pulsed neutron source is used, analysis of the measured thermal capture cross section as a function of time—the thermal neutron die-away—reveals the chemical constituents in conjunction with the porosity of the formation. The combination of (n, n) and (n,γ) devices adds a new dimension to well-logging. For example, FNA and puled fast neutron analysis can be applied for the analysis of the C/O ratio in the formation. From PGAA, H, Si, Ca, Fe, S, Cl, and other elements can be identified. Oil and water flow can be monitored by measuring the neutron activation of injected tracers of radioactive particles. For details regarding such practices, see chapters 13–15 of [138].

Nuclear techniques based on (n, γ) and (γ, γ) reactions are widely used in the minerals industry. On-line identification and quantification of elemental contents by neutron interrogation, chiefly by PGAA and delayed neutron activation analysis, as well as transmission measurements, have contributed enormous economic value to the industry. For coal processing alone, for example, continuous determination of the carbon content (hence the calorific value), incombustible minerals (hence better control in burning and coal ash treatment), and moisture (hence improved furnace performance) in raw coal on conveyors and in slurries offer attractive economical and environment-friendly incentives for the industry.

Industries have employed ^{241}AmBe (average ~4 MeV neutrons, usage time 20 years, ~6.6×10^6 n/s, <1g) or ^{252}Cf (average ~2-MeV neutrons extending to ~10 MeV, usage time ~2 years, 3 μg) radioisotopes as neutron sources for many decades. Recently, concerns have been raised regarding the safety, control, and supply of these radioactive isotopes; meanwhile, seal-tube-type d-d and d-t neutron generators have become available commercially. Furthermore, by virtue of the pulse-mode operation of neutron generators, PFTNA can be applied for elemental analysis. For example, the μs-width, 14-MeV fast

neutron bursts from a d-t seal tube enable online measurements of sulfur in coal with a precision of 0.5 wt % and of carbon with a precision of ~1 wt %. [139] However, the technology transfer from radioisotope sources to neutron generators has been slow. A major challenge is the adverse conditions of well-logging (tight spaces like ~12–25 cm diameter boreholes, a high pressure of 150 MPa, elevated temperatures up to 180°C, the presence of water or mud) and mineral processing (a contaminant milieu near conveyor belts or slurries). Thus sealed-tube neutron generators must be engineered to achieve compactness, robustness, and reliability somewhat on a par with the radioisotope sources. Industries also must invest in the development of new calibration schemes, gauges, and data interpretation algorithms.

6.4 Irradiation Effects of Electronics

The interactions of cosmic rays with the earth's atmosphere produce showers of high-energy ionizing particles, including high-energy neutrons, most of which are eventually intercepted by matter in the biosphere. This "cosmic neutron radiation" hits the top of the atmosphere and generates, through particle reactions and nuclear reactions, a cascade of neutrons. Showers of cosmic neutron radiation are intense enough that they can potentially disrupt the normal operation of electronic systems and represent a particular threat to aircraft avionics, with problems ranging from wiping a device's memory, to interrupting its normal behavior, to permanently damaging the electronics. At normal aircraft flying altitudes (30,000 to 35,000 feet) these neutron showers are intense enough to potentially disrupt the correct operation of avionic electronics through single event effects (SEEs). Neutron-induced SEEs on electronics may result in recoverable soft errors such as a single event upset (SEU), e.g., temporary memory data corruption or logic circuit status changes, as well as a permanent hard error, e.g., single event latch-up, a short circuit due to power supply failure. This kind of disruption can also occur at ground level, causing damage to electronic systems used in everyday life.

The increasing density of circuitries as a result of miniaturization renders chips more susceptible to the infliction of an event of this sort. Fast neutrons as high-kinetic-energy neutral particles are hard to shield against. Good design and testing of electronics is necessary to mitigate SEE disruptions to ensure the safety of aircraft systems. Since the end of the 20th century, neutron SEE testing has been moving outside the aerospace sector into other areas such as transport, communications, medicine, and computing systems, where reliable and fault-free electronic systems are required.

A reasonable approach is to understand the microscopic mechanism of neutron-induced radiation damage and to quantify/certify the impact on chip performance. This can be done through accelerated irradiation studies at laboratory sources that produce fast neutron spectra emulating those of atmospheric neutrons at sea level and at avionic altitudes. The acceleration factor, the neutron flux ratio of laboratory sources to the atmospheric environment, would be 10^6 or higher, enabling efficient and accurate measurement. [140]

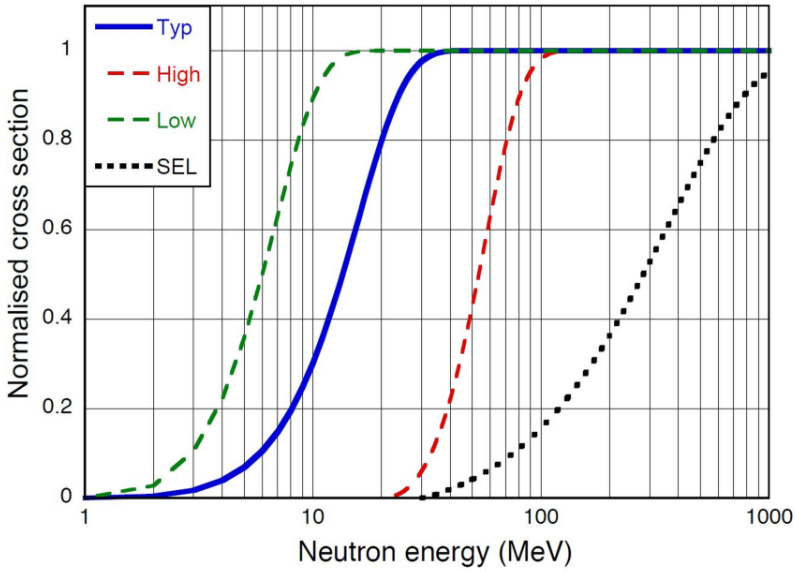

Figure 6.4 Typical cross sections of single event effects (Weibull curves [141]) as a function of neutron energy for cases with typical (Typ), low (Low), and high (High) thresholds and for a single event latch-up.

The energy of the inflicting neutron varies from below 10 MeV to 1 GeV. While large neutron sources such as the TRIUMF, LANSCE, and ISIS facilities have been used to investigate high-energy events, [142] the cross section of SEE, $\sigma_{SEE}(E)$, for $1\ \text{MeV} < E < 60\ \text{MeV}$, is best studied at quasi-mono-energetic (QM) CANS. The underlying rationale is illustrated by the energy dependences of $\sigma_{SEE}(E)$ in Figure 6.4. The profile of an SEU cross section, the so-called Weibull curve, specific to an electronic device can be accurately determined by measurements at a QMCANS with neutron energies below and above the threshold; whereas in the case of white-beam sources, the product of the cross section and the neutron flux integrated over an energy interval is measured. Experiments carried out so far at the HUNS in Japan and at LENS in the United States provided only characterization of the response to an SEE integrated on the all energy spectrum. At these facilities, accelerated testing of electronic devices and systems (between a million and 100 million times) are possible; a measurement of just 1 hour at the facility is equivalent to exposing microchips to high-energy neutrons over hundreds of years of flying time in an aircraft.

At present, only a handful of general-purpose QMCANS—TIARA, CYRIC, and RCNP in Japan; iThembaLabs of South Africa; and TSL of Sweden—are in operation. This small number is inadequate and suboptimal even for initial testing of electronics products. The NEPIR facility at the SPES source—a proton cyclotron–driven QMCANS in Italy that is currently under construction—aims to be a CANS dedicated to studies of SEEs by fast-neutron-irradiation with a quasi mono-energetic and tunable neutron energy option. [143] The latter is made possible by an assortment of thin lithium and beryllium targets, which permit studies of energy-dependent neutron interactions. The accessible energy range of NEPIR is 1 to 65 MeV, which comprises more than 60% of fast atmospheric neutrons. NEPIR will use a specialized neutron production target, the ANEM, capable of producing neutrons with a continuous energy distribution similar to that of atmospheric neutrons over the 1–65 MeV range. New CANS such as the SPES are designed to include a suite of flexible but individually optimized neutron and proton facilities to serve users from academia and industry across multiple disciplines, from neutron scattering and irradiation to isotope production.

6.5 Nuclear Data

Nuclear data are measured properties and numerical quantities that describe nuclear reactions. For example, the information about various cross sections, decay half-lives, gamma-ray emission characteristics, spin states, *Q*-values, and so on mentioned in Section 5 belongs to nuclear data. Because we are not yet able to calculate and predict precisely nuclear phenomena, for example, from first-principles formulism, our understanding of nuclear matter and interactions is rooted in the establishment of nuclear data. Such data, organized and managed by the international nuclear science community, encompass an enormous energy range from 10^{-5} to 10^{9} eV for hundreds of nuclides and thousands of radioisotopes. [144] The main reasons for furnishing new and better data are twofold: to validate theoretical calculations derived from analytical models and numerical simulations which in turn use the database, and to secure new experimental results and improved previous data that are needed to advance the field of nuclear physics and the technology of nuclear applications. Nuclear astrophysics is one of the important areas on the fundamental side. Fission reactors, fusion research, accelerator-driven transmutation and energy amplification systems; nuclear medicine, including health physics; materials characterization and processing; and so on are burgeoning sectors on the applied side.

International communities have contemplated road maps for the acquisition of nuclear data. [145-147] The TOF beamline and the ANNRI at n_TOF-CERN and J-PARC, respectively, permit measurement of nuclear data at energies (up to GeV) and for small amount of sample (less than mg) beyond the capability of CANS [148-150]. Other facilities such as GELINA, FNG, KURRI-LINAC, PAL-PNF [151] contribute nuclear-data measurements at lower energies (see Section 4.1). New CANS such as SPES, LENOS, nELBE, and UTCANS include dedicated beam lines for nuclear data collection (see Section 4.2).

At cold, thermal, and epithermal neutron energies, the scattering enters the “phonon” regime where scatterers in a condensed state are not free. Here phonons are generalized to include atomic and/or molecular vibrations; rotations (free-like or hindered, classical jump or quantum tunneling) of sub-molecular units; and diffusive migration of single atoms, subject to chemical force fluctuations due to binding and dissociation and thermodynamical interactions. The measured total scattering cross section would vary depending on the sample environment and the instrument’s dynamic range. To delineate the phonon effects, experimenters must measure the elastic, quasielastic, and inelastic scattering, which usually requires measurements using specialized spectrometers, at different sample conditions. Traditionally, nuclear data consist of datasets of individual isotope from which data of any substances can, presumably, be formulated according to their chemical compositions provided the result in the thermal-energy region is corrected by modeling of the collective and individual motions of the atoms. Several efforts are underway within the community to develop and exploit more models that are suitable for describing the interactions of neutrons with specific materials. The collection of suitable data against which models may be compared and the validation of this modeling of atomic motions for important nuclear substances is an area where CANS facilities are currently having an increasing a scope.

Furthermore, the data obtained consist of coherent and incoherent scattering, which represents collective and single-particle motion, respectively. Measurements of hydrogenous materials such as water and hydrocarbons, owing to the extraordinarily large incoherent scattering cross section of hydrogen atoms, allow an approximate interpretation of uncorrelated hydrogen-atom motions. Technologies such as fission reactors, nuclear medicine, and well-logging rely on accurate neutron cross section databases of key materials such as light and heavy water, graphite, uranium, plutonium, steels and alloys, hydrocarbons, and proteins that can be obtained by instruments at CANS. A recent example is the re-measurements of the total cross section of heavy water in the 0.0001–1 eV energy range at 20° and 50°C at the Bariloche e-linac-driven neutron source and at LENS. [152]

6.6 Experimental Nuclear Astrophysics

Nuclear astrophysics concerns all the nuclear phenomena in the cosmos, with an emphasis on stellar evolution and the nucleosynthesis of heavy elements beyond iron, which have occurred since a few minutes after the Big Bang (primordial time), including events being observed in the present day. Experimental nuclear astrophysics ranges from observation of the sky on the Earth to satellites, and from analyses of meteorites to measurements of nuclear-reaction parameters at laboratories. The cumulative data constitute a library for the validation of astrophysical models and calculations. Clearly, a comprehensive and accurate database will permit rigorous tests of modeling and aid discrimination of competing theories, leading to a better understanding of the universe as a whole. Man-made accelerators have created particles with sufficient kinetic energies [1 eV (K.E.) = 7,740K] to reach the temperatures of stellar interior or exploding supernovas

We recall the different processes of synthesis of nuclei. They include charged-particle fusion reactions that are responsible for making light elements with mass numbers below ~60. The heavier elements are made by neutron captures in conjunction with competing β decays. When the neutron capture time, τ_n, is much larger than the β lifetime, τ_β, the slow neutron-capture process (s-process) prevails and produces nuclei along the valley of stability. Occasionally, branching points occur on the path when τ_n and τ_β are comparable. The rapid neutron-capture process (r-process), requiring $\tau_n \ll \tau_\beta$, runs into the neutron-rich region toward the neutron drip line, creating unstable nuclei. The rapid proton-capture process (rp-process) runs near the proton drip line. Additionally, photodisintegration reactions (γ-process) produce rare p-nuclei.

A major challenge in experimental nuclear astrophysics is the study of reactions and decay processes far from stability (e.g., the r- and rp-process) for the understanding of nucleosynthesis during stellar explosions such as Type II supernova. The ongoing development of new facilities to provide clean radioactive beams is expected to command a promising role in future experimentation. Here, we point out examples of key experiments on the s-process in nucleosynthesis that can be done at laboratory neutron sources.

One of the challenges in experimental nuclear astrophysics is the study of very low energy at stability to interpret charged particle-induced nucleosynthesis processes during stellar evolution. Small accelerators operating by ^{7}Li(p,n)^{7}Be reaction–produced keV neutrons are ideal for measurements of neutron-capture cross section at very low energies, such as those of $^{143, 145, 146}$Nd obtained by Veerapaspong [153].

Another area of interest regards neutron-induced reactions near stability for the understanding of the s-process. TOF facilities at larger pulsed neutron sources such as the n_TOF-CERN are useful for measurements of capture cross sections up to hundreds of MeV, as well as decay half-lives of the associated (n, γ) reactions. For example, high-precision data of the energy dependence of neutron-source reactions, e.g., ^{13}C(α,n)^{16}O and ^{11}Na(α,n)^{25}Mg, and neutron-poison reactions, e.g., ^{14}N(n,p)^{14}C, ^{16}O(n,γ)^{17}O, and ^{25}Mg(n,γ)^{26}Mg, are critical to s-process calculation of the convection and mixing nature during carbon-nitrogen-oxygen burning stages. An interesting situation arises at the s-process branching points where matter flows can occur by both neutron capture and β decay. Since neutron captures are sensitive to the number of neutrons, accurate measured neutron-capture cross sections and β half-lives allow an assessment of the neutron density. Furthermore, the β half-lives are expected to differ for nuclei in the stellar environment, where the excited states are thermally populated, from those of nuclei in the laboratory, where only the nuclear ground state decays. Thus measurements of s-process abundances at branching points permit determination of the temperatures inside stars. Successful data were obtained from neutron experiments; see [154] and the references therein.

Previous-generation compact neutron sources driven by low-energy ion accelerators imply low flux and long pulses, which severely limit the capability of TOF measurements of weak cross sections. The FRANZ facility, current under construction, is a new CANS capable of producing high-flux, tunable, low-energy neutrons for TOF measurements by virtue of a novel rebunching-compressor design (see Section 4.2.2.2). The ^{7}Li(p,n)^{7}Be reaction of FRANZ is well-suited for the simulation of stellar neutron spectra. It is scheduled to attempt measurements of a series of extremely small neutron-capture cross sections and unstable branch-point nuclei which are essential to further the understanding of *s*-process in nucleosynthesis. [154, 155].

6.7 Neutron Capture Therapy

Neutron capture therapy is a cancer treatment based on targeting neutron-capture-induced radiation (see Section 5.1.3) at cancer cells. It is a complex, multidisciplinary enterprise. This subsection addresses only the prospects for employing CANS as a neutron source for BNCT and the associated neutronics. Details of other prerequisite elements needed in parallel R&D, such as pharmaceuticals, medical imaging, radiobiology, clinical planning and implementation, can be found in [156-160].

BNCT takes advantage of the neutron-capture reaction of ^{10}B(n, α)^{7}Li. The linear energy transfers (LET) of the emitted α-particles and ^{7}Li nuclei are ~100 times higher than those of x-, γ- and β-rays administered by other radiation treatments. Furthermore, the average ranges of ~9 and ~5 μm for α and ^{7}Li, respectively, are comparable to the dimension (~10 μm) of a cell. If a sufficient amount of ^{10}B can be delivered and concentrated on the surface, or preferably in the interior, of *only* cancerous tumor cells, neutron irradiation of the cancer will generate a superlative relative biological effectiveness (RBE) for killing tumor cells while preserving normal tissue. Because the neutron capture cross section of ^{10}B is high for thermal neutrons, and fast neutrons impose negative biological effects on healthy cells, BNCT should be administered with epithermal neutrons (eV to keV range) after taking into account the neutron-thermalization effect by traversing tissues. With regard to neutron sources, there are the concerns regarding fissile materials in the reactor fuel and the difficulty of integrating a nuclear reactor into hospitals or clinical facilities. Therefore, fission reactors (see Section 3.2.1) are not ideal sources for BNCT in spite of the most common practice to date. CANS are a desirable alterative.

The preferable neutron-generating reactions and the corresponding CANS parameters are given in Table 6.2. The CANS correspond to (p, n)- and (d, n)-reaction-driven neutron generators and p/d-linac accelerator-driven sources, in conjunction with a proper target and BSA. In general, the technologies of the front-end proton or deuteron accelerators are well established, although their compactness and efficiency could be improved. Proton linac systems and neutron generators based on the ^{2}H(d, n)^{3}He and ^{3}H(d, n)^{4}He reactions are available commercially. The target and the BSA, on the other hand, require substantially more research.

Among the reactions given in Table 6.2, ^{7}Li(p, n)^{7}Be, ^{9}Be(p, n)^{9}B, ^{9}Be(d, n)^{10}B, and ^{13}C(d, n)^{14}N are the feasible ones. The ^{7}Li(p, n)^{7}Be reaction presents itself as the best candidate when the projectile energy is just above the threshold energy of the reaction so that a maximum number of "soft" epithermal neutrons are produced in the forward direction (in the laboratory frame of reference) with minimum γ-radiation, fast neutrons, and daughter nuclei. [161] However, the flammable and low-melting-point lithium target presents a number of technical challenges, such as heat removal and target protection against radiation damage by the proton beam, which have yet to be overcome. Additionally, each (p,n) reaction will produce a ^{7}Be nucleus which is a gamma (478 keV) emitter with a half-life of 53.3 days. Thus the

accumulative exposure to this radiation of workers who maintain the operation of the BNCT unit on a regular basis deserves due consideration and control. The $^{9}Be(p, n)^{9}B$ reaction is the second-best option, provided a satisfactory BSA can be realized. The other (d, n) reactions require substantial development of both the neutron-generating devices and the BSA.

Table 6.2. Neutron-generating reactions and CANS suitable for BNCT

Reaction	**$E_{projectile}$ (MeV)**	**$E_{threshold}$ (MeV)**	**$<E_{neutron}>$ (MeV)**	**Neutron yield (n/mA/s)**	**Accelerator/target (approximate linear dimensions and cost)**
$^{7}Li(p,n)^{7}Be$	~2.5	1.88	~0.6	9.09×10^{11}	p-electrostatic accelerator/lithium (technically challenging); ~5 m and ~$5+M
$^{9}Be(p,n)^{9}B$	~4–20	2.06	~1.6-8	$0.5–1.2\times10^{12}$	p-linac/beryllium (achievable); ~5–10 m and ~$5-10M
$^{9}Be(d,n)^{10}B$	1.5	0	1.66	3.3×10^{11}	d-linac/beryllium (achievable); ~5 m and ~$5M
$^{2}H(d,n)^{3}He$	0.15	0	2.5	$\sim2\times10^{9}$	Neutron generator/d-Ti; ~1m and ~$0.2M
$^{3}H(d,n)^{4}He$	0.15	0	14.1	$\sim5\times10^{10}$	neutron generator/d-Ti; ~1 m and ~$0.3M
$^{13}C(d,n)^{14}N$	1.5	0	1.08	1.9×10^{11}	Under study
$^{12}C(d,n)^{13}N$	1.5	0.33	0.55	6×10^{10}	Under study

Motivated by the potential benefits of epithermal neutron production of the $^{7}Li(p, n)^{7}Be$ reaction, neutronics engineers have undertaken design studies and experimentation aimed at attaining a workable system. Considerable progress has been made, such as the prototypes associated with the LENOS (Section 4.2.3) [162] and the NUANS (Section 4.2.6) projects, which reported success in initial testing. [161-164].

As described in a survey by Wagner *et al*.[165], all BNCT facilities where patients have been treated between 2002 and 2011 were neutron reactors, many of which the treatment programs are no longer active. In recent years accelerator-based neutron sources have been under development for BNCT in Argentina, Belgium, Italy, Japan, Russia, UK, and other countries [155]. Results from first clinical tests are expected around 2016 from studies carried out at a CANS based on 30-MeV protons from a cyclotron and a Be target for neutron production, jointly developed by Sumitomo Heavy Industries, Ltd. And KURRI in Japan [166].

A number of BSA designs have been proposed for BNCT [167, 168]. The rationale typically stems from a two-stage neutron slowing-down, first of fast neutrons by heavy shields such as iron and subsequently by lighter materials such as AlF_3, in conjunction with a neutron reflector (e.g., lead) and a gamma shield.

Such a design of BSA typically permits mainly transmission of the epithermal neutrons of a few keV that are needed for BNCT treatment.

The CANS application for neutron capture therapy is motivated by three major factors: (1) the continuing improvement of the source and the BSA system; (2) the compactness, transportability, and commercial availability of major components; and (3) the substantial savings in capital investment and operational overhead. At present, several BNCT projects based on CANS have been proposed in Japan and in European countries. [167, 169-172] In conjunction with developments of ^{10}B-containing drugs, boron imaging techniques, and protocols for clinical management, the medical, pharmaceutical, medical, and neutron communities are hopeful for expedient preclinical trials of BNCT for an expanded scope of cancer treatments.

6.8 Isotope Production

Modern societies rely critically on the use of a multitude of stable and radioactive isotopes in all aspect of life. Over the years, the increase in demand for isotopes has superseded the production capacity, typically from fission reactors and cyclotron-driven facilities. Currently, the National Isotopes Program under the US Department of Energy is deemed underfunded and not "mission-ready," while demand is expected to increase considerably in the future. Commercial producers are mainly small cyclotrons specialized to produce a limited set of isotopes such as those (^{18}F, ^{11}C, ^{15}O) for positron emission tomography (PET) at hospitals. The situation, in the United States, for example, has been scrutinized by numerous expert panels and committees. [173, 174] In the following paragraphs, we use the case of the production of ^{99m}Tc to illustrate the potential for isotope production by CANS via neutron capture reactions. ^{99m}Tc (m denotes the metastable state (half-life of ~6 h) decays to essentially stable ^{99}Tc (half-life >105 years) by emission of 140 keV photons. The short half-life and the emitted photons detectable outside a patient's body make ^{99m}Tc the most-used isotope for medical imaging. It is applied to over 70% of all nuclear medicine procedures, from diagnosis of blood clots in the brain, lung, and coronary artery to scanning of bone infection, to monitoring and treatment of cancers.

Because ^{99m}Tc has such a short half-life, it must be extracted at or near a hospital from a chromatographic column containing ^{99}Mo (half-life of 67 h) in solution—a ^{99}Mo/^{99m}Tc-generator. Conventional production of ^{99}Mo is via neutron irradiation of a ^{235}U target, typically made from fission products containing either low-enriched uranium (LEU) or high-enriched uranium (HEU). Therefore, LEU or HEU targets must be shipped to an isotope-producing reactor for irradiation. The products are purified in a nearby processing facility, yielding ^{99}Mo solutions to feed ^{99}Mo/^{99m}Tc generators at a manufacturing facility so that the final useable product can be delivered to hospitals. Until 2010, the ^{99}Mo supply for the world was produced principally at six reactors, all of which were over 40 years of age. Any prolonged shutdown of these reactors, scheduled or unexpected, may cause dire consequences to the end-users. For example, the November 2007 extended shutdown of the National Research Universal reactor reportedly affected tens of thousands of patient procedures in the United States. Ideally, one envisages using a CANS to generate ^{99}Mo or generate ^{99m}Tc directly (at the user's location) by means of neutron-capture reactions that require neither fission products such as ^{235}U nor enriched Mo targets such as ^{100}Mo. This would eliminate the hazard of transporting radioactive LEU/HEU materials and generating radioactive wastes. [148, 175, 176]

Despite the small neutron-capture cross sections, promising results have been reported for the possible production of ^{99}Mo and ^{99m}Tc by CANS. Bertsche [177] considered alternative ^{99}Mo-producing reactions using low- and high-energy accelerators. Dovbnya et al. [178] investigated the ^{98}Mo(n,γ)^{99}Mo→^{99m}Tc reaction and speculated on the feasibility of producing the ^{99m}Tc radioisotope using a neutron generator of a thermal-neutron flux ~10^2 n/cm^2/s. Nagai et al. [179, 180] exploited the substantial cross section of the ^{100}Mo(n, 2n)^{99}Mo reaction in the neutron energy range of 12–17 MeV (~1.5 b) and demonstrated the

production of 79-GBq/g specific activity of ^{99}Mo after irradiating an enriched ^{100}Mo target for 198 h with a 14-MeV neutron flux of ~10^{13} n/cm^2/s. The demand for ^{99}Mo and ^{99m}Tc radioisotopes is expected to grow at a annual rate of ~5%. Considering this outstanding case, together with the projected increasing need for many other isotopes, it is perhaps not far-fetched to imagine having hundreds of CANS as suppliers of isotopes at various locations in the near future. [174] The SPES project will develop the Isotope Separation On Line facility for production of radioisotopes for medical use.

7. Perspectives

In the last 5 years, scientists and engineers involving in building and using CANS have taken on expanding roles in R&D, engineering, and education. The reasons for the increasing activities are manifold. First, as high-power (~0.5–5 MW) neutron-scattering facilities become available to users through competitive proposal systems, increasing numbers of beginners and research students will seek training or practice in scattering experiments at compact sources. Second, compact sources are ideal test beds for R&D and validation of advanced instrumentation and techniques, leading to eventual utilization at existing and future big facilities. Third, there are other disciplines, as discussed in Section 6, the advancement of which depends on experimentation at moderate-energy neutron sources.

These factors accentuate the complementary and supplementary nature of CANS with respect to large-scale, high-power neutron sources commissioned to fulfill users' demand for basic research, particularly for cutting-edge experiments vital to materials research. However, as the neutron scattering capacity prompted by the retiring of mainstream reactor sources is not replaced, the role of CANS in the neutron landscape is shifting. In the past, CANS often stemmed from spin-offs of legacy accelerator projects; the current trend points to competitively innovative CANS for serving user needs in both basic and applied research over a network of gridded local or regional interests and collaborations[181-183].

Therefore, on the front of basic materials research, we anticipate a suite of CANS that are optimized in source brilliance, beam line capacity, and variety of end stations. Innovations in accelerator multiplexing, moderators with tailored performance, novel neutron optics, and advanced detectors may warrant a revised definition of CANS in the future. On the applied side, as the neutron production and instrumentation of CANS excel, the use of epithermal to fast neutrons for technologies involving energy, interrogation, security, biomedical, and cultural heritage applications will prevail. Groundbreaking developments may be possible. For example, probing microscopic magnetism in engineering materials, biological systems and complex structures that contain hydrogen are benefited by the capability of magnetic interactions and sensitivity to hydrogen atoms unique to the neutron. Furthermore, exploiting the associated functionalities through the utilization of polarized neutrons in conjunction with nuclear-spin-polarized hydrogen techniques made available by the next-generation CANS and advanced instrumentation integrated in cultural, medical and industrial enterprises will open a new frontier of neutron applications.

8. Conclusions

The development of a diverse set of compact accelerator-driven neutron sources is providing the research community with a range of versatile tools for neutron beam research and taking the place of difficult-to-replace research reactors. The compact nature of such sources makes them accessible to many institutions and even, in some cases, portable. We can foresee expanded use of CANS as the technology for accelerators, targets, moderators, and instrumentation advances. Clearly, advances in this field are aided by sustained international inter-laboratory collaborations, the realization of which incentivized, in 2009, the foundation of the Union of Compact Accelerator-driven Neutron Sources, UCANS, [184] now subscribed to by more than 15 institutions. The union holds regular meetings that rotate among the

participating organizations, about once per year, and the published proceedings provide an excellent resource for information about the various sources and their applications.

Acknowledgments

This work was partially supported within the CNR-STFC Agreement (2014-2020) concerning collaboration in scientific research at the ISIS spallation neutron source. We thank T. Brückel, B. Galnander, R. Granada, T. Gutberlet, A. Junghans, Y. Kiyanagi, K. R. Kim, P. Mastinu, C. Massimi, E. Passoth, M. Pillon, A. Prokofiev, U. Ratzinger, P. Schillebeeckx, F. Sordo Balbin, M. Uesaka, X. Wang, and J. Wyss, for providing updated information on the parameters, drawings, and images, of the CANS described in this work. We are grateful to C. D. Frost for providing updated information on the ChipIr beam line at ISIS.

References

[1] D. Richter, T. Springer, A Twenty Years Forward Look at Neutron Scattering Facilities in the OECD Countries and Russia, OECD, (1998).
[2] K.N. Clausen, Fission, spallation or fusion-based neutron sources, PRAMANA - Journal of Physics, 71 (2008) 623-628.
[3] J.M. Carpenter, W.B. Yelon, Neutron Sources, Methods of Experimental Physics, 23 Part A (1987).
[4] E. Fermi, Radioattività indotta dal bombardamento di neutroni, La Ricerca Scientifica, 5 (25 March 1934) 283.
[5] E. Fermi, "Fermi's Own Story". The First Reactor., Oak Ridge, Tennessee: United States Atomic Energy Commission, Division of Technical Information., (December 1982) 22–26.
[6] T.E. Mason, T.J. Gawne, S.E. Nagler, M.B. Nestor, J.M. Carpenter, The early development of neutron diffraction: science in the wings of the Manhattan Project, Acta Crystallography A, 69 (2013) 37–44.
[7] J.S. Fraser, R.E. Green, J.W. Hilborn, J.C.D. Milton, W.A. Gibson, E.E. Gross, A. Zucker, Neutron production in thick target bombarded by high energy protons, Physics in Canada, 21 (1965) 17.
[8] V.A. Nikolaev, V.I. Yurevich, R.M. Yakovlev, R.S. Vassil'kov, Neutron Production in Thick Lead Target, ICANS-XI International Collaboration on Advanced Neutron Sources, KEK. Tsukuba, October 22-26, 1990, (1990).
[9] J.M. Carpenter, T.A. Gabriel, E.B. Iverson, D.W. Jerng, The 10-GeV question: What is the best energy to drive a pulsed spallation neutron source?, Physica B: Condensed Matter (Amsterdam), 270 (1999) 272-279.
[10] IAEA, Determination of Absorbed Dose in Reactors, International Atomic Enargy Agency, Vienna, TECHNICAL REPORTS SERIES No. 127 (1971).
[11] https://www.euro-fusion.org/jet/.
[12] http://www.pppl.gov/Tokamak%20Fusion%20Test%20Reactor.
[13] A. Taylor, M. Dunne, S. Bennington, S. Ansell, I. Gardner, P. Norrys, T. Broome, D. Findlay, R. Nelmes, A route to the brightest possible neutron source?, Science, 315 (2007) 1092-1095.
[14] M. Drosg, DROSG-2000v2.1: Neutron source reactions. Data files with computer codes for 57 accelerator-based two-body neutron source reactions, IAEA, report IAEA-NDS-87 (2002).
[15] K.H. Y Yamagata, J Ju, S Wang, S Morita, J Kato, Y Otake, A Taketani et al., Development of a neutron generating target for compact neutron sources using low energy proton beams, Journal of Radioanalytical and Nuclear Chemistry, 305 (3) (2015) 787-794.
[16] J.M. Carpenter, W.B. Yelon, Neutron Sources, Methods of Experimental Physics, Neutron Scattering, 23 (1986) 99-196.
[17] L.D. Stevens, A.J. Miller, Radiation studies at a medium energy accelerator, Lawrence Livermore Laboratory report, UCRL-19386, (1969).
[18] M.R. Hawkesvorth, Neutron Radiography Equipment and Methods, Atomic Energy Review of Modern Physics, 15 (1977) 169 - 220.
[19] W.P. Swanson, Calculation of neutron yields released by electrons incident on selected materials, Health Physics, 35 (1978) 353.
[20] B. Khaykovich, M.V. Gubarov, Y. Bagdasarova, B.D. Ramsey, D.E. Moncton, From x-ray telescopes to neutron scattering: using axisymmetric mirrors to focus a neutron beam, Nuclear Instrument and Methods A, 631 (2011) 98-104.
[21] Micklich, personal communication, (2011).
[22] J. Davis, G.M. Petrov, Angular distribution of neutrons from high-intensity laser-target interactions, Plasma Phys. Controlled Fusion, 50 (2008) 065016.
[23] S. Nakai, K. Mima, Y. Kato, K. Tanaka, Y. Ikeda, H.Azechi, K. Miyanaga, M. Nakai, M. Perlado, R.G. Arrabal, Industrial applications of laser neutron source, Journal of Physics: Conference Series, 244 (2010) 042027.
[24] L.A.R. Palomino, J.J. Blostein, J. Dawidowski, Performance of the second deep inelastic neutron scattering spectrometer at the Bariloche electron LINAC, Journal of Instrumentation, 8 (2013) P08016.

[25] Y. Xiao, Z. Chen, Y. Yang, X. Wang, Development Progress of the Neutron Imaging Station in CPHS, Physics Procedia, 69 (2015).
[26] http://www.cyric.tohoku.ac.jp/english/index.html.
[27] A. Terakawa, H. Suzuki, K. Kumagai, Y. Kikuchi, T. Uekusa, T. Uemori, H. Fujisawa, N. Sugimoto, K. Itoh, M. Baba, H. Orihara, K. Maeda, New fast neutron time-of-flight facilities at CYRIC, Nuclear Instruments and Methods in Physics Research A, 491 (2002) 419-425.
[28] http://www.fusione.enea.it/LABORATORIES/Tec/FNG.html.en.
[29] https://www.rpi.edu/dept/ne/public_html/Gaerttner_LINAC.html.
[30] A.M. Daskalakis, R.M. Bahran, E.J. Blain, B.J. McDermott, S. Piela, Y. Danon, D.P. Barry, G. Leinweber, R.C. Block, M.J. Rapp, R. Capote, A. Trkov, Quasi-differential neutron scattering from 238U from 0.5 to 20 MeV, Annals of Nuclear Energy, 73 (November 2014) 455-464.
[31] F.J. Saglimen, Y. Danon, R.C. Block, M.J. Rapp, R.M. Bahran, G. Leinweber, D.P. Barry, N.J. Drindak, A system for differential neutron scattering experiments in the energy range from 0.5 to 20 MeV, Nuclear Instruments and Methods in Physics Research Section A, 620 (2010) 401-409.
[32] R.C. Block, Y. Danon, F. Gunsing, R.C. Haight, Neutron Cross Section Measurements, Handbook of Nuclear Engineering, E. Cacuci and D. Gabriel (eds), Springer US (2010).
[33] https://ec.europa.eu/jrc/en/research-facility/linear-electron-accelerator-facility.
[34] W. Mondelaers, P. Schillebeeckx, GELINA, a neutron time-of-flight facility for neutron data measurements, Notiziario Neutroni e Luce di Sincrotrone, 11 (2006) 19 - 25.
[35] P. Schillebeeckx, B. Becker, Y. Danon, K. Guber, H. Harada, J. Heyse, A.R. Junghans, S. Kopecky, C. Massimi, M.C. Moxon, N. Otuka, I. Sirakov, K. Volev, Determination of resonance parameters and their covariances from neutron induced reaction cross section data, Nucl. Data Sheets, 113 (2012) 3054 – 3100.
[36] D. Tronc, J.M. Salome, K. Böckhoff, A new pulse compression system for intense relativistic electron beams, Nuclear Instruments and Methods, 228 (1985) 217-227.
[37] P. Schillebeeckx, B. Becker, H. Harada, S. Kopecky, Neutron Resonance Spectroscopy for the Characterisation of Materials and Objects, Report EUR 26848 EN.
[38] http://phi.phys.nagoya-u.ac.jp/JCANS/huns.html.
[39] M. Furusaka, H. Sato, T. Kamiyama, M. Onhuma, Y. Kiyanagi, Activity of Hokkaido University Neutron Source, HUNS, Physics Procedia, 60 (2014).
[40] http://tlabs.ac.za/.
[41] M. Mosconi, E. Musonza, A. Buffler, R. Nolte, S. Rottger, F.D. Smith, Characterization of the High-Energy Neutron Beam Facility at iThemba LABS, Radiation Measurements, 45 (2010).
[42] http://pal.postech.ac.kr/.
[43] G.N. Kim, H.S. Kang, Y.S. Lee, M.H. Cho, I.S. Ko, W. Namkung, Pulsed neutron source using 100-MeV electron linac at Pohang Accelerator Laboratory, Proceedings of 20th International Linac Conference, Monterey (CA), (2002) 621-623.
[44] http://phi.phys.nagoya-u.ac.jp/JCANS/kuans.html.
[45] S. Tasaki, T. Nagae, M. Hirose, Y. Yamashita, K. Hironaka, Y. Abe, Y. Yamagata, Y. Otake, K. Hirota, Properties and Possible Applications of Kyoto University Accelerator Based Neutron Source (KUANS), Physics Procedia, 60 (2014) 181.
[46] http://www.rri.kyoto-u.ac.jp/LINAC/.
[47] K. Kobayashi, S. Lee, S. Yamamoto, T. Kawano, Neutron capture cross-section measurement of 99Tc by linac time-of-flight and the resonance analysis, Nuclear Science and Engineering, 146 (2004) 209–220.
[48] http://www.indiana.edu/~lens/.
[49] D.V. Baxter, J.M. Cameron, V.P. Derenchuk, C.M. Lavelle, M.B. Leuschner, M.A. Lone, H.O. Meyer, T. Rinckel, W.M. Snow, Status of the low energy neutron source at Indiana University, Nuclear Instruments and Methods B, 241 (2005) 209-212.
[50] C.M. Lavelle, D.V. Baxter, M.A. Lone, H. Nann, J.M. Cameron, V.P. Derenchuk., H. Kaiser, M.B. Leuschner, W. Lozowski, H.O. Meyer, R. Pynn, N. Remmes, T. Rinckel, W.M. Snow, P.E. Sokol, Neutronic Design and Measured Performance of the Low Energy Neutron Source Target Moderator Reflector System, Nuclear Instruments and Methods A, 587 (2008) 324-341.

[51] Z. Guo, Y. Lu, Y. Zou, K. Zhu, S. Peng, J. Zhao, S. Gao, W. Wen, H. Li, Q. Zhou, H. Ren, P. Lü, H. Zeng, S. Wang, G. Tang, D. Mo, Z. Yuan, D. Xie, X. Yan, J. Chen, Progress of PKUNIFTY – a RFQ Accelerator based Neutron Imaging Facility at Peking University, Physics Procedia, 43 (2013).
[52] http://rans.riken.jp/en/index.html.
[53] Y.Otake, M.Olbinado, Y.Seki, K.Hirota, Y.Yamagata, J.Ju, T.Adachi, S.Morita, Y.Iwashita, M.Hino, M.Ichikawa, M.Kitaguchi, T.Takahashi, H.Yoshizawa, S.W.Lee, W.Yashiro, A.Momose, Research toward the development of compact neutron interference imaging instrument with gratings, Journal of Physics Conference Series, 340 (2012) 012035.
[54] http://www.tsl.uu.se/irradiation-facilities-tsl/.
[55] A.V. Prokofiev, J. Blomgren, O. Bystrom, C. Ekstrom, S. Pomp, U. Tippawan, V. Ziemann, M. Osterlund, The TSL neutron beam facility, Radiation Protection Dosimetry, 126 (2007).
[56] A.V. Prokofiev, CUP–A New High-Flux Irradiation Position at the ANITA Neutron Facility at TSL, IEEE Transactions on Nuclear Science, 61 (2014) 1929.
[57] http://www.essbilbao.org/index.php/en/.
[58] R. Vivanco, A. Ghiglino, J.P.d. Vicente, F. Sordo, S. Terrón, M. Magán, J.M. Perlado, F.J. Bermejo, Basic concept for an accelerator-driven subcritical system to be used as a long-pulse neutron source for Condensed Matter research, Nuclear Instruments and Methods in Physics Research A, 767 (2014) 176-187.
[59] http://exp-astro.physik.uni-frankfurt.de/franz/.
[60] C. Wiesner, L.P. Chau, H. Dinter, M. Droba, M. Heilmann, N. Joshi, D. Mäder, A. Metz, O. Meusel, I. Müller, D. Noll, H. Podlech, U. Ratzinger, H. Reichau, R. Reifarth, A. Schempp, S. Schmidt, W. Schweizer, K. Volk, C. Wagner, Proton Driver Linac for the Frankfurt Neutron Source, AIP Conference Proceedings, 1265 (2010) 487-492.
[61] L.P. Chau, M. Droba, O. Meusel, D. Noll, U. Ratzinger, C. Wiesner, Proc. of the LINAC2010 Conf., Tsukuba, Japan, (2010) 292.
[62] http://www.lnl.infn.it/index.php/en/.
[63] http://www.lnf.infn.it/acceleratori/btf/.
[64] M. Prata, D. Alloni, P.D. Felice, M. Palomba, A. Pietropaolo, M. Pillon, L. Quintieri, A. Santagata, P. Valente, Italian neutron sources, Euro Physics Journal Plus, 129 (2014) 255.
[65] https://www.hzdr.de/db/Cms?pNid=317.
[66] A.R. Junghans, R. Beyer, Z. Elekes, E. Grosse, R. Hannaske, T. Kogler, R. Massarczyk, R. Schwengner, A. Wagner, Fast-neutron Induced Reactions at the nELBE Time-of-flight Facility, Nuclear Data Sheets, 119 (2014) 349–352.
[67] D. Bisello, J. Esposito, P. Mastinu, G. Prete, L. Silvestrin, J. Wyss, The QMN Beam Line of the Neutron-induced Single Event Effects Facility at the 70 MeV Cyclotron of LNL-INFN, Physics Procedia, 60 (2014) 271-277.
[68] http://phi.phys.nagoya-u.ac.jp/riko/NUANS/index.html.
[69] H. Tanaka, Y. Sakurai, M. Suzuki, S. Masunaga, Y. Kinashi, G. Kashino, Y. Liu, T. Mitsumoto, S. Yajima, H. Tsutsui, A. Maruhashi, K. Ono, Characteristics comparison between a cyclotron-based neutron source and KUR-HWNIF for boron neutron capture therapy, Nuclear Instruments and Methods in Physics Research B, 267 (2009) 1970-1977.
[70] http://phits.jaea.go.jp/.
[71] https://ec.europa.eu/jrc/en/research-facility/van-de-graaff-accelerator.
[72] C. Cohen-Tannoudji, B. Diu, F. Laloë, Méchanique Quantique, Hermann Editeurs des Sciences et des Arts, Paris, Tome I et Tome II (1977, 1986).
[73] S.W. Lovesey, Theory of Neutron Scattering from Condensed Matter, Oxford University Press, (1984).
[74] https://www.ncnr.nist.gov/resources/n-lengths/.
[75] E.L. N. Kardjilov, E. Steichele, and P. Vontobel, Phase-contrast radiography with a polychromatic neutron beam, Nuclear Instruments and Methods in Physics Research A, A527 (2004) 519–530.
[76] H. Sato, T. Kamiyama, Y. Kiyanagi, A Rietveld-type analysis code for pulsed neutron Bragg-edge transmission imaging and quantitative evaluation of texture and microstructure of a welded α -iron plate, Materials Transactions, 52 (2011) 1294-1302.

[77] A. Steuwer, P.J. Withers, J.R. Santisteban, L. Edwards, Using pulsed neutron transmission for crystalline phase imaging and analysis, Journal of Applied Physics, 97 (2005) 074903.
[78] T. Adachia, K. Ikeda, T. Okua, J. Guo, W. Lin, H. Ohmori, T. Morishima, H.M. Shimizu, K. Sakaia, J. Suzuki, K.C. Littrell, C.-K. Loong, Possible application of compound Fresnel lens for neutron beam focusing, Physica B, 350 (2004) e775-778.
[79] https://mcnp.lanl.gov/.
[80] https://geant4.web.cern.ch/geant4/.
[81] T.R. R. M. Moon, and W. C. Koehler, Polarization Analysis of Thermal-Neutron Scattering, Physics Review Letters, 181 (Published 10 May 1969) 920.
[82] F. Tasset, Zero field neutron polarimetry, Physica B: Condensed Matter, 156-157 (1989) 627.
[83] https://www.gemeasurement.com/radiation-detection.
[84] A.J. Hurd, R.T. Kouzes, Why new neutron detector materials must replace helium-3, The European Physical Journal, 129 (2014).
[85] F. Sacchetti, N. Colonna, R. Faccini, B. Guerard, R. Hall-Wilton, F. Murtas, C. Petrillo, A. Pietropaolo, N. Rhodes, L. Quintieri, M. Tardocchi, P. Valente, 3He-free neutron detectors and their applications, The European Physical Journal Plus, 130 (2015).
[86] F. Piscitelli, Novel boron-10-based detectors for neutron scattering science Helium-3-free detectors for large- and small-area applications: The Multi-Grid and the Multi-Blade prototypes., The European Physical Journal Plus, 130 (2015).
[87] C. Andreani, A. Pietropaolo, R. Senesi, G. Gorini, M. Tardocchi, A. Bracco, N. Rhodes, E. Schooneveld, Electron-volt spectroscopy at a pulsed neutron source using a resonance detector technique, Nuclear Instruments and Methods in Physics Research A, 481 (2002) 509–520.
[88] A. Pietropaolo, C. Andreani, M.Rebai, L. Giacomelli, G.Gorini, E.P. Cippo, M. Tardocchi, A. Fazzi, G.V. Rinati, C.Verona, M. Marinelli, E. Milani, C.D. Frost, E.M. Schooneveld, Single-crystal diamond detector for time-resolved measurements of a pulsed fast-neutron beam., Europhysics letter, 92 (2010) 68003.
[89] M. Tardocchi, A. Pietropaolo, C. Andreani, A. Bracco, A. D'Angelo, G. Gorini, S. Imberti, R. Senesi, N.J. Rhodes, E.M. Schooneveld, Cadmium–Zinc–Telluride photon detector for epithermal neutron spectroscopy—pulse height response characterisation, Nuclear Instruments and Methods in Physics Research A, 526 (2004) 477–492.
[90] G.F. Knoll, Radiation detection and measurement,, Wiley, 4th edition (2010).
[91] B. Gebauer, Towards detectors for next generation spallation neutron sources, Nuclear Instruments and Methods in Physics Research A, 535 (2004) 65-78.
[92] R.G. Cooper, SNS detector plans, Nuclear Instruments and Methods in Physics Research A, 529 (2004) 394-398.
[93] C.W.E.v. Eijk, Neutron PSDs for the next generation of spallation neutron sources, Nuclear Instruments and Methods in Physics Research A, 477 (2002) 383-390.
[94] H. Sato, O. Takada, K. Iwase, T. Kamiyama, Y. Kiyanagi, Journal of Physics Conference Series, 251 (2010) 012070.
[95] K. Iwase, H. Sato, K. Mori, T. Kamiyama, T. Ishigaki, Y. Kiyanagi, Metallurgical and Materials Transactions A, 42 (2011) 2296.
[96] K. Iwase, H. Sato, S. Harjo, T. Kamiyama, T. Ito, S. Takata, K. Aizawa, Y. Kiyanagi, In situ lattice strain mapping during tensile loading using the neutron transmission and diffraction methods, Journal of Applied Crystallography, 45 (2012) 113.
[97] Y. Kiyanagi, T. Shinohara, T. Kai, T. Kamiyama, H. Sato, K. Kino, K. Aizawa, M. Arai, M. Harada, K. Sakai, K. Oikawa, M. Ooi, F. Maekawa, H. Iikura, T. Sakai, M. Matsubayashi, M. Segawa, M. Kureta, Present status of research on pulsed neutron imaging in Japan, Physics Procedia, 43 (2013) 92.
[98] Y. Kiyanagi, K. Mizukami, T. Kamiyama, F. Hiraga, H. Iwasa, Images obtained by neutron transmission measurement using time-of-flight method, Nuclear Instrument and Methods A, 542 (2005).
[99] Y. Kiyanagi, N. Sakamoto, H. Iwasa, T. Kamiyama, F. Hiraga, S. Sato, H. Sagehashi, T. Ino, M. Furusaka, J. Suzuki, A. Gorin, I. Manuilov, A. Ryazantsev, K. Kuroda, K. Sakai, F. Tokanai, H. Miyasaka,

T. Adachi, T. Oku, K. Ikeda, S. Suzuki, K. Morimoto, H.M. Shimizu, Some experimental studies on time-of-flight radiography using a pulsed neutron source, IEEE Transactions on Nuclear Science, 52 (2005) 371.
[100] H. Sato, O. Takada, S. Satoh, T. Kamiyama, Y. Kiyanagi, Development of material evaluation method by using a pulsed neutron transmission with pixel type detectors, Nuclear Instruments and Methods A, 623 (2010) 597.
[101] S. Uno, T. Uchida, M. Sekimoto, T. Murakami, K. Miyama, M. Shoji, E. Nakano, T. Koike, K. Morita, H. Sato, T. Kamiyama, Y. Kiyanagi, Physics Procedia, 37 (2012) 600.
[102] K. Tokuda, T. Kamiyama, Y. Kiyanagi, R. Moreh, S. Ikeda, Jpn. Journal of Applied Physics, 40 (2001).
[103] G. Charpak, Nuclear Instruments and Methods in Physics Research, 62 (1968) 262.
[104] A.S. F Sauli, Micropattern gaseous detectors, Annual Review of Nuclear and Particle Science, 49 (1999) 341-388.
[105] N.J. Rhodes, A.G. Wardle, A.J. Boram, M.W. Johnson, Pixelated neutron scintillation detectors using fibre optic coded arrays, Nuclear Instrumnets and Methods A, 392 (1997) 315.
[106] T. Nakamura, T. Kawasaki, T. Hosoya, K. Toh, K. Oikawa, K. Sakasai, M. Ebine, A. Birumachi, K. Soyama, M. Katagiri, A large-area two-dimensional scintillator detector with a wavelength-shifting fibre readout for a time-of-flight single-crystal neutron diffractometer, Nuclear Instrument and Methods A, 686 (2012) 64.
[107] F. Piscitelli, Boron-10 layers, Neutron Reflectometry and Thermal Neutron Gaseous Detectors,, PhD Thesis, Uni. Perugia (2014). arXiv:1406.3133.
[108] J. Correa, PhD Thesis, Uni Zaragoza, (2012).
[109] G. Croci, F. Murtas, F. Resnati, Prospects in MPGDs development for neutron detection (Summary of RD-51 Academia-Industry Matching Event Second Special Workshop on Neutron Detection with MPGDs), RD51-NOTE-2015-012:, (2015).
[110] http://www.neutron.anl.gov/ipns/icans.html.
[111] F.S. F.J. Bermejo, M. Ohnuma, Y. Kiyanagi, H. Sato, 3rd International Meeting of the Union for Compact Accelerator-driven Neutron Sources, UCANS III, 31 July–3 August 2012, Bilbao, Spain & the 4th International Meeting of the Union for Compact Accelerator-driven Neutron Sources, UCANS IV, 23-27 September 2013, Sapporo, Hokkaido, Japan, Physics Procedia, 60 (2014).
[112] M.M. S. Terrón, F. Sordo, A. Ghiglino, F. Martınez, F.J.Bermejo, J.M. Perlado, Proceedings of the Union for Accelerator-driven Neutron Sources., Physics Procedia, 26 (2012) 196-204.
[113] U. Rücker, T. Cronert, J. Voigt, J.P. Dabruck, P.-E. Doege, J. Ulrich, R. Nabbi, Y. Beßler, M. Butzek, M. Büscher, C. Lange, M. Klaus, T. Gutberlet, T. Brückel, The Jülich High Brilliance Neutron Source Project, The European Physical Journal Plus, 113 (2016).
[114] IAEA, Neutron generators for analytical purposes, IAEA, 2012.
[115] IAEA, Database of prompt gamma rays from slow neutron capture fro elemental analysis, IAEA, 2007.
[116] H.R. Verma, Atomic and Nuclear Analytical Methods. XRF, Mossbauer, XPS, NAA and Ion-beam Spectroscopic Techniques, 2007.
[117] A. Vértes, S. Nagy, Z. Klencsár, R.G. Lovas, F. Røusch, Handbook of Nuclear Chemistry, Springer, 2011.
[118] E.M. A. Hussein, Handbook on Radiation Probing, Gauging, Imaging and Analysis. Volume I: Basics and Techniques, 2004.
[119] D. Creagh, The Use of Neutron Technology in Archaeological and Cultural Heritage Research, in: C. Grupen, I. Buvat (Eds.) Handbook of Particle Detection and Imaging, Springer2012, pp. 813-831.
[120] G. Harbottle, Neutron Activation Analysis in Archaeological Chemistry, Top. Curr. Chem., 157 (1990) 57-91.
[121] T. Tzotzas, G. Karanikas, G.E. Krassas, Body Composition Analysis Using Radionuclides, in: V.R. Preedy (Ed.) Handbook of Anthropometry: Physical Measures of Human Form in Health and Disease, Springer2012, pp. 185-203.

[122] FHWA, Corrosion Costs and Preventive Strategies in the United States, CC Technologies Laboratories, Inc., Dublin, Ohio, 2002.
[123] H. Czichos, Handbook of Technical Diagnostics, Springer-Verlag, Berlin, 2013.
[124] D. Breysse, Non-Destructive Assessment of Concrete Structures: Reliability and Limits of Single and Combined Techniques, Springer-Verlag, Berlin, 2012.
[125] Physical Techniques in the Study of Art, Archaeology and Cultural Heritage, Elsevier, 2 (D. Creagh and D. Bradley).
[126] C.-K. Loong, A. Scherillo, G. Festa, Scattering Techniques: Small- and Wide-Angle Neutron Diffraction, in Neutron Methods for Archeology and Cultural Heritage Ed. N. Kardjilov and G. Festa, (2016).
[127] Y.S. S. Nagashima, H. Sato, T. Kamiyama, M. Ohnuma, and Y. Kiyanagi, Imaging of crystalline structural information of Japanese swords by pulsed neutron transmission spectroscopy, Physics Procedia 60, (2014) 327-331.
[128] C. Bruschini, Commercial Systems for the Direct Detection of Explosives for Explosive Ordnance Disposal Tasks, Subsurface Sensing Technologies and Applications, 2 (2001) 299-336.
[129] A. Buffler, Contraband detection with fast neutrons, Radiation Physics and Chemistry, 71 (2004) 853-861.
[130] A. Bakalyarov, M. Karetnikov, V. Lebedev, G. Muradyan, Y. Skorik, N. Turpikin, G. Yakolev, Experimental model of the device for detection of nuclear materials by pulsed photoneutron technology, in: S. Apikyan, D. Diamond, R. Way (Eds.) and Response to Nuclear Prevention, Detection and Radiological Threats, Springer, Dordrecht, The Netherlands, 2008, pp. 173-181.
[131] J.R. Granada, R.E. Mayer, J. Dawidowski, J.R. Santisteban, F. Cantargi, J.J. Blostein, L.A. Rodríguez Palomino, A. Tartaglione, The sciences and applications of the Electron Linac-driven neutron source in Argentina, The European Physical Journal Plus, (2016).
[132] J.C. Rynes, Gamma-ray and Neutron Radiography for a Pulsed Fast Neutron Analysis Cargo Inspection System, Nuclear Engineering, University of California, Berkeley, Berkeley, 1999.
[133] S.M. McConchie, Detection of hazardous materials in vehicles using neutron interrogation techniques, Purdue University, West Lafayette, Indiana, 2007.
[134] R. Miklaszewski, U. Wiącek, D. Dworak, K. Drozdowicz, V. Gribkovc, Detection of explosives and other illicit materials by a single nanosecond neutron pulses — Monte Carlo simulation of the detection process, Journal of Instrumentation, 7 (2012) C07006.
[135] T. Žagar, J. Galy, J. Magill, M. Kellett, Laser-generated nanosecond pulsed neutron sources: scaling from VULCAN to table-top, New Journal of Physics, 7 (2005) 253.
[136] G. Nebbia, J. Gerl, Detection of buried landmines and hidden explosives using neutron, X-ray and gamma-ray probes, Europhysics News, July/August (2005) 119-123.
[137] K. Yoshikawa, K. Masuda, T. Takamatsu, Y. Yamamoto, H. Toku, T. Fujimoto, Development of a High-performance Landmine Detection System Through Gamma-ray Detection by Using a Compact Fusion Neutron Source and Dualsensors, in: K. Furuta, J. Ishikawa (Eds.) Anti-personnel Landmine Detection for Humanitarian Demining, Springer-Verlag2009, pp. 157-173.
[138] D.V. Ellis, J.M. Singer, Well Logging for Earth Scientists, Springer Science+Business Media B.V., Dordrecht, The Netherlands, 2008.
[139] L. Dep, M. Belbot, G. Vourvopoulos, S. Sudar, Pulsed neutron-based on-line coal analysis, Journal of Radioanalytical and Nuclear Chemistry, 234 (1998) 107-112.
[140] C. Andreani, A. Pietropaolo, A. Salsano, G. Gorini, M. Tardocchi, A. Paccagnella, S. Gerardin, C.D. Frost, S. Ansell, S.P. Platt, Facility for fast neutron irradiation tests of electronics at the ISIS spallation neutron source, Applied Physics Letters, 92 (2008) 114101.
[141] N. Kanekawa, E.H. Ibe, T. Suga, Y. Uematsu, Dependability in Electronic Systems, Spinger, New York, (2011).
[142] C. Andreani, G. Gorini, T. Materna, Novel Neutron Imaging Techniques for Cultural Heritage Objects, in: I.S. Anderson, R.L. McGreevy, H.Z. Bilheux (Eds.) Neutron Imaging and Applications, Springer-Verlag, Berlin, 2009, pp. 229-252.

[143] J.E. D. Bisello, P. Mastinu, G. Prete, L. Silvestrin, J. Wyss, The QMN Beam Line of the Neutron-induced Single Event Effects Facility at the 70 MeV Cyclotron of LNL-INFN, Physics Procedia, 60 (2014) 271-277.
[144] K. Shibata, JENDL: Nuclear databases for science and technology, Journal of Nuclear Science and Technology, 50 (2013) 449-469.
[145] M.B. Chadwick, H.G. Hughes, R.C. Little, E.J. Pitcher, P.G. Young, Nuclear Data for Accelerator-Driven Systems, Progress in Nuclear Energy, 38 (2001) 179-219.
[146] D.D. Sood, P. Oblozinsky, M. Herman, O. Schwerer, Nuclear data for applications, Journal of Radioanalytical and Nuclear Chemistry, 243 (2000) 227-233.
[147] Y.A. Korovin, V.V. Artisyuk, A.V. Ignatyuk, G.B. Pilnov, S.A. Yu., Y.E. Titarenko, S.G. Yavshits, Transmutation of radioactive nuclear waste – present status and requirement for the problem-oriented nuclear data base, PRAMANA - Journal of Physics, 68 (2007) 181-191.
[148] IAEA, Nuclear data for the production of therapeutic radionuclides, International Atomic Energy Agency, Vienna, 2010.
[149] Y. Kiyanagi, Accurate Neutron Nucleus Reaction Measurement Instrument (ANNRI) for Capture Cross Section Measurements at J-PARC, Journal of the Korean Physical Society, 59 (2011) 779-784.
[150] P.F. Mastinu, U. Abbondanno, G. Aerts, H. Álvarez, F. Alvarez-Velarde, S. Andriamonje, J. Andrzejewski, P. Assimakopoulos, L. Audouin, G. Badurek, N. Bustreo, P. aumann, F.B. vá, E. Berthoumieux, F. Calviño, D. Cano-Ott, R. Capote, A.C.d. Albornoz, P. Cennini, V. Chepel, E. Chiaveri, N. Colonna, G. Cortes, A. Couture, J. Cox, M. Dahlfors, S. David, I. Dillmann, R. Dolfini, C. Domingo-Pardo, W. Dridi, I. Duran, C. Eleftheriadis, M. Embid-Segura, L. Ferrant, A. Ferrari, R. Ferreira-Marques, L. itzpatrick, H. Frais-Kölb, K. Fujii, W. Furman, C. Guerrero, I. Goncalves, R. Gallino, E. Gonzalez-Romero, A. Goverdovski, Gramegna, E. Griesmayer, F. Gunsing, B. Haas, R. Haight, M. Heil, A. Herrera-Martinez, M. Igashira, S. Isaev, E. Jericha1, Y. Kadi, Käppeler, D. Karamanis, D. Karadimos, M. Kerveno, V. Ketlerov, P. Koehler, V. Konovalov, E. Kossionides, M.K. ka, C. Lamboudis, H. Leeb1, A. Lindote, I. Lopes, M. Lozano, S. Lukic, J. Marganiec, L. Marques, S. Marrone, C. Massimi, A. Mengoni, P.M. Milazzo, C. Moreau, M. Mosconi, F. Neves, H. Oberhummer, S. O'Brien, M. Oshima, J. Pancin, C. Papachristodoulou, C. Papadopoulos, C. Paradela, N. Patronis, A. Pavlik, P. Pavlopoulos, L. Perrot, R. Plag, A. Plompen, A. Plukis, A. Poch, C. Pretel, J. Quesada, T. Rauscher, R. Reifarth, M. Rosetti, C. Rubbia, G. Rudolf, P. Rullhusen, J. Salgado, L. Sarchiapone, I. Savvidis, C. Stephan, G. Tagliente, J.L. Tain, L. Tassan-Got, L. Tavora, R. Terlizzi, G. Vannini, P. Vaz, A. Ventura, D. Villamarin, M.C. Vincente, V. Vlachoudis, R. Vlastou, F. Voss, S. Walter, H. Wendler, M. Wiescher, K. Wisshak, Neutron cross section measurements at n-TOF for ADS related studies, Journal of Physics: Condensed Matter, 41 (2006) 352-360.
[151] G.N. Kim, M.W. Lee, K.S. Kim, H.S. Kang, M.H. Cho, I.S. Ko, W. Namkung, Nuclear Data measurements with a pulsed neutron facility based on an electron LINAC, The 1st International Particle Accelerator Conference, IPAC'10, Kyoto, Japan, 2010.
[152] J.M. Damian, J.R. Granada!, D. Baxter, S. Parnell, D. Evans, Measurement of the total cross section of heavy water in the 0.1 meV -1 eVenergy range at 20 and 50!!C, in: G. Prete, P. Mastinu (Eds.) The Fifth Meeting of the Union for Compact Accelerator-driven Neutron Sources, Il Nuovo Cimento-Colloquia and communications in physics, 2015.
[153] T. Veerapaspong, M. Igashira, S. Mizuno, J.-i. Hori, T. Ohsaki, Measurement of keV-Neutron Capture Cross Sections and Capture Gamma-Ray Spectra of ^{143,145,146}Nd, Journal of Nuclear Science and Technology, 36 (1999) 855-864.
[154] F. Käppeler, R. Gallino, S. Bisterzo, W. Aoki, The s process: Nuclear physics, stellar models, and observations, Review of Modern Physics, 83 (2011) 157-193.
[155] I. Dillmann, R. Reifarthc, Nuclear astrophysics with neutrons, Journal of Instrumentation,, 7 (2012).
[156] W.A.G. Sauerwein, A. Wittig, R. Moss, Y. Nakagawa, Neutron Capture Therapy, Springer-Verlag, Berlin, 2012.
[157] S. Liberman, A. Kreiner, M. Casal, P. Menendez, A. Schwint, A. Dagrosa, G.S. Cruz, S. Gonzalez, A. Valda, G.S. Martin, G. Juvenal, M. Pisarev, V. Tribillin, New Challenges in Neutron Capture Therapy 2010, in: S. Liberman, A. Kreiner, M. Casal, P. Menendez, A. Schwint, A. Dagrosa, G.S. Cruz, S. Gonzalez,

A. Valda, G.S. Martin, G. Juvenal, M. Pisarev, V. Tribillin (Eds.) The 14th International Congress on Neutron Capture Therapy, Buenos Aires, Argentina, 2010.
[158] T.E. Blue, J.C. Yanch, Accelerator-based epithermal neutron sources for boron neutron capture therapy of brain tumors, Journal of Neuro-Oncology, 62 (2003) 19-31.
[159] IAEA, Current Status of Neutron Capture Therapy, International Atomic Energy Agency, Vienna, 1999.
[160] R.F. Barth, Boron neutron capture therapy at the crossroads: Challenges and opportunities, Applied Radiation and Isotopes, 67 (2009) S3–S6.
[161] F. Hiraga, T. Okazaki, Y. Kiyanagi, Neutronic Design on a Small Accelerator-Based ^{7}Li (p, n) Neutron Source for Neutron Scattering Experiments, Physics Procedia, 26 (2012) 97-107.
[162] P. Mastinu, J. Praena, G. Martín-Hernándezc, N. Dzysiuk, G. Pretea, R. Capoted, M. Pignatari, A. Ventura, Status of the LEgnaro NeutrOn Source facility (LENOS), Physics Procedia, 26 (2012) 261-273.
[163] K. Tsuchida, Target for neutron-generating device and manufacturing method therefor, Google Patents n. 20150216029 http://www.google.com/patents/EP2874473A1?cl=ena, (2015).
[164] J.P. I. Porras, F. Arias de Saavedra, M. Pedrosa, P. L. Esquinas and P. Jimenez-Bonilla, Epithermal neutron beams from the 7Li(p,n) reaction near the threshold for neutron capture therapy, IL NUOVO CIMENTO C, 38 (2015).
[165] F.M. Wagner, B. Loeper-Kabasakal, H. Breitkreutz, Neutron medical treatment of tumours – a survey of facilities, Journal of Instrumentation, 7 (2012) C03041.
[166] http://www.shi.co.jp/english/info/index.html.
[167] C.-K. Loong, R. Sollychin, R.K. Wong, K. Bradley, M.A. Piestrupc, T. Liang, The Pros and Cons of Preliminary R&D of Boron Neutron Capture Therapy Based on Compact Neutron Generators: A Plan of Collaboration, Physics Procedia, 60 (2014) 264-270.
[168] J.K.Kim, K.-O. Kim, Current research on accelerator-based boron neutron capture therapy in Korea, Nuclear Engineering and Technology, 41 (2009).
[169] H. Kumada, A. Matsumura, M. Yoshioka, H. Kobayashi, H. Matsumoto, T. Kurihara, S.-i. Kurokawa, T. Nakamoto, T. Nakamura, T. SuganoS, Development of a linac-based neutron source for BNCT with beryllium three-layer neutron target system, in: G. Prete, P. Mastinu (Eds.) The Fifth Meeting of the Union for Compact Accelerator-driven Neutron Sources, Il Nuovo Cimento-Colloquia and communications in physics, Padova, Italy, 2015.
[170] A. Pisent, E. Fagotti, P. Colautti, D. Moro, S. Bortolussi, MUNES project: an intense Multidisciplinar Neutron Source for BNCT and other applications based on a high intensity RFQ accelerator, in: G. Prete, P. Mastinu (Eds.) The Fifth Meeting of the Union for Compact Accelerator-driven Neutron Sources, Il Nuovo Cimento-Colloquia and communications in physics, Padova, Italy, 2015.
[171] I. Postuma, S. Bortolussi, N. Protti, J. Valsecchi, S. Fatemi, S. Altieri, BNCT neutron beam from accelerator, in: G. Prete, P. Mastinu (Eds.) The Fifth Meeting of the Union for Compact Accelerator-driven Neutron Sources, Il Nuovo Cimento-Colloquia and communications in physics, Padova, Italy, 2015.
[172] P.C. A. Pisent, J Esposito, L. De Nardo, V. Conte, D. Agosteo, G. Jori, P.A. Posocco, L.B. Tecchio, R. Tinti, G. Rosi, Progress on the accelerator based SPES-BNCT project at INFN Legnaro, Journal of Physics: Conference Series, 41 (2006).
[173] DOE, The Nation's Needs for Isotopes: Present and Future, US Department of Energy, 2008.
[174] NSAC, Isotopes for the Nation's Future A Long Range Plan, US Department of Energy, 2009.
[175] M. Lyra, P. Charalambatou, E. Roussou, S. Fytros, I. Baka, Alternative production methods to face global molybdenum-99 supply shortage, Hellenic Journal of Nuclear Medicine, January-April (2011) 49-55.
[176] OECD, The Supply of Medical Radioisotopes: Review of potential molybdenum-99/techetium-99m production technology, Organization for Economic Co-operaton and Development, 2010.
[177] K. Bertsche, Accelerator production options for ^{99}Mo, The 1st International Particle Accelerator Conference, , IPAC'10, Kyoto, Japan, 2010.

[178] A.N. Dovbnya, E.L. Kuplennikov, V.A. Tsymbal, V.V. Krasil'nikov, Possibility of 99mTc production at neutron generator, Problems of Atomic Science and Technology N5 Series: Nuclear Physics Investigations, 52 (1999).
[179] Y. Nagai, Y. Hatsukawa, Production of 99Mo for nuclear medicine by 100Mo(n; 2n)99Mo, Journal of Physical Soc. Jpn., 78 (2009).
[180] Y. Nagai, Y. Hatsukawa, T. Kin, K. Hashimoto, S. Motoishi, C. Konno, K. Ochiai, K. Takakura, Y. Sato, Y. Kawauchi, N. Sato, A. Ohta, H. Yamabayashi, M. Tanase, S. Fujisaki, T. Teranaka, N. Takeuchi, T. Igarashi, Successful Labeling of 99mTc-MDP Using 99mTc Separated from 99Mo Produced by 100Mo(n; 2n)99Mo, Journal Physical Soc. Jpn., 80 (2011).
[181] E. Cartlidge, Europe on course for a neutron drought, Science, 351 (2016) 1251.
[182] T. Feder, Seeking to bridge Europe's impending neutron gap, Physics Today, (March 2016) 25-27.
[183] C. Andreani, C.-K. Loong, G. Prete, Focus point on compact accelerator-driven neutron sources, The European Physical Journal Plus, (2016).
[184] Y. Kiyanagi, C.-K. Loong, The Fourth Meeting of the Union for Compact Accelerator-Driven Neutron Sources (UCANS), in: N. news (Ed.), 2014.

List of symbols (in order of appearance) and acronyms:

SYMBOLS: [alphabetically sorted, first Greek, then English] Many symbols and vector notations do not appear correctly, some are known MS Word problems, please double check.

A_{pot} = potential scattering

A_{res} = resonance scattering

A = mass number

β = Beta particle

b = scattering length

$\langle b \rangle$ = average coherent scattering length

$\vec{B}$ = magnetic field

ξ = variable that describe the efficiency of neutron thermalization and slowing down hinges upon the average gain of lethargy by a scattering event

d = sample of thickness

d = deuterium

δ = neutron-energy-dependent phase shift

δ' = real part of δ

δ'' = imaginary part of δ

e^- = electron

eV = electron Volt

E_n = resonance energy

E = energy

$f(E)$= spectrum of fission neutrons

F(r) = force of the neutron

$\overrightarrow{G_{hkl}}$= reciprocal lattice vector

$\Gamma_{s,n}$ = half-width of the n^{th} resonance for scattering

$\Gamma_{r,n}$ = half-width of the n^{th} resonance for reaction

i, j = states of spin of the neutron

$\hbar$ = reduced Planck constant

k_b = Boltzmann constant

kW = chilo-watt

$\overrightarrow{k_1}$= outgoing neutron wave vector

$\overrightarrow{k_0}$= incoming neutron wave vector

λ = wavelength

m_n = neutron mass

M = mass of the atoms

n = neutron

n_d = atomic number density

N = number of scattering units in the sample

$\mathrm{N(E)}$ = evaporation spectrum of neutrons

N_A = Avogadro's number

$\overline{\nu}_e$ = electron anti-neutrino

η = refractive index

ϑ_o = neutron incident angle

ϑ_T = transmitted angle of neutrons

f = scattering amplitude

μ_N= nuclear magneton

μ_n= magnetic moment

γ = gamma particle

γ_n = gyromagnetic ratio

p = proton

π_0 = pion particle

$\vec{q}$= reduced wave vector

$\vec{Q}$= neutron momentum transfer

ρ = mass density

R_X = nucleus' radius

Σ = "macroscopic" cross sections

σ = cross-section

σ_{ij} = scattering kernel

$\vec{\sigma}$ = spin

σ_r = reaction cross section

σ_{coh} = coherent cross-section

σ_{inc} = incoherent cross-section

σ_S = scattering cross section

S_{coh} = coherent scattering function

S_{inc} = incoherent scattering function

t = time

t_e = mean lifetime

$t_{1/2}$ = half-life

t = tritium

τ_n = neutron capture time

T = pulsing period

T = Temperature

T_r = probability of transmission

v = neutron speed

υ (also f) = frequency

V(r) = potential energy

Y(E,A) = yield

ω_L = Larmor frequency

ACRONYMS:

Technical acronyms:

ADS Imaging - Accelerator Driven System Imaging

ANEM - Atmospheric Neutron EmulatorLPSSs - long-pulse spallation sources

APT - associated particle technique

BNCT –Boron neutron capture therapy

BSA = Beam Shaping Assembly

CANS - Compact Accelerator-based Neutron Sources

DGAA - Delayed Gamma Activation Analysis

DINS - Deep Inelastic Neutron scattering

FNA - fast neutron analysis

FNAA – Fast Neutron Activation Analysis

FWHM - Full width at half maximum

GEM – the Gas Electron Multiplier

GNP - gross national product

HC - hydrocarbon

HEU - high-enriched uranium

HPGe - High purity germanium detector

LET = linear energy transfers

LEU - low-enriched uranium

MB - Maxwell-Boltzmann

MCNP - Monte Carlo N-Particle code

MPNCX = a Monte Carlo code

MSc and PhD - Master of Science and Doctor of Philosophy

MWPC = multi-wire proportional chamber

NRCA - Neutron Resonance Capture Analysis

NRTA - Neutron Resonance Transmission Analysis

NRTI - Neutron resonance transmission imaging

NT – Neutron Tomography

PET - positron emission tomography

PGAA - Prompt gamma activation analysis

PHITS – a Monte Carlo simulation code

PKA - primary knock-on atom

PFTNA - pulsed fast and thermal neutron analysis

QMCANS - quasi-mono-energetic CANS

QMN - Quasi Mono-energetic Neutrons

RBE = relative biological effectiveness

RF - Radiofrequency

RFQ - Radio-Frequency Quadrupo

RITS - Rietveld-type analysis code

SANS - Small Angle Neutron Scattering

SEE – Single Event Effect

SEU - single event upset

TNA - thermal neutron analysis

TOF - Time of flight

UCANS - Union of Compact Accelerator-based Neutron Sources

Facilities:

ANITA - Atmospheric-like Neutrons from thIck TArget

ANL - Argonne National Laboratory

ANEM - Atmospheric-Neutron Emulator

CARR - The 60MW China Advanced Research Reactor

CERN - The European Organization for Nuclear Research

CP1 - Chicago Pile-1

CP2 - Chicago Pile-2

CPHS - Compact Pulsed Hadron Source

CSNS - China Spallation Neutron Source

CNEA - Centro Atómico Bariloche

CPHS - Compact Pulsed Hadron Source of Tsinghua University

CYRIC - Cyclotron and Radioisotope Center

EC-JRC - Joint Research Centre of the European Commission

ELBE - Low background experimental hall of Helmholtz-Zentrum Dresden-Rossendorf

ENEA - Agenzia nazionale per le nuove tecnologie, l'energia e lo sviluppo economico sostenibile

ESS - The European Spallation Source

ESRF - European Synchrotron Radiation Facility

ESSB – European Spallation Source-Bilbao

EVEDA - The Engineering Validation and Engineering Design Activities

FRMII - Forschungs-Neutronenquelle Heinz Maier-Leibnitz

FAIR- Facility for Antiproton and Ion Research

FNG – Frascati Neutron Generator

FARETRA - A next generation reactor simulator for transmutation studies at LKNL

FNG - The Frascati Neutron Generator

FRANZ - Frankfurt Neutron Source at the Stern-Gerlach-Zentrum

GELINA- Geel Electron LINear Accelerator Facility

HFBR - High Flux Beam Reactor

HFIR - High Flux Isotope Reactor

HFR - High Flux Reactor

HUNS- The Hokkaido University Neutron Source

KENS - National Laboratory of High Energy Physics

KEK – High Energy Accelerator Research Organization (Tsukuba, Japan)

KIGAM - Korea Institute of Geoscience and Mineral Resources

KIRAMS - The Korea Institute of Radiological and Medical Sciences

KOMAC - Korea Multi-purpose Accelerator Complex

KUANS - Kyoto University Accelerator-driven Neutron Source

KURRI - Kyoto University Research Reactor Institute – Electron Linear Accelerator

IAEA - International Atomic Energy Agency

IBR-2 - Fast pulsed reactor

ISIS - STFC Rutherford Appleton Laboratory

IFMIF - International Fusion Materials Irradiation Facility

ILL - Institut Laue-Langevin

IPNS - Intense Pulsed Neutron Source

IRMM - Institute for Reference Materials and Measurements

ISIS-FETS - Centre for research in the physical and life sciences at the STFC Rutherford Appleton Laboratory - Front End Test Stand

iThemba or iTL – Laboratory for Accelerator Based Science

LANSCE - Los Alamos National Laboratory

LENOS - LEgnaro NeutrOn Source

LENS - The Low-Energy Neutron Source

LNL – Laboratori Nazionali di Legnaro

LPSSs - Pulses from long-pulsed spallation sourcesn@BTF - The Frascati electron-driven source

nELBE - Neutron source and low background experimental hall

NEPIR - NEutron and Proton IRradiation Facility

NST – National Research Council of Science. & Technology- Korea

NUANS - Nagoya University Accelerator-driven Neutron Source

MLS - Japanese Materials and Life Sciences Facility

MTR – Medical Therapy Reactor

NRU - National Research Universal reactor

NRX - National Research Experimental

OPAL - Australia's Open Pool Australian Lightwater reactor

PNF - Pohang *Neutron* Facility

PAL- Pohang Accelerator Laboratory

PKUNIFTY - Peking University Neutron Imaging Facility

PROTON - Direct low current proton beam line at LNL

QMN -beam lines at NEPIR facility at Laboratori Nazionali di Legnaro

RANS - Riken Accelerator-driven Neutron Source

RIKEN - Rikagaku Kenkyūsho, a large research institute in Japan

RCNP – Research Center for Nuclear Physics

SESAME - Spin-Echo Scattering Angle Measurement

SINQ and SINQII - Swiss Spallation Neutron Source

SLOWNE - A high intensity slow neutron beam line at LNL

SNS and SNSII - Spallation Neutron Source

SNS - Spallation Neutron Source

SPES - Cyclotron-driven fast neutron irradiation facility

SPSSs – short pulsed spallation sources

TIARA - Takasaki Ion Accelerators for Advanced Radiation Application

TSL - The Theodor Svedberg Laboratory

TFTR - Tokamak Fusion Test Reactor

TRIUMF – Canada's national laboratory for particle and nuclear physics and accelerator-based science

JET - Europe's largest fusion device

JSNS - Japan Spallation Neutron Source

UTCANS - U-Tokyo CANS

XFEL - European X-Ray Free-Electron Laser

X-10 - Oak Ridge Graphite Reactor

ZING-P - prototype pulsed spallation source at Argonne